OXIDATION OF GeSi AND APPLICATIONS

Thesis by

Wen-Shu Liu

In Partial Fulfillment of the Requirements

for the Degree of

Doctor of Philosophy

California Institute of Technology

Pasadena, California

1994

(submitted May 2, 1994)

ACKNOWLEDGEMENTS

First and foremost, I would like to thank my advisor, Professor Marc-A. Nicolet for his support, inspiration and encouragement throughout my graduate work at Caltech. I am also grateful to Professor Thad Vreeland, Jr. who supported me in my early graduate study and is always very helpful to me.

I am indebted to the members of Professor Nicolet's group, past and present, especially Dr. S.G. Park who contributed part of this thesis; also J.S. Chen, Dr. E.W. Lee and D.Y.C. Lie who have helped through collaborations to the completion of this thesis. Special thanks are due to J. Reid, Dr. E. Kolawa, and Dr. G. Bai for either their valuable discussions or preparation of some of my samples and to R. Gorris and M. Easterbrook for their technical assistance.

I enjoyed the collaboration with Dr. V. Arbet-Engels, Dr. T. Carns, M. Tanner and Prof. K.L. Wang at UCLA who provided me the epitaxial samples and constructive suggestions. I also benefited from the TEM work with C. Garland. I wish to thank Dr. T. Workman, Dr. H. Kubota, Dr. A. Vantomme, Dr. A. Bachli, Dr. J.H. Song and X. Sun for their generous help and friendship.

Finally I would like to thank my family for their support and encouragement. This thesis was made possible by the financial support of the Semiconductor Research Corporation.

ABSTRACT

The thermal oxidation of epitaxial and polycrystalline Ge_xSi_{1-x} has been studied in a dry or wet ambient at various temperatures. It is found that the composition of the resulting oxide depends on temperature, ambient, Ge content, structure of the Ge_xSi_{1-x} alloy, and the oxidation procedure. While in a wet ambient, and following the preheating procedure, a uniform $Ge_xSi_{1-x}O_2$ oxide is observed for a high Ge content at low oxidation temperatures, a SiO_2 oxide is obtained for a low Ge content at high temperatures. A $Ge_ySi_{1-y}O_2$ oxide with reduced Ge content ($y < x$) is found in between. Ge piles up behind the oxide when SiO_2 or $Ge_ySi_{1-y}O_2$ forms. When a uniform $Ge_xSi_{1-x}O_2$ grows, its thickness is proportional to the square root of the oxidation duration, which indicates that the rate-limiting process is the diffusive transport across the oxide of, most probably, the oxidant. The rate increases with the Ge content in the alloys. It is proposed that, in general, the oxidation behavior is determined by the competition between the speed of the diffusive process in the unoxidized GeSi alloy and the velocity at which the oxidation front progresses. The controlling factors are the oxidation temperature, the composition, and the structure of the Ge_xSi_{1-x} alloy. A model is proposed that is based on these three factors.

The stability of an amorphous $Ge_xSi_{1-x}O_2$ in contact with an epitaxial (100)Ge_xSi_{1-x} layer obtained by partially oxidizing an epitaxial Ge_xSi_{1-x} layer on a (100)Si substrate in a wet ambient at 700°C has been investigated. It is noticed that $Ge_xSi_{1-x}O_2$ is thermodynamically unstable in contact with Si or GeSi, or in the presence of hydrogen and GeO_2 will be reduced to elemental Ge.

When $Ge_{0.38}Si_{0.62}O_2$ films are exposed to hydrogen, germanium nucleates homogeneously and the result is a suspension of nanocrystalline Ge grains embedded in a film of SiO_2. This nanocrystalline Ge is photoluminescent, as would be surmised by

analogy with porous Si. When some parameters of the reduction experiment just described are altered, the outcome is radically different. This is accomplished by annealing a $Ge_{0.82}Si_{0.18}/Ge_{0.82}Si_{0.18}O_2$ bilayer on a Si substrate in a 5% H_2 ambient. A heterogeneous nucleation occurs on the interface between the epitaxial $Ge_{0.82}Si_{0.18}$ and the oxide, with the consequence that Ge grows in the form of an epitaxial layer there as it precipitates out of the oxide. Surprisingly, this Ge layer is of a superior crystalline quality than that of $Ge_{0.82}Si_{0.18}$ seed layer on which it grows.

Finally, we oxidized amorphous Ge/Si bilayers on Si substartes. Epitaxial Ge_xSi_{1-x} layers can be produced this way. Vacuum annealing of these samples only results in polycrystalline Ge_xSi_{1-x} layers.

TABLE OF CONTENTS

LIST OF TABLES

LIST OF FIGURES

LIST OF PUBLICATIONS

"Wet oxidation of epitaxial $Ge_{.36}Si_{.64}$ on (100)Si," W.S. Liu, G. Bai, M.-A. Nicolet, C.H. Chern, V. Arbet, and K.L. Wang, Mat. Res. Soc. Symp. Proc., **220**, 259 (1991).

"Importance of sample preheating in oxidation of Ge_xSi_{1-x}," W.S. Liu, E.W. Lee, M.-A. Nicolet, V. Arbet-Engels, and K.L. Wang, J. Appl. Phys. **71**, 3626 (1992).

"Wet oxidation of GeSi at 700°C," W.S. Liu, E.W. Lee, M.-A. Nicolet, V. Arbet-Engels, K.L. Wang, N.M. Abuhadba, and C.R. Aita, J. Appl. Phys. **71**, 4015 (1992).

"Epitaxial Ge_xSi_{1-x} films on Si: (1) oxidation and nitridation of Ge_xSi_{1-x} (2) ion implantation of Ge_xSi_{1-x}," M.-A. Nicolet, D.Y.C. Lie, W.S. Liu, and A. Vantomme, Proc., 14th Solid State Phys. Symp. on the Semiconductor Surface and Metal-Semiconductor Interface, (Korean Physical Society, June 26-27, 1992, pp. 1-37).

"Instability of a $Ge_xSi_{1-x}O_2$ film on Ge_xSi_{1-x}," W.S. Liu, J.S. Chen, M.-A. Nicolet, V. Arbet-Engels, and K.L. Wang, J. Appl. Phys. **72**, 4444 (1992).

"Nanocrystalline Ge in SiO_2 by annealing of $Ge_xSi_{1-x}O_2$ in hydrogen," W.S. Liu, J.S. Chen, M.-A. Nicolet, V. Arbet-Engels, and K.L. Wang, Appl. Phys. Lett. **62**, 3321 (1993).

"A Ge epilayer of high quality on a Si substrate by solid-phase epitaxy," W.S. Liu, J.S. Chen D.Y.C. Lie, and M.-A. Nicolet, Appl. Phys. Lett. **63**, 1405 (1993).

"A GaAs on Ge on Si technology via $Ge_xSi_{1-x}O_2$ reduction," W.S. Liu, M.-A. Nicolet, T. K. Carns, and K.L. Wang, presented at 35th Electronic Materials Conference, Santa Barbara, June, 1993.

"Epitaxial Ge layers on Si via $Ge_xSi_{1-x}O_2$ reduction: the roles of hydrogen partial pressure and the Ge content," W.S. Liu, M.-A. Nicolet, T.K. Carns and K.L. Wang, to be published in J. Elec. Mate.

"Kinetics and mechanism of wet oxidation of Ge_xSi_{1-x} alloys," S.G. Park, W.S. Liu, and M.-A. Nicolet, J. Appl. Phys. **75**, 1764 (1994).

"Nitridation and hydridation of GeSi oxide in ammonia," W.S. Liu and M.-A. Nicolet, to be submitted to J. Appl. Phys.

"Epitaxial Si/Ge_xSi_{1-x} heterostructure from oxidized amorphous Ge/Si bilayer on Si(100)," W.S. Liu, S.G. Park, and M.-A. Nicolet, to be submitted to J. Appl. Phys.

Chapter 1
Introduction

Heterojunction devices have superior electronic properties due to their unique energy band alignment at the interface. For example, higher frequency and higher current densities can be achieved in a heterojunction bipolar transistor than a conventional bipolar transistor [1]. In a conventional npn transistor, the concentration ratio of injected electrons from the emitter to the base to injected holes in the reverse direction is equal to the concentration ratio of dopants in the emitter and base regions. To obtain a high current gain, it is necessary to make the donor concentration in the emitter much greater than the acceptor concentration in the base. However the limitation to a light doping of the base is that the series resistance of the base is too high for high speed application. In contrast, the current gain of a npn heterojunction bipolar transistor is proportional to the ratio of dopant concentration multiplied by $e^{\Delta E_v/kT}$, where ΔE_v is the valence band offset between the base and emitter. Therefore, by using materials with band offsets between the two regions, it is possible to achieve higher current gains without sacrificing the speed of the transistor. Another application of heterojunctions is for modulation doping which spacially separates mobile carriers from ionized impurities so that carriers can attain a mobility that is unaffected by impurities scattering. This situation exists near heterojunction interfaces [2].

Ge_xSi_{1-x}, in bulk form or as strained thin film, has a smaller bandgap than Si [3]. It has been shown that high quality, pseudomorphic Ge_xSi_{1-x} layers can be grown on Ge_ySi_{1-y} and Si substrates [4-6]. The bandgap engineering possible with the GeSi/Si material system can be exploited for the fabrication of various devices utilizing the heterojunction characteristics as described above, large wavelength optoelectronics devices, and tunneling and supperlattice devices [7-10]. One of the main attractions of the GeSi-based

system over other compound semiconductor system is its compatibility with current processing techniques of Si. Thermal oxidation of Si is one of the critical process steps in the fabrication of Si bipolar and metal-oxide-semiconductor technology. In Si-based devices and integrated circuits, thermal oxides are used as gate dielectrics, field oxides, for photolithographic masking, and for device isolations. Correspondingly, the growth of a thermal oxide of high quality on GeSi is a very desirable processing step for many potential device applications of GeSi.

The basic understanding of the kinetics of thermal oxidation in Si comes from a model developed by Deal and Grove [11]. It assumes that the growth occurs by diffusion of the oxidant through the oxide to the Si/oxide interface where the oxidant reacts with Si to form SiO_2. This model yields the familiar equation,

$$x^2 + Ax = B\,(t + t_i),$$

where x is the oxide thickness, t is the oxidation duration, and A and B are constants for a given set of oxidation conditions. The quantity $t_i = (x_i^2 + Ax_i)/B$ is related to the initial condition, where x_i is the thickness of a pre-existing oxide. Two different regimes of growth are generally identified: a linear regime when $t \leq A^2/4B$ which leads to the relation $x = B/A(t + t_i)$ and a parabolic regime when $t \geq A^2/4B$ which gives $x^2 = Bt$. In the linear regime, the oxide growth is limited by the Si/SiO_2 interface kinetics while in the parabolic regime, the growth rate is controlled by the diffusion of oxidant through the oxide. The activation energy of B, the diffusion rate constant, is similar to that for diffusion of oxygen or water in fused silica for dry and wet oxidation respectively, while the interfacial rate constant B/A is the same for wet and dry conditions and has an activation energy similar to the energy to break a Si-Si bond (~ 2 eV).

It is of scientific and technological interests to investigate how the oxidation of GeSi proceeds and to compare it to that of pure Si. Besides us, and as would be expected from

the importance of this subject, several other groups have been involved with this subject recently [12-19]. Depending on oxidation conditions and alloy composition, both segregation of Ge in front of the growing oxide [12-19] and trapping of Ge in the growing oxide [15-19] have been observed. The properties of the resulting oxide are also of interest. Polycrystalline Ge_xSi_{1-x} has been proposed as a promising material for thin film transistor [20]. Its oxidation behavior and the comparison with that of epitaxial Ge_xSi_{1-x} is certainly important.

This thesis is devoted to the study of the kinetics and associated mechanisms of wet oxidation of epitaxial and polycrystalline Ge_xSi_{1-x} and the properties of the resulting oxides. Chapters 2, 3 and 4 describe how one can form uniform $Ge_xSi_{1-x}O_2$ layers out of either epitaxial or polycrystalline Ge_xSi_{1-x} alloys. As a gate oxide, $Ge_xSi_{1-x}O_2$ is not useful, however, because the oxide is thermodynamically unstable in contact with Si or GeSi. Chapter 5 describes this instability and its thermodynamic origin. Chapters 6 and 7 deal further with this instability of $Ge_xSi_{1-x}O_2$ and exploit it for a novel and versatile method to synthesize nanostructured Ge in SiO_2 and for an unusual epitaxial growth of Ge. In Chapter 8, the formation of an epitaxial Si/Ge_xSi_{1-x} heterostructure from oxidized amorphous Ge/Si bilayers is reported. The last chapter draws conclusions and discusses future works.

Reference

[1] H. Kroemer, Proc. IEEE **70**, 13 (1982).

[2] S. Wang, *Fundamentals of Semiconductor Theory and Device Physics* (Prentice-Hall, Inc, New Jersy) p. 542.

[3] R. People, Phys. Rev. **B32**, 1405 (1985).

[4] J.C. Bean, L.C. Feldman, A.T. Fiory, S. Nakahara, and I.K. Robinson, J. Vac. Sci. Technol. **A2**, 436 (1984).

[5] H. Daembkes, H.-J. Herzog, H. Jorke, H. Kibbel, and E. Kasper, IEEE Trans. Electron Devices **33**, 633 (1986).

[6] C.A. King, C.M. Gronet, J.F. Gibbson, and S.D. Wilson, IEEE Electron Device Lett. **9**, 229 (1988).

[7] R. People, J. Quantum Electron. **22**, 1696 (1986).

[8] S.S. Iyer, G.L. Patton, J.M.C. Stork, B.S. Meyerson, and D.L. Harame, IEEE Trans. Electron Devices **36**, 2043 (1989).

[9] S.S. Rhee, J.S. Park, R.P.G. Karunasiri, Q. Ye, and K.L. Wang, Appl. Phys. Lett. **53**, 204 (1988).

[10] J.S. Park, R.P.G. Karynasiri, K.L. Wang, S.S. Rhee, and C.H. Chern, Appl. Phys. Lett. **54**, 1564 (1989).

[11] B.E. Deal and A.S. Grove, J. Appl. Phys. **36**, 3770 (1965).

[12] D. Fathy, O.W. Holland, and C.W. White, Appl. Phys. Lett. **51**, 1337 (1987).

[13] F.K. LeGoues, R. Rosenberg, and B.S. Meyerson, Appl. Phys. Lett. **54**, 644 (1989).

[14] D.K. Nayak, K. Kamjoo, J.S. Park, J.C.S. Woo, and K.L. Wang, Appl. Phys. Lett. **57**, 369 (1990).

[15] J. Eugene, F.K. LeGous, V.P. Kesan, S.S. Iyer, and F.M. d'Heurle, Appl. Phys. Lett. **59**, 78 (1991).

[16] H.K. Liou, P.Mei, U. Gennser, and E.S. Yang, Appl. Phys. Lett. **59**, 1200 (1991).

[17] D.C. Paine, C. Caragianis, and A.F. Schwartzman, J. Appl. Phys. **70**, 5076 (1991).

[18] W.S. Liu, E.W. Lee, M.-A. Nicolet, V. Arbet-Engels, K.L. Wang, N.M. Abuhadba, and C.R. Aita, J. Appl. Phys. **71**, 4015 (1992).

[19] E.C. Frey, N.Yu, B.Patnaik, N.R. Parikh, M.L. Swanson, and W.K. Chu, J. Appl. Phys. **74**, 4750 (1993).

[20] H.C. Lin, T.G. Jung, H.Y. Lin, C.Y. Chang, and T.F. Lei, J. Appl. Phys. **74**, 5395 (1993).

Chapter 2
Oxidation of Ge_xSi_{1-x}: General Behavior

2.1 Introduction & experiment

While performing oxidation experiments, care must be exercised. The details of the procedure affects the results in ways that significantly modify their correct interpretation. In this chapter, we demonstrate the importance of the procedure adopted in the oxidation of GeSi. Similar effects have previously been noted in the oxidation of silicides [1]. Also, we show that by controlling the oxidation temperature, two different oxides (pure SiO_2 vs. uniform $Ge_xSi_{1-x}O_2$) can be formed. A simple model is given that explains the difference.

The samples used in this study were pieces of a 470 nm film of $Ge_{0.36}Si_{0.64}$ grown epitaxially on a (100)Si substrate by molecular beam epitaxy. The film is elastically relaxed as determined from x-ray double crystal diffractometry. The samples were oxidized in a tube furnace at 1000°C in dry oxygen or in a wet ambient obtained by bubbling nitrogen gas through 95°C water. Two oxidation procedures were used. In the first, the furnace was flushed with the oxidant, followed by introducing the cold sample into the hot furnace. In the second oxidation procedure (referred subsequently the method with preheating) the hot tube was flushed with nitrogen for approximately 1 h. The sample was then introduced into the furnace. After about 10 min, the furnace atmosphere was switched from nitrogen to the oxidizing ambient. Another sample was oxidized in a wet ambient at 700°C following the preheating procedure. The samples were analyzed after oxidation by backscattering and infrared absorption spectrometry.

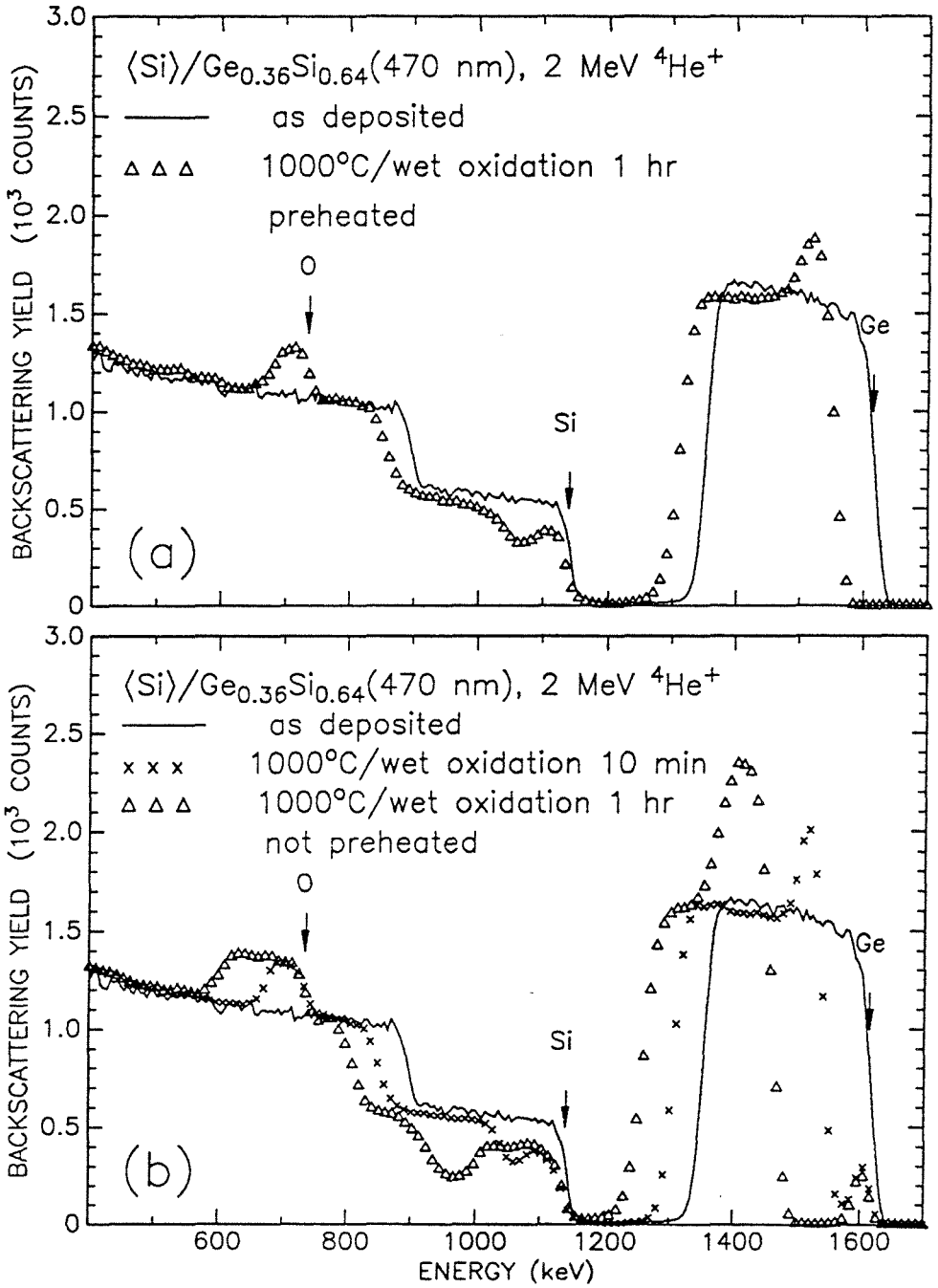

Fig. 2.1 2 MeV $^4He^+$ backscattering spectra of epitaxial $Ge_{0.36}Si_{0.64}$ films on (100)Si oxidized in steam at 1000°C: (a) after 1 hr with preheating (b) after 10 min and 1hr without preheating, showing no Ge oxidized after the first few min. (when temperature reaches 1000°C)

2.2 Importance of samples preheating

Figure 2.1 compares the backscattering spectra of two samples oxidized at 1000°C in a wet ambient with and without preheating. It is clear that with preheating only SiO_2 is formed and that Ge piles up behind it. However, the oxide formed without preheating obviously includes Ge initially. We will show later in Section 2.3 that below 700°C in a wet ambient, Ge and Si are immobile compared to the oxidation velocity. Ge as well as Si are oxidized in this temperature range and the reaction rate is quite large. The samples oxidized without preheating thus pass transiently through this temperature range as they warm up and incorporate Ge into the initially growing oxide. As the temperature rises further, the diffusivities of Ge and Si in GeSi increase so that Ge begins to be rejected, the reaction rate enhancement diminishes until pure SiO_2 is ultimately formed at 1000°C. The Ge concentration profile in the oxide measured from the surface thus reaches a maximum and then decays. Although the heating rate of the samples is fast (on the order of 1000°C/min), the oxidation rate is large enough to incorporate significant amounts of Ge into the oxide in this first few minutes of the transient warm-up. Figure 2.1(b) indeed shows that the Ge is incorporated into the oxide during the first few minutes; only SiO_2 forms after this initial period when the temperature nears 1000°C.

In contrast to the wet oxidation behavior just discussed, Fig. 2.2 shows that in dry oxygen preheating is of no consequence. No Ge is contained in the oxide for either oxidation method. This outcome is explained by the fact that the oxidation rate in dry oxygen is much less than that in wet oxygen. The oxidation rate in dry oxygen is so small that an insignificant amount of GeSi is oxidized during the initial heating-up transient.

To place a cold sample in a hot oxidizing furnace clearly complicates the correct interpretation of the oxidation data in the case of GeSi. It is therefore prudent to preheat the samples before it is oxidized and adopt this as a standard one. We certainly follow this procedure in our following oxidation experiments.

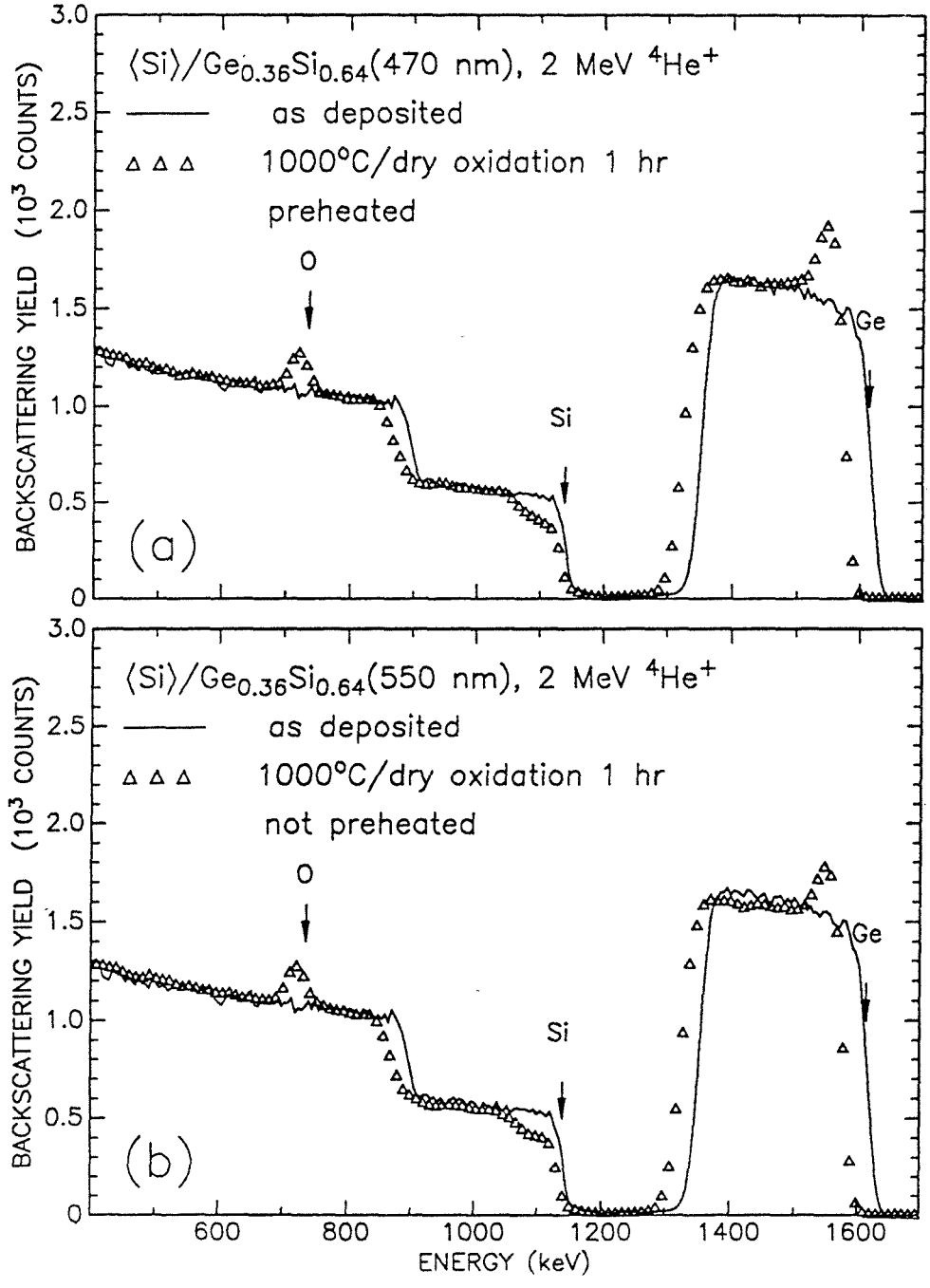

Fig. 2.2 2 MeV $^4He^+$ backscattering spectra of epitaxial $Ge_{0.36}Si_{0.64}$ films on (100)Si oxidized for 1 hr in dry oxygen at 1000°C: (a) with preheating (b) without preheating.

2.3 Dependence of the oxide composition on the temperature: SiO_2 vs. $Ge_xSi_{1-x}O_2$

Figure 2.3 compares the backscattering spectra of two samples oxidized at 1000°C and 700°C following the preheating procedure. It is clear that at 1000°C a surface of pure SiO_2 is formed and Ge piles up behind it as has been seen in previous studies [2-5]. However, the oxide formed at 700°C obviously includes Ge which is uniformly distributed in depth. Within the resolution of backscattering spectrometry, no germanium is lost in both cases. The composition of the oxide at 700°C is $Ge_{0.35}Si_{0.65}O_2$ which differs insignificantly from the original epilayer of composition of $Ge_{0.36}Si_{0.64}$. No pile-up of Ge or Si is seen behind the oxide. Its structure is x-ray amorphous. These facts strongly suggest that the GeSi layer is oxidized and that the oxide is a mixture of SiO_2 and GeO_2. The consumption rate of the GeSi layer is 120 nm per hour which is quite large when compared to that of pure Si which is a few nm of Si per hour for similar conditions.

To test the oxidation state of the layer, a $Ge_{0.36}Si_{0.64}$ sample was oxidized at 700°C for 48 hours which completely consumed the GeSi layer and also some of the substrate Si. A Nicolet Model MX-1 Fourier transform infrared spectrometer was used to obtain infrared absorption spectra of the layer. The instrument was calibrated to an accuracy of ±4 cm^{-1} using a polystyrene standard. A spectrum taken between 400 and 1500 cm^{-1} (25.0 and 6.7 mm) is shown in Fig. 2.4. The absorption peak assignment is as follows [6,7]: SiO_2 features characteristic of the quartz-derived bonding of [SiO_4] tetrahedra in melt-quenched SiO_2 glass include major peaks at 460 cm^{-1}, attributed to Si-O bending, and 1072 cm^{-1}, attributed to Si-O stretching. Minor peaks at 675 and 806 cm^{-1} are attributed to Si stretching. In addition, a peak at 610 cm^{-1} is attributed to Si stretching in [SiO_4] tetrahedra bonded in a manner characteristic of crystobalite, another modification of SiO_2.

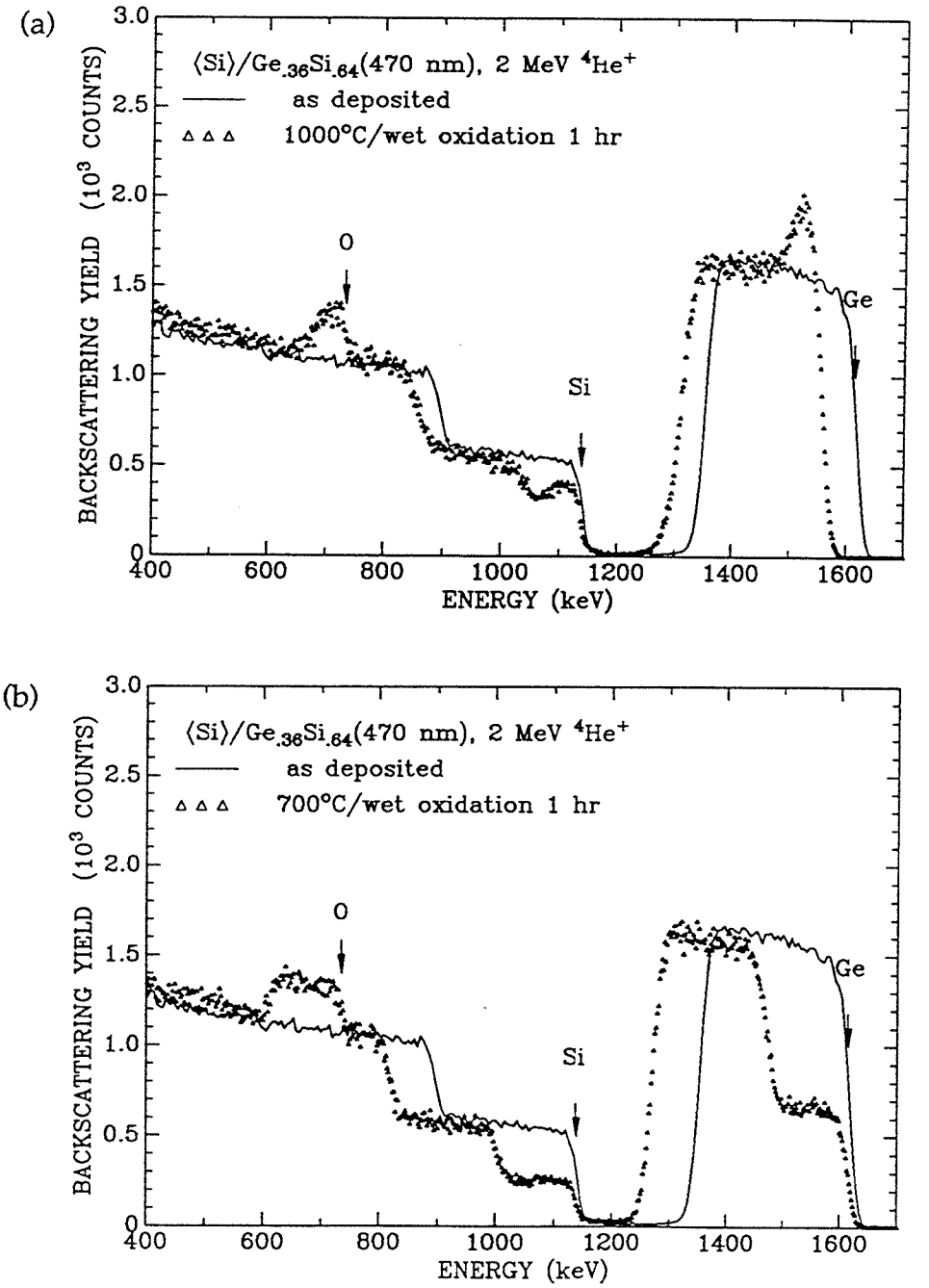

Fig. 2.3 2 MeV $^4He^+$ backscattering spectra of epitaxial $Ge_{0.36}Si_{0.64}$ films on (100)Si oxidized for 1 h in steam: (a) at 1000°C (b) at 700°C.

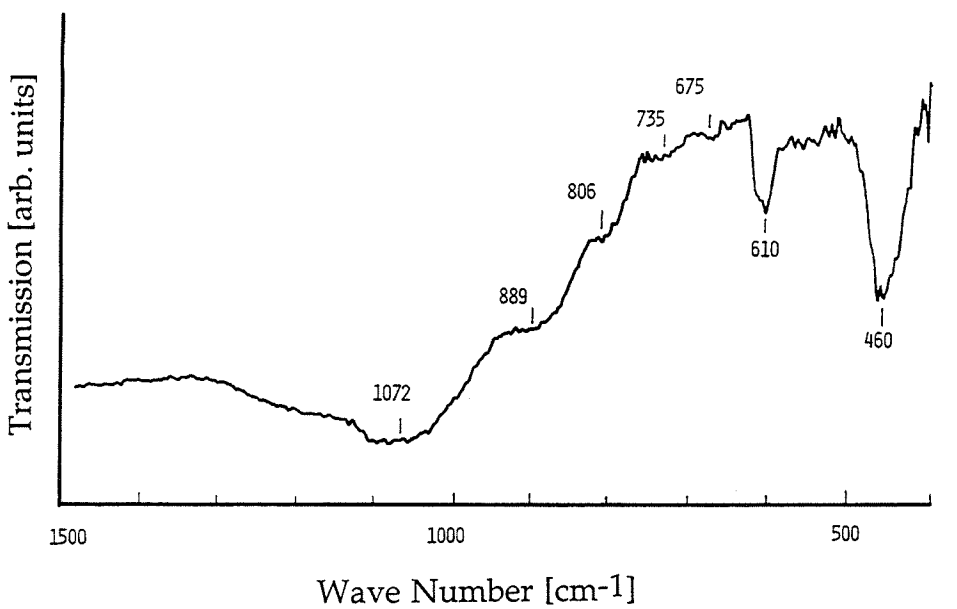

Fig. 2.4 Infrared transmission as a function of wave number for an oxidized $Ge_{0.36}Si_{0.64}$ layer.

GeO_2 crystallizes in two forms: a hexagonal form analogous to quartz in which $[GeO_4]$ tetrahedra are the building blocks, and a tetragonal rutile form in which the basic units are $[GeO_6]$ octahedra. Short range order characteristic of both coordinations are observed here. The major GeO_2 peak at 889 cm^{-1} is attributed to Ge-O stretching in $[GeO_4]$ tetrahedra. In addition, a small peak at 735 cm^{-1} is attributed to Ge-O stretching in $[GeO_6]$ octahedra. Both Ge and Si are therefore oxidized at 700°C as implied from the backscattering spectrum.

To interpret these results, we show in Fig. 2.5 some thermodynamical data of silicon oxide and germanium oxides. Since the GeSi oxidation reaction is governed by the addition of oxygen, the free energy of reaction should be measured in terms of kilocalorie per gram atom of oxidant. Therefore, we describe our system by the reaction

$$(1-x+xy/2)\ Si + x\ GeO_y = (xy/2)\ SiO_2 + Ge_xSi_{1-x}.$$

The free energy of formation of the GeSi alloy, when approximated by an ideal solution, only contributes an entropy term which amounts to some thousands of calories over the experimental temperature range and is much smaller than the free energy of formation of the oxides. We can therefore compare the free energies of formation of the oxides to determine the equilibrium state of the system. We find that it is SiO_2 with the GeSi alloy that has the lowest free energy over the temperature range of interest. This is so for every x and means that, barring the unlikely possibility of ternary compounds, there is a tieline between Ge and SiO_2 in the ternary phase diagram. In other words, as long as there is Si, SiO_2 is the only stable oxide in this system. The pure SiO_2 formed at 1000°C follows this thermodynamical prediction. The uniform GeSi oxide formed at 700°C, however, does not, which must be due to kinetic constraints.

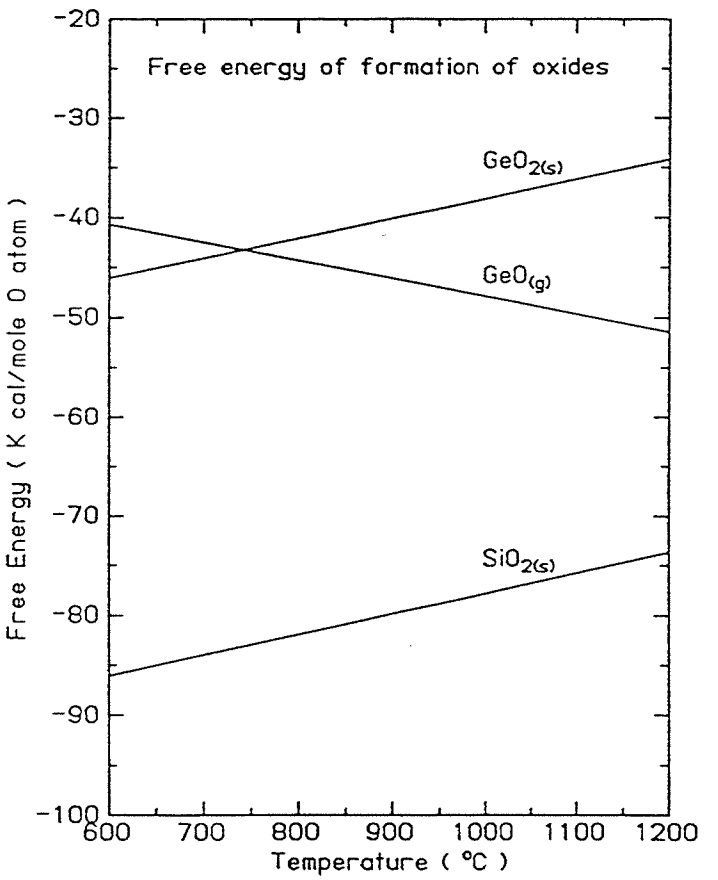

Fig. 2.5 The free energies of formation of $GeO_{2(s)}$, $GeO_{(g)}$, and $SiO_{2(s)}$; the reference states: $Ge_{(s)}$, $Si_{(s)}$, and $O_{2(g)}$.

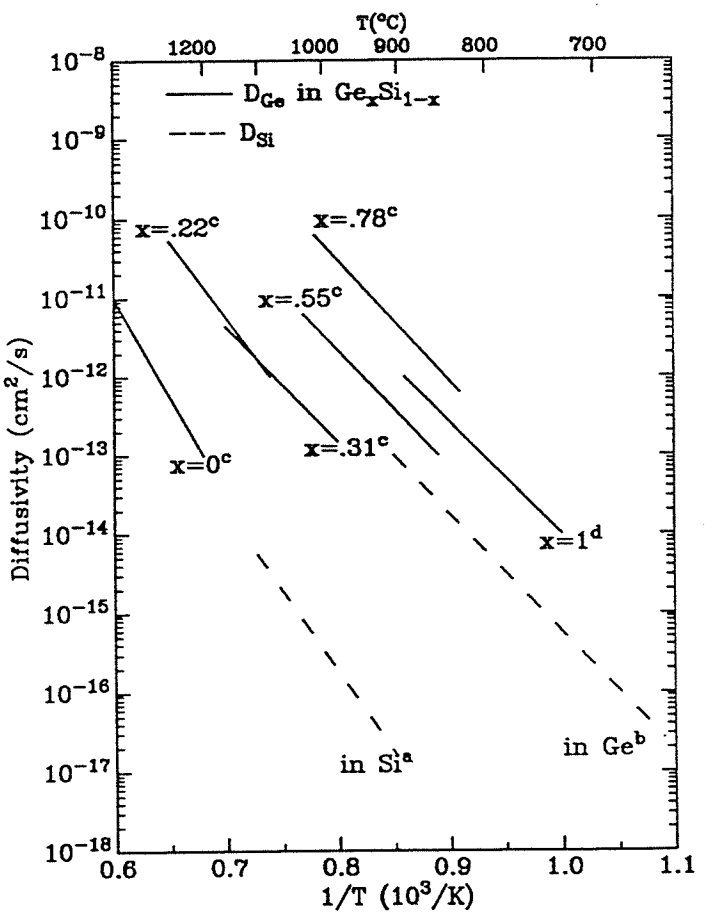

Fig. 2.6 Temperature dependence of the diffusion coefficients of Ge and Si; activation energies range from 3 to 5 eV.

a: ref. 8 b: ref. 9 c: ref. 10 d: ref 11

There are two kinetic factors involved with the reaction: the velocity of oxidation front (proportional to oxidation rate) and the Si supply rate (proportional to Ge or Si diffusivity). That of the diffusivities of Si and of Ge in either Si or Ge ranges from 3 to 5 eV. The same values apply for the diffusivity of Ge in GeSi (Fig. 2.6). As we will show in Chapter 4, the rate of oxidation of these samples is parabolic with the annealing duration employed here and has an activation energy of 1.1 eV. The oxidation thus will slow down little compared to the decrease of the diffusivities in GeSi when the temperature falls. The reason for the different oxide formed at 1000°C and at 700°C becomes clear: at 1000°C, the diffusion of Ge and Si relative to each other is fast compared to the motion of the oxidation front. Thermodynamics controls the outcome in that case and only SiO_2 forms. At 700°C, Ge and Si are immobile compared to the oxidation velocity. Germanium and Si are uniformly oxidized in this case. A similar situation is found in the oxidation of $TiSi_2$, which is explained in the same way [1].

References

[1] W. J. Strydom and J. C Lombaard, Thin Solid Films **131**, 215 (1985).

[2] F. K. LeGoues, R. Rosenberg, T. Nguyen, F. Himpsel, and B. S. Meyerson, J. Appl. Phys. **65**, 1724 (1989).

[3] F. K. LeGoues, R. Rosenberg, and B. S. Meyerson, Appl. Phys. Lett. **54**, 664 (1989).

[4] D. Nayak, K. Kamjoo, J. C. S. Woo, J. S. Park, and K. L. Wang, Appl. Phys. Lett. **56**, 66 (1990).

[5] D. K. Nayak, K. Kamjoo, J. S. Park, J. C. S. Woo, and K. L. Wang, Appl. Phys. Lett. **57**, 369 (1990).

[6] E.R. Lippincott, A. Van Valkenburg, C.E. Weir, and E.N. Bunting, J. Res. NBS **61**, 61 (1958).

[7] K. Suzuki, Diff. Defect Data **53-54**, 233 (1987).

[8] J. Hirvonen and A. Anttila, Appl. Phys. Lett. **35**, 703 (1979)

[9] J. Raisanen, J. Hirvonen and A. Anttila, Solid-State Electron. **24**, 333 (1981)

[10] G. L. Mcvay and A. R. Ducharme, Phys. Rev. **B9**, 627 (1974)

[11] H. Widmer and G. R. Gunther-Mohr, Helv. Phys. Acta **34**, 635 (1961)

Chapter 3
Wet Oxidation of Epitaxial Ge_xSi_{1-x}

3.1 Introduction & experiment

We have demonstrated in chapter 2 that at low temperatures (T < 700°C), the Si supply at the reaction interface is restricted, and Ge can also be oxidized, resulting in the formation of a GeSi oxide. The oxide formed at low temperatures in a wet ambient shows a uniform composition with the same Ge/Si ratio as that of the virgin GeSi epilayer. No pileup of Ge is observed in that case and the oxidation rate is very large. The consequent low thermal budget of this wet oxidation process of GeSi at low temperature is of practical interest. We thus present in this chapter the kinetics of the oxidation of epitaxial Ge_xSi_{1-x} samples of two different Ge contents at 700°C in a wet ambient.

The GeSi samples for this study were grown epitaxially onto (100)Si substrates by molecular beam epitaxy without intentional doping. One sample is a layer of $Ge_{0.36}Si_{0.64}$ about 470 nm thick, the other a layer of $Ge_{0.28}Si_{0.72}$ about 550 nm thick. Both films are elastically relaxed as determined from x-ray double crystal diffractometry. The large thickness was chosen to ensure that the oxide would never reach the substrate under the conditions of our experiments. The oxidation was done in a tube furnace at 700°C in a wet ambient by bubbling nitrogen gas through 95°C de-ionized water.

3.2 The structure characterization of $Ge_xSi_{1-x}O_2$ on Ge_xSi_{1-x}

Figure 3.1 (a) and (b) show the backscattering spectra of the two Ge_xSi_{1-x} samples before and after they were oxidized at 700°C for 1 h. It is clear that in both cases the oxide includes Ge which is uniformly distributed in depth. Within the resolution of

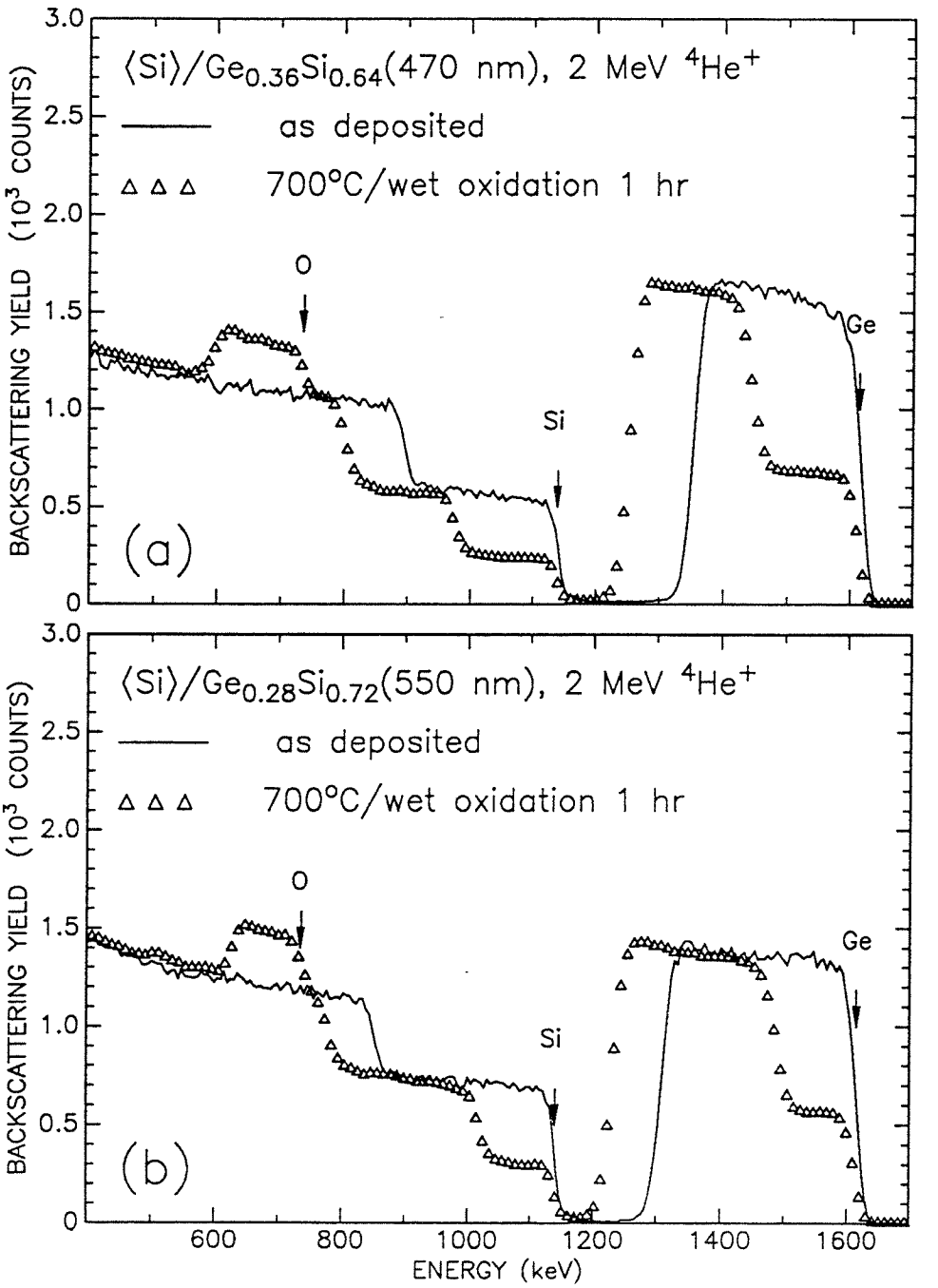

Fig. 3.1 2 MeV $^4He^+$ backscattering spectra of epitaxial layers of (a) $Ge_{0.36}Si_{0.64}$ (b) $Ge_{0.28}Si_{0.72}$ on (100)Si before and after oxidation for 1 h in wet ambient at 700°C, showing a uniform composition of the GeSi oxide. The scattering angle of detected particles is 170°.

backscattering spectrometry, no germanium is lost in both cases. The composition of the oxide derived from the backscattering spectrum of the $Ge_{0.36}Si_{0.64}$ sample is $Ge_{0.35}Si_{0.65}O_2$ with an error of ± 5%. The Ge:Si ratio in the oxide differs insignificantly from that of the original epilayer. A similar result holds for the $Ge_{0.28}Si_{0.72}$ sample. No pileup of Ge or Si is seen behind the oxide and the oxide structure is x-ray amorphous in both cases. These facts prove that the Ge and Si in the GeSi layer are fully oxidized simultaneously. The composition of the oxide is consistent with that of a mixture of SiO_2 and GeO_2. For the same 1 h duration of oxidation the oxide of the $Ge_{0.36}Si_{0.64}$ sample is about 1.4 times thicker than that of the $Ge_{0.28}Si_{0.72}$ sample, as follows from the comparison of the area of the two oxygen signals in the spectra.

Figure 3.2 shows a cross-sectional transmission electron micrograph of the $Ge_{0.36}Si_{0.64}$ sample after oxidation at 700°C for 1 h. Two distinct uniform layers are clearly seen. The thickness of the oxide varies laterally by about 10%; that of the remaining unoxidized GeSi layer is laterally constant. Included in the figure is a transmission electron diffraction pattern obtained with a beam that was probing both the oxidized and the unoxidized GeSi layers. The transmission electron diffraction pattern contains diffuse rings characteristic of a noncrystalline structure which originate from the oxide layer as was established by independent diffraction experiments. The remaining unoxidized $Ge_{0.36}Si_{0.64}$ layer is still single crystalline by electron diffraction. There is no indication of a region with a changed Ge content in the remaining GeSi layer as Ge pileup would produce. The cross-sectional transmission electron micrograph of the sample with only 28 at% Ge for oxidation at 700°C for 1 h shows a similar structure but with a thinner oxide (about 240 nm) than that of the sample with 36 at% Ge (about 340 nm). From these oxide thicknesses and the corresponding backscattering data, we calculate the density of $Ge_{0.36}Si_{0.64}O_2$ and $Ge_{0.28}Si_{0.72}O_2$ to be 2.1×10^{22} formula units/cm^3, with an estimated error of 10%. This density is similar to that of amorphous SiO_2 (2.25×10^{22} molecules/cm^3).

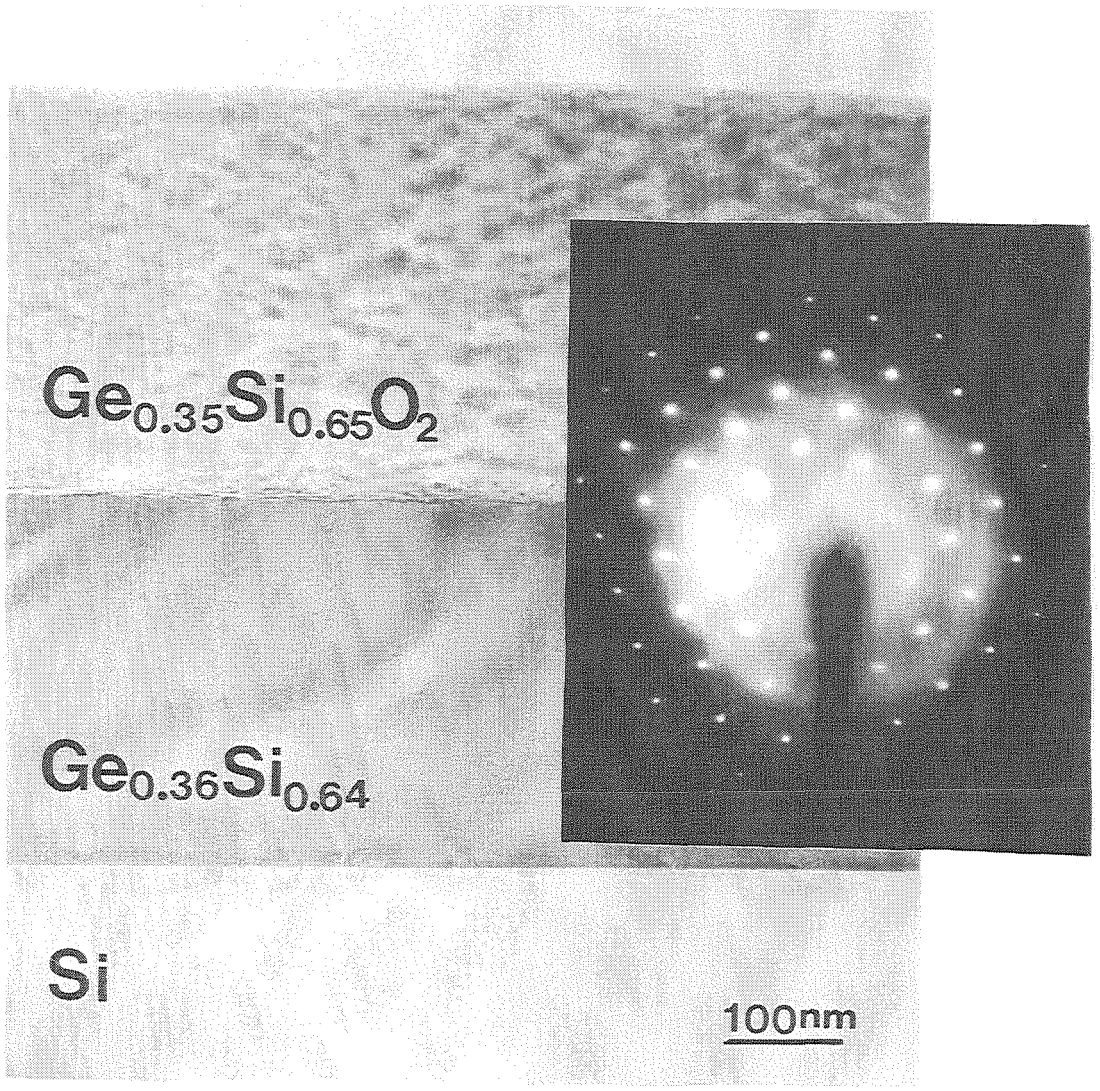

Fig. 3.2 Cross-sectional transmission electron micrograph of GeSi/GeSi oxide layer for $Ge_{0.36}Si_{0.64}$ after oxidation at 700°C for 1 h, showing the smooth GeSi/GeSi oxide layer interface. The diffraction pattern that samples both the oxidized and the unoxidized GeSi layer is also inserted.

The oxides of our two samples appear quite similar in the cross-sectional transmission electron micrographs. This is noteworthy because in the SiO_2-GeO_2 quasi-binary phase diagram [1] at 700°C GeO_2 (which has the tetragonal rutile structure) is soluble in SiO_2 (which has the hexagonal β-quartz structure) up to a limit of 32% only. No such boundary exists between 28 and 36% in the amorphous phase, probably because much of the Ge is tetrahedrally bonded in the same way Si is.

3.3 Kinetics and mechanisms

The square of the oxide thickness, calculated from backscattering spectra and the known density of the oxides, versus oxidation duration at 700°C is shown in Fig. 3.3 for the $Ge_{0.36}Si_{0.64}$ sample and $Ge_{0.28}Si_{0.72}$ sample. All oxidized samples have spectra similar to those of Fig. 3.1 reflecting a uniform oxide composition, but with different thicknesses. The oxidation of both samples can be expressed by a parabolic growth law as can be seen from Fig. 3.3 where the square of the oxide thickness is plotted linearly with the oxidation duration. The parabolic rate constant is 1.1×10^5 nm²/h for the $Ge_{0.36}Si_{0.64}$ sample and 6.4×10^4 nm²/h for the $Ge_{0.28}Si_{0.72}$ sample. The latter one is still larger than that for wet oxidation of pure Si (4×10^4 nm²/h, which is also plotted in the figure) extrapolated from Deal and Grove's paper [2]. However, at this temperature, the oxide growth of pure Si in wet ambient actually follows the linear law within this range of oxide thicknesses.

Oxidation consists of two major processes: reaction and diffusion, the slower one of which determines the kinetics of oxidation. Regarding the diffusion process, no direct determination of the moving species during thermal oxidation of Ge or Ge_xSi_{1-x} alloys has been reported in the literature for either wet or dry ambients. Law and Meigs [3] assume that Ge moves in the oxidation of Ge, following the behavior observed in most metals, but experiments by Crisman *et al.* [4] later provided strong evidence to the contrary. For Si, it is well established that the oxidant is the moving species for both wet and dry ambients in

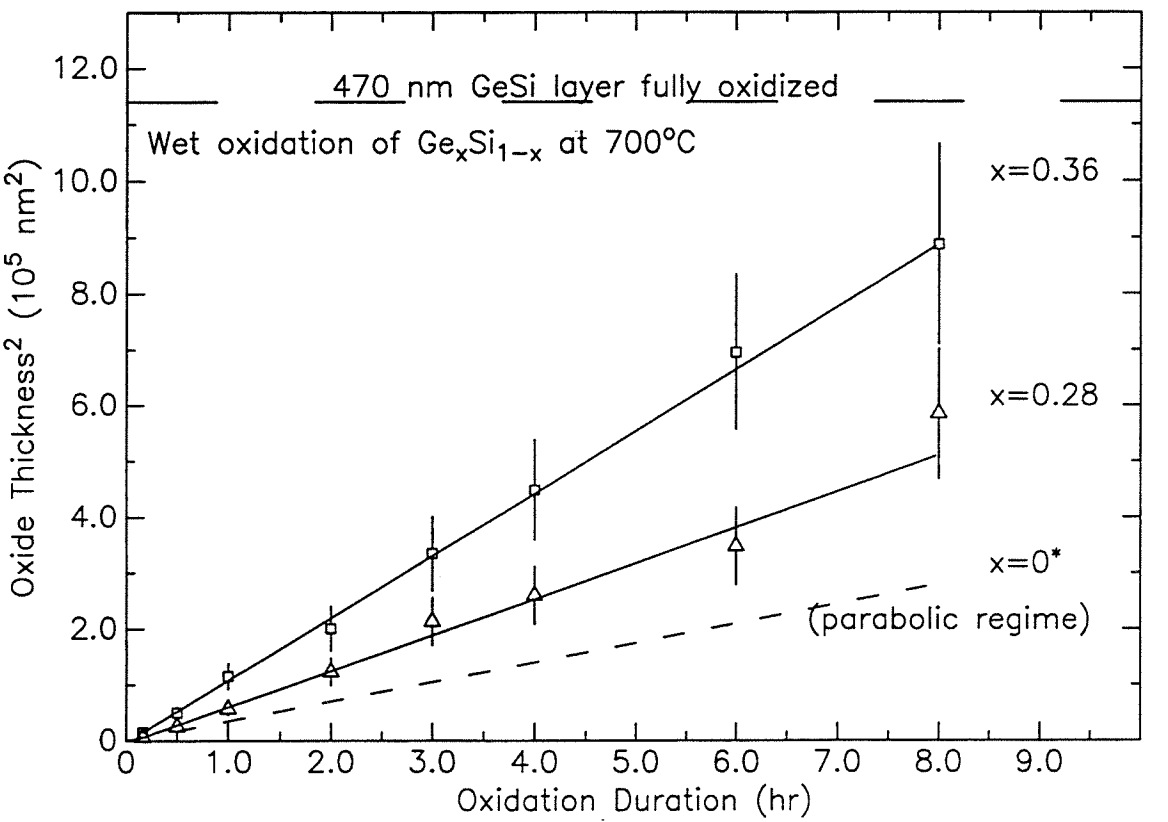

Fig. 3.3 The square of the oxide thickness vs the duration of wet oxidation for the $Ge_{0.36}Si_{0.64}$ and $Ge_{0.28}Si_{0.72}$ samples. The solid straight lines through the origin indicate a pure parabolic growth.

*From Ref. 6, with the parabolic rate constant extrapolated to 700°C.

both the linear and the parabolic regimes [5,6].

In our study, a uniform oxide is formed with a smooth oxide/semiconductor interface. If the oxidant were not the moving species, Ge and Si would have to both diffuse and in such manner that even for different diffusivities in the oxide, their fluxes toward the surface would have to be equal to keep the oxide composition uniform as it is observed to be. In addition, this would have to be true for different compositions of the oxide, as our experiments show. Although we cannot exclude this possibility, we consider it very unlikely. Most probably it is the oxidant that moves, so that the reaction occurs at the interface as in the case for pure Si. A definitive proof of this conclusion has to be carried out with a marker experiment.

A parabolic growth as observed in Fig. 3.3 indicates a diffusion-limited process. We thus compare our results with those of Si and Ge in their parabolic growth regimes. Our Ge_xSi_{1-x} epilayers show a larger parabolic constant than pure Si (Fig. 3.3). We cannot compare directly with Ge because wet oxidation data do not seem to exist in the literature. Dry oxidation of Ge, however, has been reported to be parabolic at 550, 575 and 600°C [7,8]. Extrapolating their data to 700°C, the parabolic rate constant surpasses that measured here for GeSi. Presumably, the wet oxidation of Ge will be much larger yet. The parabolic rate constants measured here thus fall between those of pure Si and Ge. We recall that the sample with 36% Ge oxidizes 1.4 times faster than that with 28% Ge. It thus appears that increasing the GeO_2 content in the oxide also raises the parabolic constant. This can be attributed to an enhanced diffusivity and/or an increased water solubility in $Ge_xSi_{1-x}O_2$.

Our GeSi oxide shows a uniform composition throughout the oxide thickness (Fig. 3.1). That is so even when the whole GeSi layer is completely oxidized (about 1.1 mm oxide). This is different from the previous oxidation studies of GeSi. In cases where $x \geq 0.5$ [9,10], although Ge oxidizes initially, it is excluded from the oxidation afterwards and only SiO_2 forms subsequently. In other cases where $x < 0.5$ [9-16] only SiO_2 forms from

the start and Ge immediately piles up behind the growing oxide. To compare the present results with others published so far, one should notice that all previous studies were performed at 800°C and above while here the temperature is 700°C. At such a low temperature, the diffusive transport of Si and Ge in the epilayer is frozen [17]. This is why the Si:Ge ratio remains constant in space and time in the present case. In this limiting case, the oxidation of Ge_xSi_{1-x} proceeds as it would for an elemental material.

Pure Si at 700°C, however, oxidizes linearly in time within the range of oxide thicknesses observed here. We see no such linear growth regime. The rate constant for the oxidation reaction of Ge_xSi_{1-x} hence must be substantially higher than it is for pure Si. In fact, the reaction rate constant for Ge_xSi_{1-x} must be increased by a factor which exceeds that by which the parabolic rate constant rises because otherwise, the growth law would be linear, as it is in pure Si. Several causes can be advanced for such an enhancement of the reaction rate constant. The stable crystalline phase of GeO_2 is that of rutile which is 6-fold coordinated. Upon oxidation Ge thus changes coordination while Si does not because it forms the 4-fold coordinated quartz. This change in coordination for Ge can enhance the reaction rate. That explanation is unlikely, however, because much of the Ge is 4-fold coordinated in the amorphous $Ge_xSi_{1-x}O_2$. Another possible cause is the increased free charge carrier concentration resulting from the reduced bandgap of Ge_xSi_{1-x}. In the case of silicides, it is well established that the semiconducting silicides have a reduced linear reaction rate constant compared to that of the metallic silicides [18]. Yet another possible cause is the local strain that must exist in the Ge_xSi_{1-x} alloy as a result of the random microscopic heterogeneities. This hypothesis suggests an experiment to compare the linear rate of oxidation for epitaxial films with different elastic strains at constant composition.

References

[1] E.C. Shafer and Rustum Roy, U. S. Army Signal Corps Contract **DA** 36-039, SC 63099 (1956).

[2] B.E. Deal and A. S. Grove, J. Appl. Phys. **36**, 3770(1965).

[3] J.T. Law and P.S. Meigs, J. Electrochem. Soc. **104**, 154(1957).

[4] E.E. Crisman, Y.M. Ercil, J.J. Loferski, and P.J. Stiles, J. Electrochem Soc. **128**, 1845 (1982).

[5] J.R. Ligenza and W.G. Spitzer, J. Phys. Chem. Solids, **14**, 131(1960).

[6] P.J. Jorgensen, J. Chem. Phys., **37**, 784(1962).

[7] J. Sladkova, Czech. J. Phys. **B 18**,801(1968).

[8] J. Sladkova, Czech. J. Phys. **B 27**,943(1977).

[9] J. Eugene, F. K. LeGoues, V. P. Kesan, S. S. lyer, and F. M. d'Heurle, Appl. Phys. Lett. **59**, 78(1991).

[10] H.K. Liou, P. Mei, U. Gennser, and E.S. Yang, Appl. Phys. Lett. **59**, 1200(1991).

[11] O.W. Holland, C. White, and D. Fathy, Appl. Phys. Lett. **51**, 520(1987).

[12] D. Fathy, O.W. Holland, and C. White, Appl. Phys. Lett. **51**, 1337(1987).

[13] F.K. LeGoues, R. Rosenberg, T. Nguyen, F. Himpsel, and B.S. Meyerson, J. Appl. Phys. **65**, 1724(1989).

[14] F.K. LeGoues, R. Rosenberg, and B.S. Meyerson, Appl. Phys Lett. **54**, 644(1989).

[15] D. Nayak, K. Kamjoo, J.C.S. Woo, J.S. Park, and K.L. Wang, Appl. Phys. Lett. **56**, 66 (1990).

[16] D.K. Nayak, K. Kamjoo, J.S. Park, J. C. S. Woo, and K.L. Wang, Appl. Phys. Lett. **57**, 369 (1990).

[17] W.S. Liu, G. Bai, M-A. Nicolet, C. H., V. Arbet and K.L. Wang, Mater. Res. Soc. Symp. Proc. **220**, 259 (1991).

[18] F.M. d'Heurle, R.D. Frampton, E.A. Irene, Hao Jiang and C.S. Petersson, Appl. Phys. Lett. **47**, 1170(1985).

Chapter 4
Wet Oxidation of Polycrystalline Ge_xSi_{1-x} and the comparison to epitaxial Ge_xSi_{1-x}

4.1 Introduction

As we can see from the previous chapters and other people's studies [1-10], the thermal oxidation behavior of epitaxial Ge_xSi_{1-x} depends on temperature, ambient (dry or wet), pressure, and Ge content. A pure SiO_2 layer grows with Ge piling up behind it for epitaxial samples of low Ge content ($x \leq 0.25$) at high temperature ($T \geq 800°C$) for wet or dry oxidations [1-4]. A uniform $Ge_xSi_{1-x}O_2$ layer is formed at low temperature ($T \leq 700°C$) using high pressure dry oxidation [5] or wet oxidation [6,7]. Ge_xSi_{1-x} substrates with Ge content of 50 % or higher exhibit multiple layers of oxides of $Ge_xSi_{1-x}O_2$ and SiO_2 at high oxidation temperature ($T \geq 880°C$) [4,8]. In this chapter, we extend the study to the wet oxidation of *polycrystalline* Ge_xSi_{1-x} alloys of different compositions ($0.10 \leq x \leq 0.47$) at 550 to 900°C and compare them with those obtained for epitaxially grown $Ge_{0.2}Si_{0.8}$ and those in Chapter 3. One other study of wet oxidation at 700°C exists so far for polycrystalline Ge_xSi_{1-x} ($0.05 \leq x \leq 0.15$) [11].

4.2 Experiment

300 nm-thick polycrystalline GeSi films were prepared by the intermixing of Ge/Si bilayers. (100) Si wafers with a 600 nm thick thermally grown SiO_2 layer served as substrates. Germanium and silicon films, whose thicknesses resulted in an overall germanium content of 10, 20, 28, and 47 atomic percent, were deposited sequentially in an electron beam evaporator of a base pressure of 7×10^{-9} torr. The silicon and germanium

charges in the electron beam evaporator had 99.9999 % purity. A 110 nm-thick capping layer, added to prevent the loss of Ge during the subsequent high-temperature treatment, was formed by oxidizing a part of the top silicon layer in a wet ambient for 20 min at 900°C. The remaining Ge/Si bilayer was then transformed into a GeSi alloy with uniformly distributed Ge and Si by annealing for 48 hours in flowing N_2 at 930°C. The capping oxide was then stripped off in a diluted aqueous HF solution. The polycrystalline structure of the films was confirmed by glancing angle x-ray diffractometry, and the compositions and thicknesses were determined by backscattering spectrometry. The grain size of the alloy thus formed is established at ≥ 100 nm from the (111) x-ray diffraction measurements [12] and is not expected to change upon the subsequent thermal oxidation carried out at lesser temperatures. For comparison, a 240 nm-thick epitaxial $Ge_{0.2}Si_{0.8}$ layer grown onto a (100) Si substrate by molecular beam epitaxy was oxidized as well. X-ray double crystal diffractometry shows that the film is pseudomorphic.

Oxidations were done in a tube furnace at various temperatures in a wet ambient obtained by bubbling N_2 gas through 95°C deionized water.

4.3 Three oxidation behaviors

Figures 4.1 (a) to (d) show the backscattering spectra of both polycrystalline and pseudomorphic $Ge_{0.2}Si_{0.8}$ samples oxidized at 600, 700, 750, and 900°C, respectively. The spectrum of the as-formed unoxidized polycrystalline sample is shown also in Fig. 4.1 (a). That spectrum indicates that the interface of the $Ge_{0.2}Si_{0.8}$ alloy layer with the substrate oxide is sharp and that the composition of Ge and Si is uniform. The spectra of Fig. 4.1 (a) show that the thickness and composition of the oxides formed at 600°C on both the polycrystalline and the pseudomorphic films are the same. The composition of these oxides is $Ge_{0.2}Si_{0.8}O_2$, i.e., the Ge:Si ratio (= 0.25) in the oxide is the same as that in the

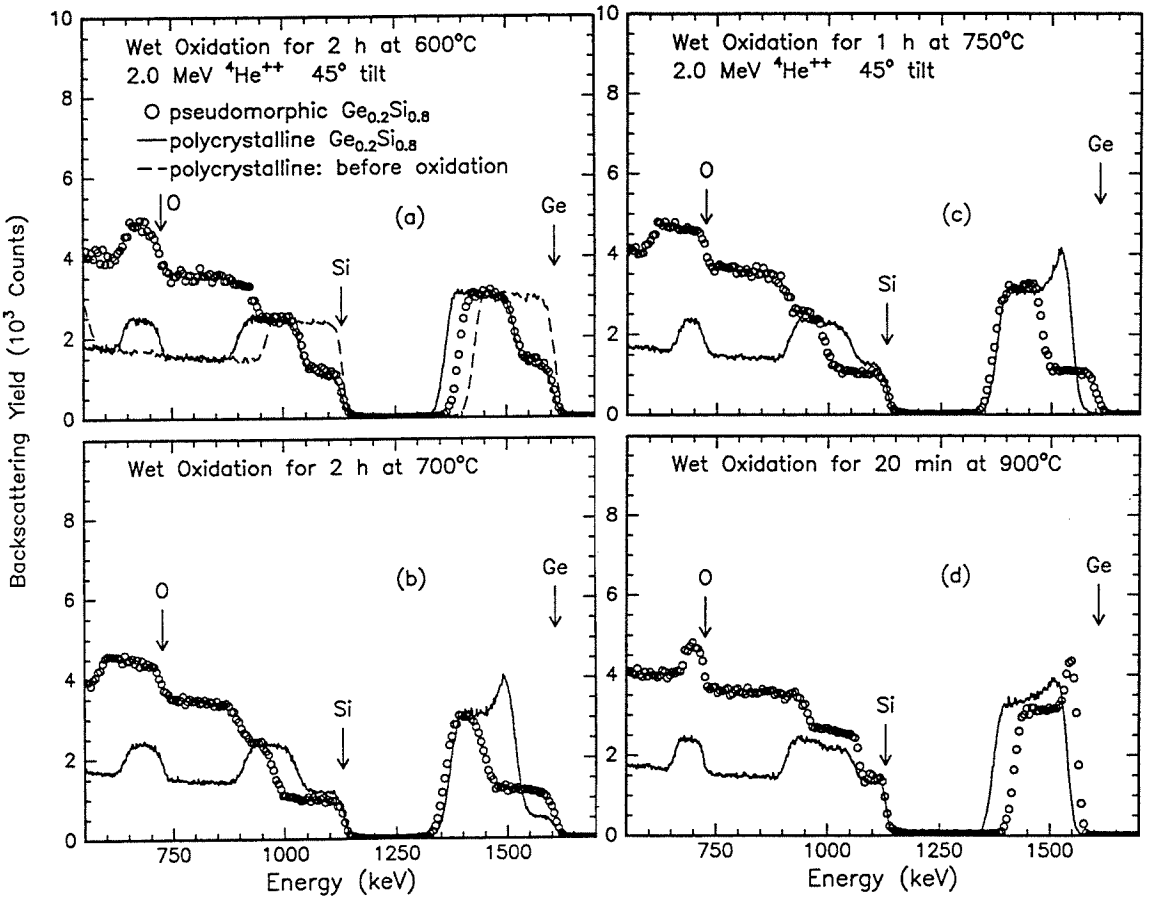

Fig. 4.1 2 MeV $^4He^{++}$ backscattering spectra of pseudomorphic and polycrystalline $Ge_{0.2}Si_{0.8}$ samples oxidized in wet ambient (a) for 2 hours at 600°C, (b) for 2 hours at 700°C, (c) for 1 hour at 750°C and (d) for 20 minutes at 900°C. The scattering angle of detected particles is 170°; the beam enters at 45° to the sample surface.

alloy within accuracy of backscattering spectrometry. This same outcome is also observed upon oxidation at 650°C. No pileup of Ge or Si is observed behind the oxide.

At 700°C after two hours (Fig. 4.1 (b)), the Ge content in the oxide formed on the polycrystalline layer begins to decrease and Ge piles up behind the oxide. The Ge:Si ratio in the oxide decreases to 14:86 (= 0.16) and the peak concentration of Ge that piles up behind the oxide increases to a ratio of about 0.67. However, the pseudomorphic sample still shows the same oxidation behavior as at 600°C ; $Ge_{0.2}Si_{0.8}O_2$ forms and no Ge piles up. The oxide on the pseudomorphic sample is thicker than that on the polycrystalline sample as the unequal widths of the oxygen peaks reveal.

At 750°C after one hour (Fig. 4.1 (c)), the Ge is almost totally rejected from the oxide of the polycrystalline sample. At this temperature, the pseudomorphic sample starts to show a decrease in the Ge content of the oxide also and the pile-up of Ge behind the oxide begins. The oxide composition is about $Ge_{0.14}Si_{0.86}O_2$. The thickness of the oxide on the pseudomorphic sample is again larger than on the polycrystalline one.

At 900°C after 20 min (Fig. 4.1 (d)), an essentially pure SiO_2 is formed and Ge piles up behind it for both polycrystalline and pseudomorphic samples. The thickness of oxide grown on pseudomorphic layer is now thinner than that on the polycrystalline layer. The spectra also show that the Ge accumulates in a narrower layer and to a higher concentration in the pseudomorphic sample than in the polycrystalline one.

This experiment reveals three distinct types of oxidation behavior. In one case, seen at 900°C, a SiO_2 layer forms with Ge piling up behind it. We shall call this behavior type A for convenience. In another case, seen at 600°C, a $Ge_xSi_{1-x}O_2$ forms whose Ge content is same as that of Ge_xSi_{1-x} alloy. Germanium and silicon are distributed uniformly within the oxide. There is no pile-up of Ge. We shall call this the type C case. Between these two limiting cases, there is a transition region where a $Ge_ySi_{1-y}O_2$ oxide forms that has a Ge content that is lower than the bulk Ge_xSi_{1-x} alloy (i.e., $y < x$), and where some Ge piles up behind the oxide. This intermediate case will be called type B.

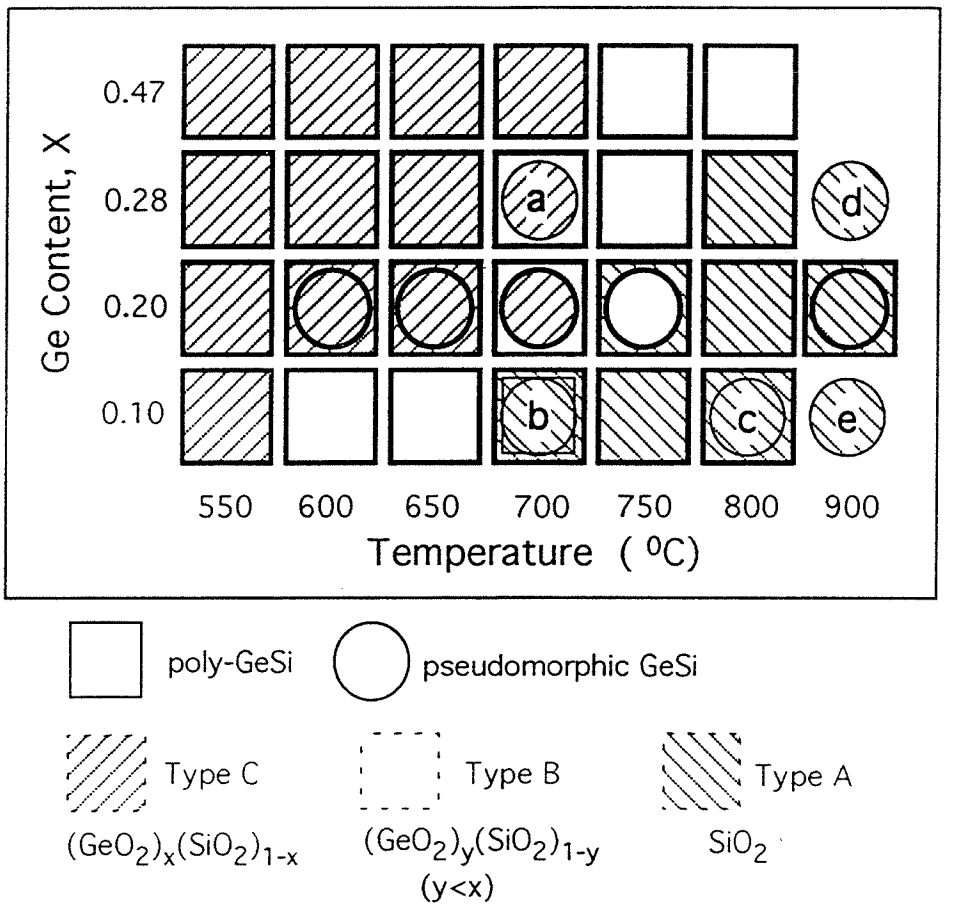

Fig. 4.2 Oxide types obtained upon wet thermal oxidation of polycrystalline and pseudomorphic Ge_xSi_{1-x} alloys in terms of the germanium content, x, and the oxidation temperature. Type A stands for SiO_2 formation, type B for $Ge_y Si_{1-y}O_2$ with $y < x$ and type C for $Ge_xSi_{1-x}O_2$. Squares indicate polycrystalline and circles pseudomorphic samples. Entries bordered by thin lines are taken from the literature,(a: from ref. 7; b: from ref. 11; c: x = 0.116 from ref. 5 ; d: x = 0.25 from ref. 4; e: x = 0.08, T = 960°C from ref. 3).

This change of behavior from type C to type A as the oxidation temperature rises is observed also for the other three polycrystalline Ge_xSi_{1-x} alloy compositions x = 0.10, 0.28, and 0.47 studied here, but the transition occurs at different temperatures. Figure 4.2 summarizes the result in terms of Ge content and oxidation temperature. It can be seen that as the Ge content in the poly-GeSi alloy decreases from 47 to 10 percent at a fixed oxidation temperature of 700°C, for example, the oxide changes from type C to type B and to type A. Conversely as the oxidation temperature increases from 550 to 800°C for a fixed Ge content in the alloy, the oxide changes from type C to type B and to type A. The transition temperature rises with the Ge content from about 600°C for 10 % to about 750°C for 47 %. One interesting observation is that for the pseudomorphic $Ge_{0.2}Si_{0.8}$ represented by circles in the figure, the transition temperature is higher than that of the polycrystalline $Ge_{0.2}Si_{0.8}$ (see also Fig. 4.1 and Fig. 4.2). This is true also for $Ge_{0.28}Si_{0.72}$ as discussed in the following section.

4.4 Kinetics for type C oxidation

Simple kinetics may be reasonably expected only within the range of type A and C oxidation. We thus selected first the temperature of 550°C to probe the time dependence of the oxide growth, because at this temperature the oxide is of type C for all alloys, regardless of Ge content. In Fig. 4.3 the square of the oxide thickness is plotted versus the oxidation duration for our four alloy compositions at 550°C [7]. The oxide thickness were derived from backscattering spectra assuming Bragg's rule for the stopping cross section of the three elements [13,14] and a fixed number density of 2.1×10^{22} formula units/cm^3. A Deal and Grove plot of oxide thickness vs (time/thickness) [15] was also constructed to determine the linear and parabolic rate constants for these oxidations, with the conclusion that the linear rate constant is zero for all four compositions within the experimental errors. The parabolic rate constants in units of 10^3 nm^2/h are 2.4, 2.7, 3.3

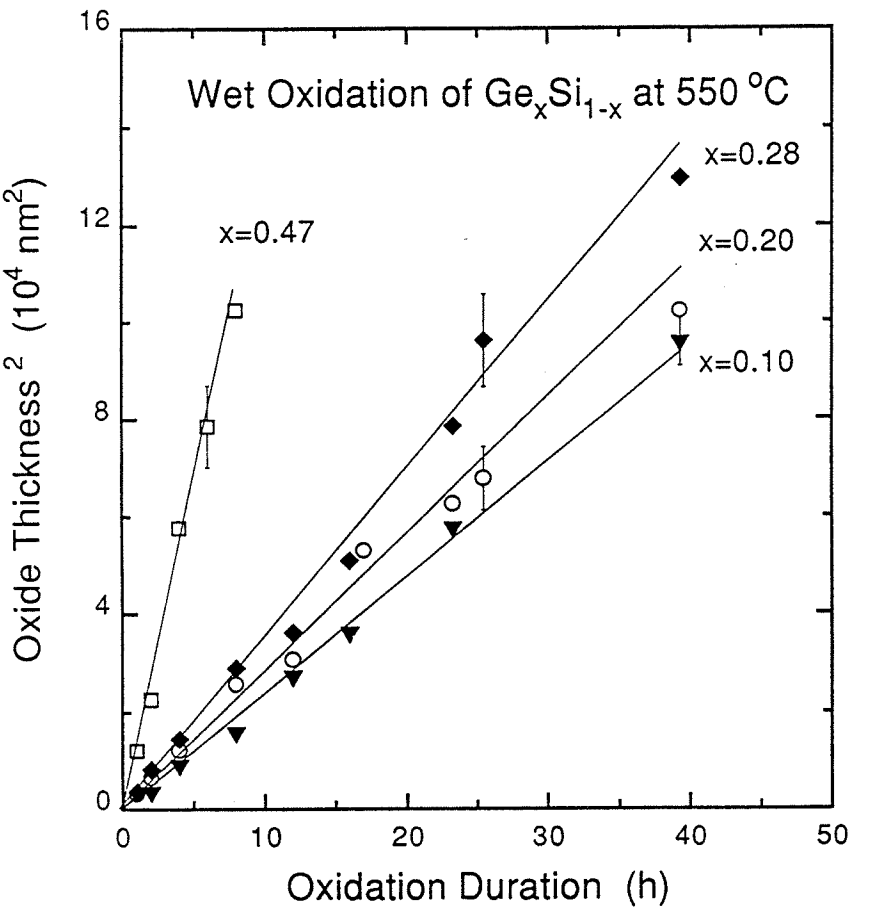

Fig. 4.3 The square of the oxide thickness formed vs the duration of wet oxidation of polycrystalline Ge_xSi_{1-x} at 550°C with a Ge contents of x = 0.10, 0.20, 0.28 and 0.47. The straight lines from the origin indicate a pure parabolic growth. The error bars give typical values of the experimental uncertainties.

and 13.8 for x = 0.10, 0.20, 0.28, and 0.47, respectively. The rate of oxide growth accelerates with the Ge content. This faster growth rate for a larger Ge content is also observed at 600 and 650°C as long as all of the oxides are of type C.

We next measured the temperature dependence of this oxidation process to determine the activation energy of the parabolic rate constant. [We define the parabolic rate constant, B, as the proportionality factor relating the oxidation duration, t, to the square of the oxide thickness, $(\Delta x)^2$.] The temperature range available for this measurement is necessarily limited (see Fig. 4.2). We selected the alloy of composition x = 0.47 to maximize the accessible temperature range and repeated the measurements of $(\Delta x)^2$ vs t for 600, 650, 675, and 700°C. The result is shown in Fig. 4.4 and yields an activation energy, E_A, for the wet oxidation of polycrystalline $Ge_{0.47}Si_{0.53}$ of E_A = 1.1 eV with an estimated error of ±0.2 eV. Additional measurement, not as thorough and complete as for x = 0.47, were also made for polycrystalline alloys with x = 0.20 and 0.28 and for pseudomorphic $Ge_{0.2}Si_{0.8}$. The experimental uncertainties are correspondingly larger. The results are plotted in Fig. 4.4 as well. They indicate that over the parameter range covered here the activation energy of the parabolic rate constant has no discernible dependence on the Ge content and on the crystallinity. For comparison, the parabolic rate constant of $(1.6 \times 10^{10}$ nm^2/h) exp[(−1.17 eV)/kT] for pure Si extrapolated from the paper of R. R. Razouk *et al.* is plotted also [16].

4.5 Discussion

A. Kinetics

Oxidation of GeSi alloys consists of diffusion and reaction. The square root dependence of the oxide thickness on the oxidation duration seen in Fig. 4.3 is characteristic of a process where diffusion across the growing layer limits the rate. We thus conclude that the kinetics of oxidation of polycrystalline Ge_xSi_{1-x} alloys in type C

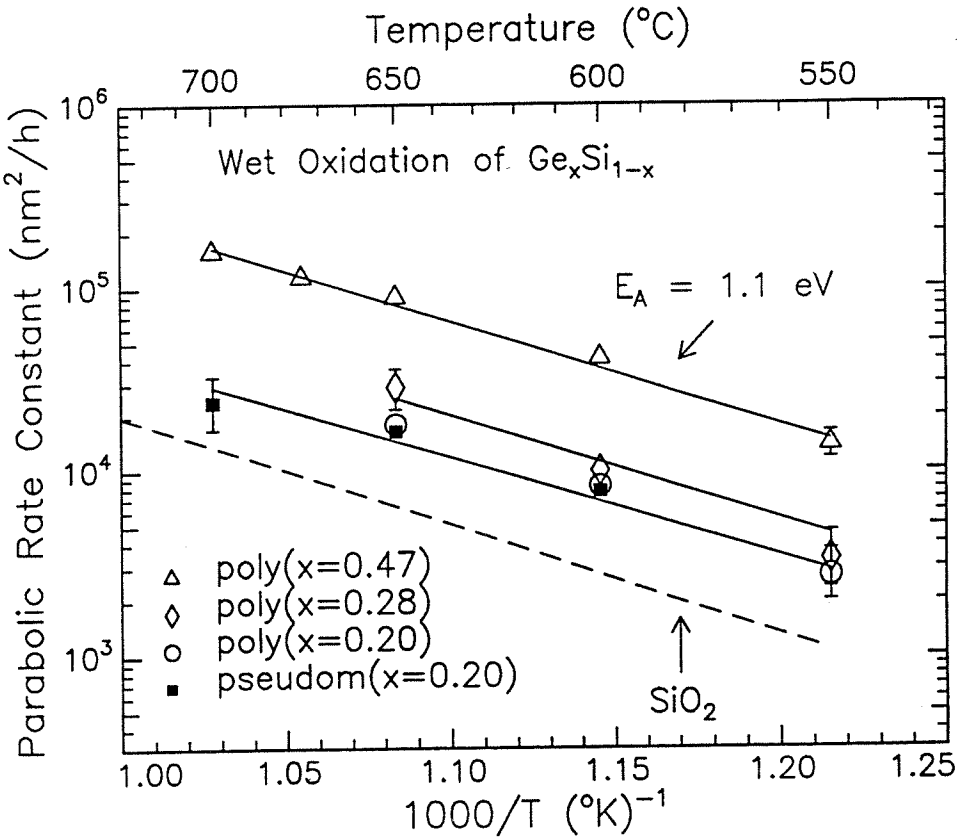

Fig. 4.4 The effect of temperature on the parabolic rate constant for polycrystalline Ge_xSi_{1-x} (x = 0.20, 0.28, and 0.47) and pseudomorphic $Ge_{0.2}Si_{0.8}$. The dashed line represents the parabolic rate constant of pure Si oxidized in steam extrapolated from ref. 14.

oxidation is controlled by transport across the GeSi oxide. No direct observation of the moving species exists for this thermal oxidation reaction, but it is almost certainly the oxidant that moves. If that were not so, Ge and Si would have to both diffuse across the oxide in such a way that their fluxes toward the surface would be equal to keep the oxide composition uniform. This would have to be so even for different diffusivities of Ge and Si in the oxide and for different oxide compositions. Such circumstances are most unlikely. For example, in the oxidation of metallic alloys, where the metallic ions are the moving species, the ratio of the components in the oxide will in general differ from the ratio of the alloy [17]. We thus suppose that it is the oxidant that moves.

A square root dependence is also observed for epitaxial $Ge_{0.28}Si_{0.72}$ oxidized in wet ambient at 700°C, and the oxide formed is also type C (see Fig. 4.2) [7]. At 600 and 650°C, the oxides grown on polycrystalline and pseudomorphic $Ge_{0.2}Si_{0.8}$ are the same in thickness and composition (see Fig. 4.1(a) and Fig. 4.4). Within experimental error, the activation energy of the parabolic rate constant B is also the same (Fig. 4.4). The microstructure of, and the strain in, the GeSi alloy thus leave this type C oxidation process unaffected. This fact is consistent with the finding that the oxidation process is controlled by the mass transport in the oxide.

The oxide is amorphous [7] and the parabolic rate constant B is of the form $B \sim D_{eff}\, c^*$, where D_{eff} is the effective diffusivity of the diffusant in the oxide and c^* the solid solubility of the oxidant in the oxide [15]. We thus infer from Fig. 4.4 specifically that the product of diffusivity and solid solubility of the oxidant is a function of the alloy composition x. But Fig. 4.4 further shows that the activation energy of the parabolic rate constant is not a function of x in the composition range we consider. As in Si [15], the solubility of H_2O in $Ge_xSi_{1-x}O_2$ is probably only a weak function of temperature. The temperature dependence of the parabolic rate constant thus probably reflects just that of D_{eff}. The mechanism of oxidant transport therefore does not change noticeably with x

either. We can again express D_{eff} in the form $D_{eff} = D_0 \exp(\frac{-E_A}{kT})$. The dependence of the parabolic rate constant with x thus originates from the solid solubility and D_0. A rising solid solubility of moisture in $(GeO_2)_x(SiO_2)_{1-x}$ with increasing x is very likely. At 1000°C the solid solubility of H_2O in SiO_2 is about 3×10^{19} molecules/cm^3 [15], but that of H_2O in GeO_2 is much higher than that since GeO_2 is hydroscopic [18]. The rise in B with the composition x is thus surely due in part to an increase in the solubility of the oxidant.

The activation energy of the parabolic rate constant has a common value of 1.1 ± 0.2 eV for all our type C oxides, regardless of the microstructure, strain, and composition of the Ge_xSi_{1-x} alloys from which they were formed (Fig. 4.4). For the oxidation of single crystalline silicon in pyrogenic steam at different pressures, the activation energy of the parabolic rate constant is 1.17 eV at temperatures below 900°C [16]. The value of 1.1 ± 0.2 eV is thus typical of x = 0 as well. It is known that a higher steam pressure raises the solid solubility of the oxidant in SiO_2 [15,16] and thus the flux of the oxidant to the interface. In our case, such an increased flux is obtained by increasing the GeO_2 content. The activation energy remains the same in both cases. The existence of GeO_2 in the oxide enhances the flux of the oxidant to the interface and therefore results in a faster growth rate of $Ge_xSi_{1-x}O_2$ than SiO_2.

This simple result for the kinetics of type C oxidation contrasts with that of type A oxidation, when only SiO_2 forms. The previous studies of wet oxidation of epitaxial Ge_xSi_{1-x} ($x \leq 0.50$) at high temperature find that the oxidation rate decreases after an initial fast growth [3,4]. An observed enhancement of the type A oxidation rate compared to that of silicon has been explained variously as the result of the weak Ge-Si bonding compare to Si-Si bonding [1], of a catalytic effect of Ge [3], or of its ability to suppress the generation of interstitials [2]. Ast *et al.* however observed a square root dependence for type A oxidation in both polycrystalline and epitaxial Ge_xSi_{1-x} samples with x = 0.05,

0.1 and 0.15 oxidized in wet ambient at 700°C [11]. The results in Fig. 4.2 are consistent with those findings.

B. Formation of different oxide types

At low temperature, the motion of Ge and Si in the Ge_xSi_{1-x} alloy is frozen and the oxidant reacts with both Ge and Si as it reaches the interface by diffusion. The Ge:Si ratio thus remains the same in the oxide layer as it is in the alloy. Generally, a type C oxide forms whenever the motion of Ge and Si in the alloy is sufficiently slow compared to the rate of progression of the oxidation front. At low temperature and wet oxidation this is true for both polycrystalline and epitaxial GeSi over the whole composition range of $0.1 \leq x < 0.5$, as seen in Fig. 4.2. The thermodynamic preference for the sole formation of SiO_2 is kinetically suppressed. At the high temperature end, both polycrystalline and pseudomorphic Ge_xSi_{1-x} have the same type A oxide. The free energy of formation of SiO_2 is more negative than that of GeO_2 through the temperature range considered here [6]. For example, at 700°C the free energy of formation of SiO_2 is -730 kJ/mol and that of GeO_2 is -360 kJ/mol [19]. Because of that the oxidation of silicon is thermodynamically preferred over that of Ge as long as Si is available. The activation energy of the diffusivities of Si and Ge in GeSi alloys ranges between 3 and 5 eV [6] and is much larger than the 1.1 eV of the parabolic rate constant of type C oxidation measured in this work. As the temperature rises, the diffusivities of Si and Ge in the alloy thus increase much faster than that of the oxidant in the oxide. The movement of Si and Ge eventually becomes significant and outpaces that of the oxidation front. Only SiO_2 is then formed; Ge is excluded from the oxide and piles up behind it.

C. Transition between type A and C oxides

The transition from C to B behavior sets in when in the alloy the diffusive fluxes of Si and/or Ge become commensurate with that of the oxidant in the oxide. For the same

composition x, this occurs at lower temperatures in polycrystalline than in epitaxial samples (see cases x = 0.20 and 0.28 in Fig. 4.2). Since the oxidant flux is independent of the alloy structure, this observation is explained by diffusivities that are enhanced in the polycrystalline alloy over those in the epitaxial alloy. We are not aware of any measurement of the dominant diffusing species in Ge_xSi_{1-x} alloys, but the literature data on the diffusion of Ge in Ge_xSi_{1-x} at 850°C to 1200°C suggests that Ge diffuses faster than Si in the composition and temperature range considered here [6]. In what follows, we shall formulate the discussion in terms of a movement of Ge in the alloy even though the opposite choice is not ruled out. At 900°C both polycrystalline and pseudomorphic samples form only SiO_2 (type A), and there too the oxide thickness on the polycrystalline substrate is larger. This then suggests that the enhancement of the Ge diffusion by the grain boundaries in the polycrystalline Ge_xSi_{1-x} alloy extends over our whole temperature range.

The signals of Ge and Si in the spectra of Fig. 4.1 (b), (c) and (d) that come from behind the oxide can, in principle, provide quantitative information on the effective Ge diffusivity in the alloy. A proper analysis is difficult though, because the problem is nonlinear, on the one hand, due to the changing alloy concentration with depth and the very strong variation of the Ge diffusivity with the composition of the alloy [6], and, on the other hand, due to the concentration-dependent progression of the oxidation front. What is easy to see is that the Ge diffusivity increases in the alloy quite rapidly as the temperature increases. In Fig. 4.1 (c) and (d), for instances, the Ge distribution in the unoxidized polycrystalline alloy is quite nonuniform after 1 h at 750°C , but is near-homogeneous after only 20 min at 900°C.

When type B oxidation sets in at rising temperature, two effects appear: (i) Ge accumulates behind the oxidation front, and (ii) the rate of the oxidation slows down, as is clearly visible from the difference in the widths of the oxygen peaks in Fig. 4.1 (b). One reason the rate decreases is that the number of Si atoms available for the reaction at the

oxidation front decreases, because the atom concentration in the alloy is very nearly independent of Ge content. This process is equivalent to reducing the apparent Si flux into the reaction front, and hence introduces a new limitation to the reaction rate. There is no equivalence to this process in the case of pure Si oxidation because there the density of Si atoms present at the reaction front is always the same. Another reason why the oxidation rate slows down is the decrease of GeO_2 that is incorporated in the oxide. This decrease reduces the oxidant flux, and adds a second retarding effect. A third effect, which acts in the opposite sense, is due to the rise of the Ge content in the alloy near the oxide interface because Ge is known to accelerate the reaction kinetics [1-3]. This accelerating influence can only exert itself fully when the kinetics becomes purely reaction-controlled. The results of Fig. 4.1 indicate that over the range of parameters discussed here, this accelerating effect remains minor.

At a fixed temperature, the oxide type changes from type A to type C as the content of Ge increases. The diffusivities of Ge and Si in GeSi alloy increase as Ge content increases [6]. This enhanced diffusion alone would predict that the appearance of the type A oxide should be facilitated as the Ge content increases, which is obviously opposite to the observation. Another stronger factor therefore determines this transition. This factor is presumably the rapidly accelerating oxidation rate due to the GeO_2-enhanced oxidant flux in the oxide, as discussed above. An attempt to substantiate this model quantitatively does raise problems, however. Firstly, only the diffusivity of Ge in single crystalline Ge_xSi_{1-x} is known and only at temperatures of 800°C and above for heat treatment in vacuum [6]. An extrapolation to 700°C indicates that the diffusivity increases exponentially with the Ge content. This is a much faster increase than that of the parabolic rate constant (see Fig. 4.4 and section 4.4). Whether this discrepancy is caused by the lack of applicable diffusivity data or by inadequacies of the model requires further study.

As the temperature rises, the diffusivity of Ge in the alloy increases sharply (activation energy = 3–5 eV), that of the oxidant in the oxide less so, and the solid solubility of H_2O

relatively little, so that the transition now occurs at a higher Ge. The result is an ascending band of type B oxide as seen in Fig. 4.2.

D. Related systems

Similar reaction behaviors can also exist in systems where the gaseous oxygen of the present study is replaced by a solid element. An example is Pt on epitaxial [20] and polycrystalline [21] Ge_xSi_{1-x} alloys. At 300°C, $Pt_2(Ge_xSi_{1-x})$ forms first by Pt diffusion into the alloy and at 400°C, $Pt(Ge_xSi_{1-x})$ starts to grow after the Pt has been consumed. At 500°C, in the case of an epitaxial alloy (x = 0.2), the Ge in the $Pt(Ge_xSi_{1-x})$ is expelled completely to the interface and only a PtSi layer is formed on the surface and a Ge rich epitaxial $Ge_{0.9}Si_{0.1}$ behind it [20]. However, the dependence of the formed phase on the combination of temperature, composition, and crystallinity of the alloy has not been investigated in this system. Another example where the role of the moving metal and the initially stationary semiconductor are reversed is that of Si reacting with a Ti_xW_{1-x} alloy [22-24]. Si is now the dominant diffusant [25]. Annealing of a Ti_xW_{1-x} alloy with $x > 0.1$ below 550°C leads to the formation of $Ti_xW_{1-x}Si_2$ which consists of a hexagonal solid solution of $TiSi_2$ and WSi_2. Above 550°C , the reacted layer contains an additional phase of tetragonal WSi_2; the temperature at which this occurs depends on x [24]. Thus this system has two distinct regimes for the reacted layer; a single hexagonal structure, and a mixed hexagonal and tetragonal structure. Above 1100°C, $TiSi_2$ is preferentially formed at the silicon-silicide interface and at the surface. This latter example demonstrates that the oxidation of Ge_xSi_{1-x} is a relatively simple case because all the reaction products are of a single (amorphous) phase. The only other such case will occur with a single crystalline phase. When the reaction products consist of multiple phases, the kinetics of the reactions will necessarily be quite complex and difficult to elucidate.

4.6. Conclusion

Figure 4.2 shows that at 500°C both Si and Ge are fully oxidized. This is so because Si and Ge in the alloy are virtually immobile compared to the rate at which the oxidant migrates through the oxide. The reaction at the interface is always very fast, so that in this regime the rate of oxidation is limited by the transport of the oxidant through the oxide. This scenario is true for all compositions ($0.1 \leq x < 0.5$) we investigated here. What does change with the Ge content of the Ge_xSi_{1-x} alloy is the rate at which the reaction proceeds at a given temperature (Fig. 4.2). The rate accelerates with the Ge content. The diffusion mechanism as reflected by the activation energy is the same in all cases ($E_A = 1.1 \pm 0.2$ eV) and also applies to pure SiO_2 At these low temperatures, however, the wet oxidation of Si is reaction-limited; it isn't in the alloy because Ge enhances the reaction rate. How germanium accomplishes this is currently being debated in the literature. Helpful new insight could be gained by investigating the concentration range of $0 < x < 0.1$ in detail.

As the temperature increases, the diffusivities in the alloy rise much more rapidly than the diffusivity of the oxidant. As a result, the preferential oxidation of Si demanded thermodynamically can take over and Ge begins to be excluded from oxidation and accumulates behind the oxidation front. This has the effect of reducing the rate of oxidation, thus giving the rapid diffusion in the alloy a further advantage. This transition takes place at higher temperatures for epitaxial than for polycrystalline Ge_xSi_{1-x} alloys because of the absence of grain boundary diffusion in the monocrystalline structure.

The oxidation of Ge_xSi_{1-x} alloys has analogies where all three elements are solids. Compared to these, the case of Ge_xSi_{1-x} is particularly simple because of the amorphousness of the reaction products.

References

[1] O.W. Holland, C. White, and D. Fathy, Appl. Phys. Lett. **51**, 520 (1987).

[2] F.K. LeGoues, R. Rosenberg, and B.S. Meyerson, Appl. Phys. Lett. **54**, 644 (1989).

[3] D.K. Nayak, K.Kamjoo, J.S. Park, J.C.S. Woo, and K.L. Wang, Appl. Phys. Lett. **57**, 369 (1990).

[4] J. Eugene, F.K. LeGoues, V.P. Kesan, S.S. Iyer, and F.M. d'Heurle, Appl. Phys Lett. **59**, 78 (1991).

[5] D.C. Paine, C.Caragianis, and A.F. Schwartzman, J. Appl. Phys. **70**, 5076 (1991).

[6] W.S. Liu, G. Bai, M-A. Nicolet, C.H. Chern, V. Arbet, and K.L. Wang, Mater. Res. Soc. Symp. Proc. **220**, 259 (1991).

[7] W.S. Liu, E.W. Lee, M-A. Nicolet, V. Arbet-Engels, K.L. Wang, N.M. Abuhadba, and C.R. Aita, J. Appl. Phys. **71**, 4015 (1992).

[8] J.P. Zhang, P.L.F. Hemment, S.M. Newstead, A.R. Powell, T.E. Whall, and E.H.C. Parker, Thin Solid Films **222**, 141 (1992).

[9] D.C. Paine, C. Caragianis, T.Y. Kim, Y. Shigesato, and T. Ishahara, Appl. Phys. Lett. **62**, 2842 (1993).

[10] W.S. Liu, J.S. Chen, M-A. Nicolet, V. Arbet-Engels, and K.L. Wang, Appl. Phys. Lett. **62**, 3321 (1993).

[11] D.G. Ast and W.J. Edwards, 1992 Ann. Rep. of SRC Res. vol. III, 187 (1992).

[12] B.D. Cullity, *Elements of X-Ray Diffraction, 2nd ed.* (Addison-Wesley, Reading, 1978), p. 284.

[13] W.K. Chu, J.W. Mayer, and M.-A. Nicolet, *Backscattering Spectrometry* (Academic Press Inc., Orlando, 1978), p. 362.

[14] J.F. Ziegler, W.K. Chu, J. Appl. Phys. **47**, 2239 (1976).

[15] B.E. Deal and A.S. Grove, J. Appl. Phys. **36**, 3773 (1965).

[16] R.R. Razouk, L.N. Lie, and B.E. Deal, J. Electrochem. Soc. **128**, 2214 (1981).

[17] C. Wagner, J. Electrochem. Soc. **99**, 369 (1952).

[18] Pieter Stroeve, *Integrated Circuits: Chemical and Physical Processing* (American Chemical Society, Washington, DC, 1985) p. 179.

[19] *CRC Handbook of Chemistry and Physics*, 70th ed., edited by R.C. Weast, D.R. Lide, M.J. Astle, and W.H. Beyer (CRC, Boca Raton, 1989).

[20] H. Kanaya, Y. Cho, F. Hasegawa, and E. Yamaka, Japan J. Appl. Phys. **29**, L85 (1990).

[21] Q.Z. Hong and J.W. Mayer, J. Appl. Phys. **66**, 611 (1989).

[22] J.M. Harris, S.S. Lau, M-A. Nicolet, and R.S. Nowicki, J. Electrochem. Soc. **123**, 121 (1976).

[23] F. Nava, C. Nobili, G. Ferla, G. Iannuzzi, G. Queirolo, and G. Celotti, J. Appl. Phys. **54**, 2434 (1983).

[24] P. Gas, F.J. Tardy, and F.M. d'Heurle, J. Appl. Phys. **60**, 193 (1986).

[25] M-A. Nicolet and S.S. Lau, in *VLSI Electronics Microstructure Science, Vol. 16. Materials and Process Characterization*, edited by N. G. Einspruch and G. B. Larrabee (Academic Press, New York, 1983), ch. 6.

Chapter 5
Instability of a $Ge_xSi_{1-x}O_2$ film on a Ge_xSi_{1-x} layer

5.1 Introduction

It was initially reported that for the oxidation of GeSi samples of low Ge content ($x < 0.2$) at high temperature ($T > 800°C$), a pure SiO_2 layer grows with Ge piling up behind it [1-6]. This resulting pileup of Ge greatly increases the interface trap density of the oxide [3] and thus should be avoided if the oxide is to be used in a device environment. At low temperatures ($T < 700°C$) (see Chapter 3 and 4) or for high Ge content [7,8], the Si supply at the reaction interface is restricted, and Ge can also be oxidized, resulting in the formation of a GeSi oxide. The oxide formed at low temperature in wet ambient shows a uniform composition with the same Ge/Si ratio as that of the virgin GeSi epilayer. No pileup of Ge is observed in that case and the oxidation rate is very large. The consequent low thermal budget of this wet oxidation process of GeSi at low temperature is of practical interest.

It has been reported that GeO_2-SiO_2 glasses can, in the proper composition range, exhibit thermal coefficients of expansion that approximate that of the silicon (approximately 40×10^{-7}/°C between 25° and 700°C) [9]. The interfacial stress between these two materials, indeed, is less than 10^9 dyne/cm^2 (almost stress-free) over a wide composition range of GeO_2 [10]. The thermal coefficient of expansion of germanium is about 70×10^{-7}/°C in the same temperature range. The $Ge_xSi_{1-x}/Ge_xSi_{1-x}O_2$ system therefore exhibits much closer thermal coefficients of expansion between the protective insulating layer and the underlying GeSi film than the Ge_xSi_{1-x}/SiO_2 system does. This fact is of interest especially for epitaxial GeSi films whose metastability might be affected by this interfacial stress. However the properties of the oxide, and especially its stability need

to be examined since the resulting interface between $GeSiO_2$ and GeSi is thermodynamically unstable and germanium oxide is also known to be unstable at high temperature [11] or in moisture [12]. We present here the results of experiments that investigate the stability of $Ge_xSi_{1-x}O_2$ on GeSi upon annealing, aging, and exposure to moisture.

5.2 Experiment

The GeSi samples for this study were grown epitaxially onto a (100)Si substrate by molecular beam epitaxy without intentional doping. One sample is a layer of $Ge_{0.36}Si_{0.64}$ about 470 nm thick, the other a layer of $Ge_{0.28}Si_{0.72}$ about 550 nm thick. Both films are elastically relaxed as determined from x-ray double crystal diffractometry. Samples from the wafers were oxidized in a tube furnace at 700°C for 1 h in wet ambient obtained by bubbling nitrogen gas through 95°C deionized water. For the annealing test, the oxidized samples were vacuum-annealed at 900°C for 3 h. Other oxidized samples were stored in air at room temperature for about 5 months. Additional oxidized samples were placed in deionized water at room temperature for several hours up to several days. The water sometimes was heated up to the boiling point to accelerate the test. The oxide film of all these samples was investigated by transmission electron microscopy and backscattering spectrometry before and after the tests.

5.3 Thermal instability

The backscattering spectra for the oxide of $Ge_{0.36}Si_{0.64}$ before and after vacuum annealing test are indistinguishable. The oxide remains uniform. No Ge is lost during annealing. Similar results are also found in the case of the oxide of $Ge_{0.28}Si_{0.72}$. This is noteworthy because germanium dioxide tends to volatize at elevated temperatures in the

presence of pure germanium due to the following reaction: $GeO_2 + Ge = 2\ GeO_{(g)}$ [11]. The conservation of Ge in the present case could be due to the absence of pure Ge or the action of the oxide as a protective cap.

Figure 5.1 shows cross-sectional transmission electron micrographs of the oxide of $Ge_{0.36}Si_{0.64}$ after 3 weeks and 5 months aging in air at room temperature and after the vacuum annealing test. This analytical technique is much more sensitive to interfacial changes at the nm scale than backscattering spectrometry. Small precipitates emerge in the oxide near the interface and alter the initially sharp interface after 5 months aging and 900°C annealing. The precipitates are located in both cases at about 10 nm from the interface. However, the size of the precipitate after 900°C annealing is generally larger than that after 5 months aging at room temperature. The precipitates are crystalline with a lattice constant similar to that of the underlying GeSi layer, as shown in Fig. 5.2 which is a high-resolution micrograph of the oxide/GeSi region after 5 months aging. Similar futures are also observed in the oxide of $Ge_{0.28}Si_{0.72}$ after the vacuum annealing and aging tests. By the lattice constants, these precipitates could be elemental Ge, elemental Si, GeSi solution, or even tetragonal GeO_2 which can grow epitaxially on the (110) plane of germanium [13]. Thermodynamic arguments given as follows predict that these precipitates should be Ge_xSi_{1-x} solid solution or in the limit, elemental Ge.

The Ge-Si-O ternary phase diagram calculated by Paine *et al.* [14] has tielines connecting SiO_2 with GeO_2 and Ge_xSi_{1-x} at 1000 K. The phase diagram is similar from room temperature to 900°C according to our calculation similar to those of Paine *et al.*. Any compound below the GeO_2-SiO_2 tieline will decompose into SiO_2 plus GeO_2 and Ge, or into SiO_2 and a Ge_ySi_{1-y} solid solution, depending on what the ratio of O/(Ge+Si) is. Cross-sectional transmission electron micrographs show that the interface between the GeSi layer and the Si substrate in our samples is still sharp after 900°C annealing, indicating only insignificant interdiffusion between them. Therefore we can exclude the Si

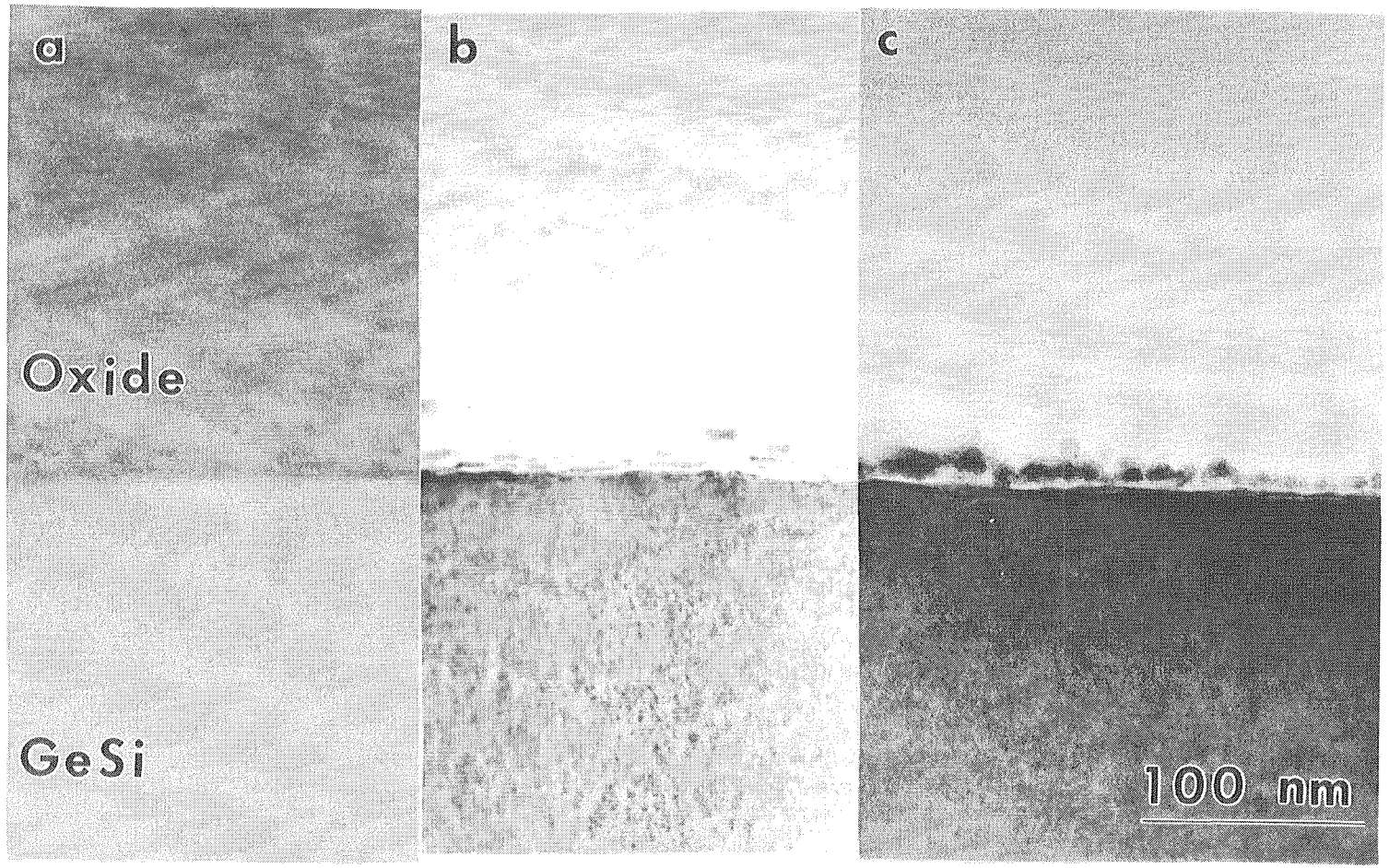

Fig. 5.1 Cross-sectional transmission electron micrograph of the GeSi layer/GeSi oxide interface for (a) 3 weeks aging in the air, (b) 5 months aging in the air and (c) 900°C annealing for 3 h after oxidation.

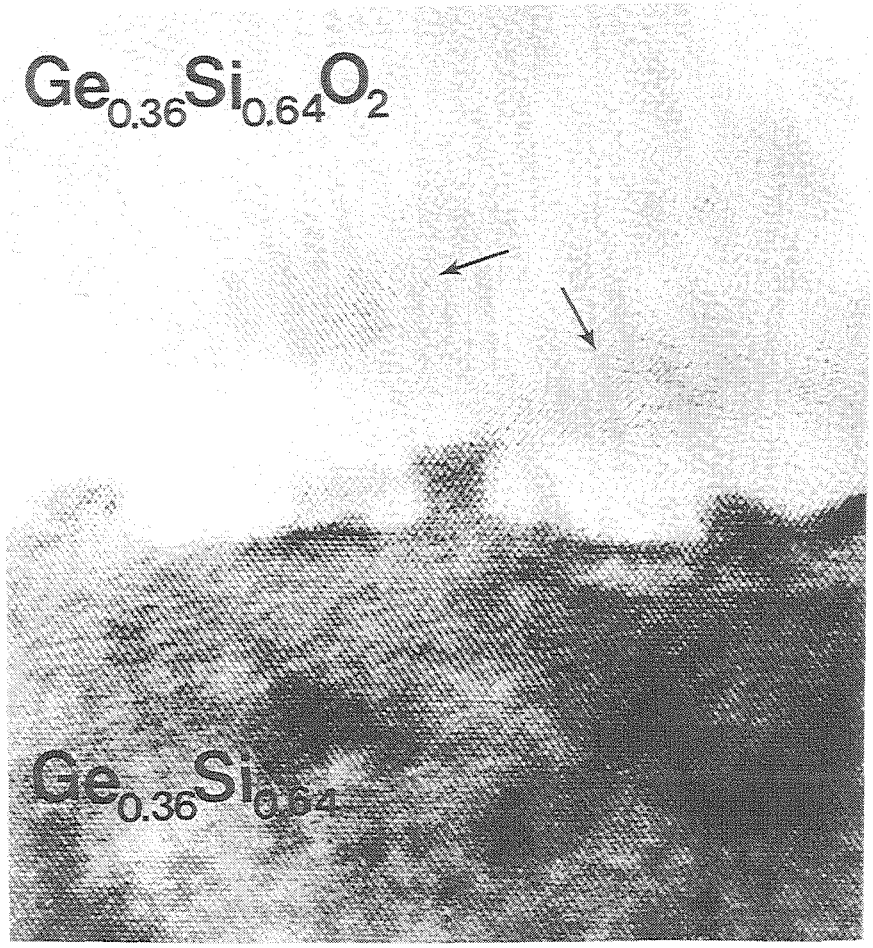

Fig. 5.2 High resolution cross-sectional transmission electron micrograph of a GeSi/$GeSiO_2$ interfacial region after aging for 5 months in air at room temperature. Crystalline precipitates with a lattice constant similar to that of the underlying GeSi layer are observed near the interface as the arrows indicate.

substrate from the system and only consider the equilibrium between the oxide and the remaining GeSi layer. The oxide then becomes unstable with the unoxidized GeSi layer since the ratio of O/(Ge+Si) for this system is less than 2 and will locate this system below the GeO_2-SiO_2 tieline in the Ge-Si-O phase diagram. This instability also exists for GeO_2-SiO_2 glasses with pure Si and is unacceptable from a device point of view.

5.4 Moisture instability

The backscattering spectra of the oxide before and after immersion in water at room temperature for 1 day are shown in Fig. 5.3. After this test, the oxide remains uniform but with a Ge content that decrease from $Ge_{0.36}Si_{0.64}O_2$ to about $Ge_{0.05}Si_{0.95}O_2$, or equivalently, a reduction from 2000 formula units/cm^2 to 1400 formula units/cm^2. This result means that about 90% of the GeO_2 is lost in the water. To see if all GeO_2 could be dissolved in the water, the sample of Fig. 5.3 was placed back in fresh deionized water for a week with water being replaced every day. No significant change was observed by backscattering spectrometry. The whole oxide including SiO_2 is totally lost after 16 h immersion in boiling water. For $Ge_{0.28}Si_{0.72}O_2$, the oxide is conserved after immersion in the water at room temperature for 1 day according to backscattering spectrometry measurements, indicating the solubility of this GeO_2-leaner oxide in room temperature water is negligible. However some amount of GeO_2 is lost after 16 h immersion in boiling water.

Hexagonal GeO_2 is known to dissolve rapidly in water; tetragonal GeO_2, on the other hand, is only very slightly soluble in room-temperature water (< 0.005 g/liter) [12]. According to IR absorption spectrometry, the state of GeO_2 in the present $Ge_{0.36}Si_{0.64}O_2$ and $Ge_{0.28}Si_{0.72}O_2$ films is mostly in the form of tetrahedrally coordinated [GeO_4] germanium (hexagonal form of GeO_2) with a little octahedrally coordinated [GeO_6]

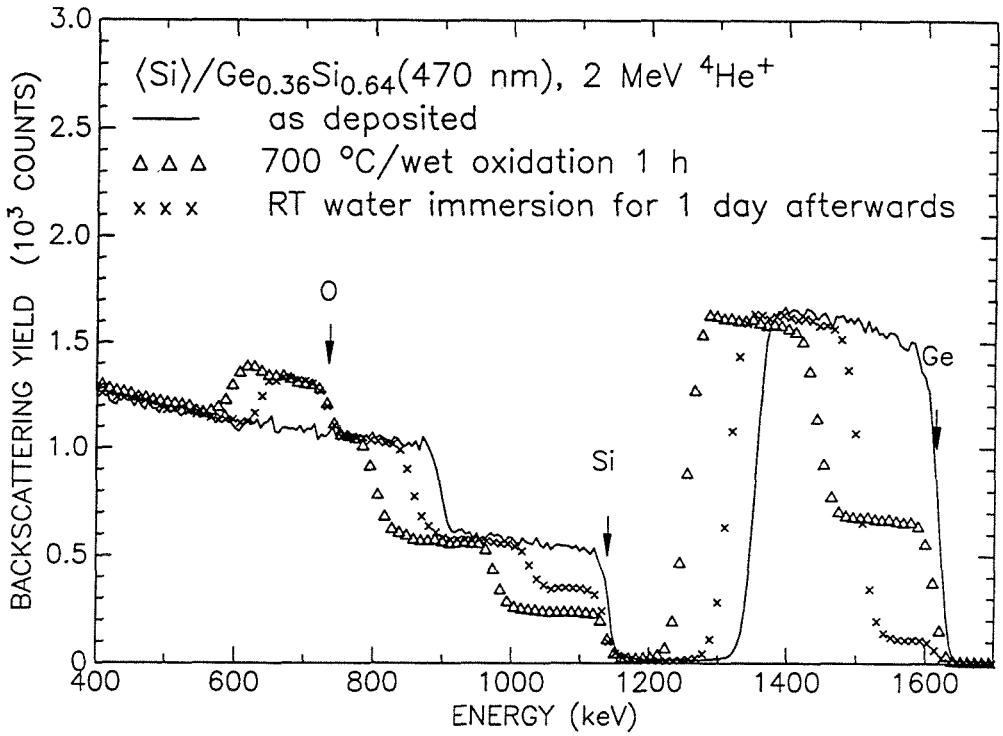

Fig. 5.3 2 MeV $^4He^+$ backscattering spectra of a $Ge_{0.36}Si_{0.64}O_2$ layer before and after immersion in water at room temperature for 1 day (Near-normal radiation beam incidence; the scattering angle of detected particles: 170°).

germanium (tetragonal form of GeO_2). By that observation, most of the GeO_2 should be water soluble in both cases. Most of the GeO_2 in $Ge_{0.36}Si_{0.64}O_2$ is in fact lost upon immersion in water at room temperature; $Ge_{0.28}Si_{0.72}O_2$, however, is completely insoluble. A similar water test has been performed on GeO_2-SiO_2 glasses deposited on Si substrates by low-pressure chemical vapor deposition by Rastani and Reisman [10]. They also find a limit (about 20% GeO_2) below which the glasses are water-insoluble. To what extent the unequal solubility of $Ge_xSi_{1-x}O_2$ films can simply be explained by a tetragonal vs. hexagonal coordination of Ge thus remains an open question.

Compositional and structural inhomogeneities can also affect the solubility. If enough SiO_2 surrounds GeO_2, it can be shielded from attack by water even though it may be tetrahedrally coordinated. The ratio of GeO_2/SiO_2 below which the oxide is completely insoluble in room-temperature water is then decided by the detailed structure of the oxide, which could be affected by the ways the oxide is formed. The effect of hot water could be to accelerate the break-up of this shielding until the remaining oxide is so porous that even the SiO_2 is eroded away.

The interface between $Ge_xSi_{1-x}O_2$ films and Ge_xSi_{1-x} or Si is thermodynamically unstable. This instability leads to the formation of GeSi precipitates by a reduction of GeO_2 near the interface. The phenomenon is detectable a few months after the formation of the interface and storage at room temperature. The instability of an oxide/semiconductor interface as that evidenced here for $Ge_xSi_{1-x}O_2$ with Ge_xSi_{1-x} or Si must be recognized and its implications have to be carefully pondered when considering possible applications of $Ge_xSi_{1-x}O_2$ films in solid-state devices. For MOS gate oxides in particular, such an instability is unacceptable. The mixed oxides are also sensitive to moisture, in ways not yet clearly explained.

References

[1] O.W. Holland, C. White, and D. Fathy, Appl. Phys. Lett. **51**, 520 (1987).

[2] D. Fathy, O.W. Holland, and C. White, Appl. Phys. Lett. **51**, 1337 (1987).

[3] F.K. LeGoues, R. Rosenberg, T. Nguyen, F. Himpsel, and B.S. Meyerson, J. Appl. Phys. **65**, 1724 (1989).

[4] F.K. LeGoues, R. Rosenberg, and B.S. Meyerson, Appl. Phys. Lett. **54**, 644 (1989).

[5] D. Nayak, K. Kamjoo, J.C.S. Woo, J.S. Park, and K.L. Wang, Appl. Phys. Lett. **56**, 66 (1990).

[6] D.K. Nayak, K. Kamjoo, J.S. Park, J.C.S. Woo, and K.L. Wang, Appl. Phys. Lett. **57**, 369 (1990).

[7] J. Eugene, F.K. LeGoues, V.P. Keason, S.S. Iyer, and F.M. d'Heurle, Appl. Phys. Lett. **59**, 78 (1991).

[8] H.K. Liou, P. Mei, U. Gennser, and E.S. Yang, Appl. Phys. Lett. **59**, 1200 (1991).

[9] R.H. Dalton, U.S. Pat. 3,542,572 (1970).

[10] S. Rastani and A. Reisman, J. Electrochem. Soc. 137, 1288 (1990).

[11] J.T. Law and P.S. Meigs, J. Electrochem. Soc. 104, 154 (1957).

[12] W.A. Albers,Jr., E.W. Valyocsik, and P.V. Mohan, J. Electrochem. Soc. **113**, 196 (1966).

[13] Pieter Stroeve, *Integrated Circuits: Chemical and physical Processing* (American Chemical Society, Washington, DC 1985), p.213.

[14] D.C. Pain, C. Caragianis and A.F. Schwartzman, J. Appl. Phys. 70, 5076 (1991)

Chapter 6
Hydridation and nitridation of $Ge_xSi_{1-x}O_2$

6.1 Introduction

As a gate oxide, $Ge_xSi_{1-x}O_2$ is not useful, as we demonstrated in Chapter 5, because the oxide is thermodynamically unstable in contact with Si or GeSi, in essence because $GeO_2 + Si = Ge + SiO_2$. Silicon dioxide and nitride (or oxynitride) are important materials in Si technology for passivation and as insulators [1]. In the case of Ge, the germanium nitride (or oxynitride) passivates the interface better than germanium oxide [2]. The oxynitrides can both be produced by annealing the dioxide in an ammonia ambient [1,2]. It is therefore of technological interest to see if this interfacial instability can be stabilized by converting the GeSi dioxide to a GeSi oxynitride. It is also scientifically interesting to nitridize the mixed GeSi dioxide in ammonia to validate the proposed mechanism for the nitridation of silicon and of germanium dioxide [1,2].

During the experiments, we noticed that GeO_2 is unstable in a hydrogen-containing ambient and will be reduced to $Ge + H_2O$. The unstable nature of this mixed oxide can be turned into an attractive feature as we will demonstrate in this chapter.

We have exposed $GeSiO_2$ films to hydrogen at 700°C for 1 h. Hydrogen will reduce GeO_2 to $Ge + H_2O$ but not SiO_2. The driving force for this reaction is large, and so are the diffusivities of hydrogen and steam. As a consequence, Ge nucleates homogeneously and the result is a suspension of nanocrystalline Ge grains embedded in a film of SiO_2. This nanocrystalline Ge is photoluminescent, as would be surmised by analogy with porous Si [3].

When some parameters of the reduction experiment just described are altered, the outcome is radically different. Instead of homogeneous nucleation, heterogeneous

nucleation prevails. This is accomplished by decreasing the free energy of the reduction reaction, using heavily diluted H_2 (forming gas: 95% N_2 + 5% H_2) instead of 100% H_2. Secondly, an oxide with a high Ge content ($Ge_{0.82}Si_{0.18}$) is used. Thirdly, the $Ge_xSi_{1-x}O_2$ layer to be reduced must have been produced by oxidizing a fraction of the thickness of an epitaxial (100) film. The heterogeneous nucleation then occurs on the interface between the epitaxial $Ge_{0.82}Si_{0.18}$ and the oxide, with the consequence that Ge now grows in the form of an epitaxial layer there as it precipitates out of the oxide. Surprisingly, this Ge layer is of a superior crystalline quality to that of the $Ge_{0.82}Si_{0.18}$ seed layer on which it grows. The (100) channeling minimum yield of a 2 MeV beam is 5% for the Ge, but 15% for the $Ge_{0.82}Si_{0.18}$. What's more, the Ge is elastically unstrained, as determined by x-ray rocking curves, meaning that the lattice misfit between the pure Ge and the $Ge_{0.82}Si_{0.18}$ has been fully accommodated by misfit dislocations. The SiO_2 from the original $Ge_{0.82}Si_{0.18}O_2$ oxide forms a uniform layer above the epitaxial Ge film.

And, finally the results on the thermal nitridation of GeSi dioxide in ammonia is presented.

6.2 Nanocrystalline Ge in SiO_2 by annealing $Ge_xSi_{1-x}O_2$ in hydrogen

When $Ge_xSi_{1-x}O_2$ is in contact with unoxidized Si or Ge_xSi_{1-x}, the system is thermodynamically unstable. The germanium dioxide can be reduced to elemental Ge by Si or Ge_xSi_{1-x} due to the large negative free energy of the reaction

$$GeO_2 + Si \text{ (or } Ge_xSi_{1-x}) = SiO_2 + Ge. \qquad (1)$$

Experiments with a $Ge_xSi_{1-x}O_2$ film on a Ge_xSi_{1-x} layer (x = 0.28 and 0.36) have shown that this reaction indeed occurs, but that the process is limited kinetically to the close vicinity (< 10 nm) of the $Ge_xSi_{1-x}/Ge_xSi_{1-x}O_2$ interface, even after annealing at 900°C for 3

h (see Chapter 5). Paine et al. [4] investigated the system with a 451-nm-thick layer of $Ge_{0.1}Si_{0.9}O_2$ on top of an 8-nm-thick SiO_2 on a Si substrate. They find that the Ge precipitates throughout the entire thickness of its oxide after a 1-h, 800°C annealing and attribute that precipitation to the reaction (1) despite the presence of an 8-nm-thick SiO_2 between the $Ge_{0.1}Si_{0.9}O_2$ layer and Si substrate. It is well established that Si is essentially immobile in pure SiO_2 at 800°C [4]. To explain a uniform distribution of Ge precipitates according to the reaction of Eq. (1) thus demands a very large hypothetical enhancement of Si diffusivity in SiO_2 whose origin remains unknown [4].

In this section, we report that by annealing $Ge_xSi_{1-x}O_2$ (with $x = 0.38$) in a H_2 ambient, Ge is also reduced from its oxidized state and precipitates in the form of nanometer-size Ge crystals that nucleate homogeneously throughout that oxide matrix. The process is driven by the reaction

$$GeO_2 \text{ (in } Ge_{0.38}Si_{0.62}O_2) + 2H_2 = Ge + 2H_2O. \qquad (2)$$

It is conceivable that this reaction also explains the results of Paine *et al.*'s experiment, thereby removing the necessity to invoke unexplained mechanisms if some H_2 was still present in the annealer. That this second pathway exists has also been pointed out by these same authors [5]. A reduction reaction of type (2) is conceivable with other species, such as CO. In principle, the reaction pathway may also depend on the structure of the oxide.

A 540-nm film of $Ge_{0.38}Si_{0.62}$ was first grown epitaxially on a Si substrate by molecular beam epitaxy. Some samples from the wafer were then oxidized in a tube furnace at 700°C for 30 min in a wet ambient. The treatment transforms the top 120 nm of the $Ge_{0.38}Si_{0.62}$ layer to amorphous $Ge_{0.38}Si_{0.62}O_2$ and leaves 420 nm of $Ge_{0.38}Si_{0.62}$ layer unoxidized. These samples shall be referred to as the "partially oxidized" samples. We also prepared some samples whose $Ge_{0.38}Si_{0.62}O_2$ film rested on a thick SiO_2 layer. The

procedure was as follows: In order not to produce a too thick layer of the $Ge_{0.38}Si_{0.62}O_2$, we first removed about 360 nm of the 540-nm-thick $Ge_{0.38}Si_{0.62}$ film by oxidizing the sample at 700°C in a wet ambient for 6 h and dissolving the oxide with a diluted HF solution afterwards. The etched sample was again oxidized at 700°C for 2 h and then at 900°C for 2 h. The treatment at 700°C fully oxidizes the remaining $Ge_{0.38}Si_{0.62}$ layer, and that at 900°C produces about 360 nm of SiO_2 by oxidizing the Si substrate. We refer to these samples as the fully oxidized samples. The purpose of using these two types of samples is to see if the presence of elemental Si in immediate contact with the Ge_xSi_{1-x} oxide, or in its vicinity with a SiO_2 barrier in between, plays a role during the hydrogen annealing. Both sample types were then annealed in a hydrogen tube furnace at 700°C for 1 h. The purity of the hydrogen gas used was about 99.95%. The pressure of hydrogen was initially 1 bar above atmospheric pressure and rose to 1.5 bar above atmospheric pressure at 700°C. This rise is less than that of the absolute oven temperature because the furnace heats up only part of the tube. Some partially oxidized samples were also annealed in vacuum for comparison.

Figure 6.1 (a) and 6.1 (b) show the cross-sectional transmission electron micrographs of the partially oxidized sample before and after the hydrogen annealing. The corresponding electron diffraction patterns derived from illumination of both the oxidized and unoxidized Ge_xSi_{1-x} layers are included. After the hydrogen annealing, the thickness of the unoxidized GeSi is about 420 nm, almost unchanged. The thickness of the oxide, however, decreases from about 240 nm to 210 nm. Only diffraction rings from amorphous but no polycrystalline material are seen in the pattern before the hydrogen annealing. Some rings of crystalline material appear in the diffraction pattern after the annealing. We identify them as belonging to polycrystalline Ge. Under high magnification, small, elongated precipitates are seen throughout the oxide (Fig. 6.2). Some of these precipitates show very clear lattice fringes of crystalline structure. No voids are observed in the oxide. We conclude from Figs. 6.1 and 6.2 that small Ge

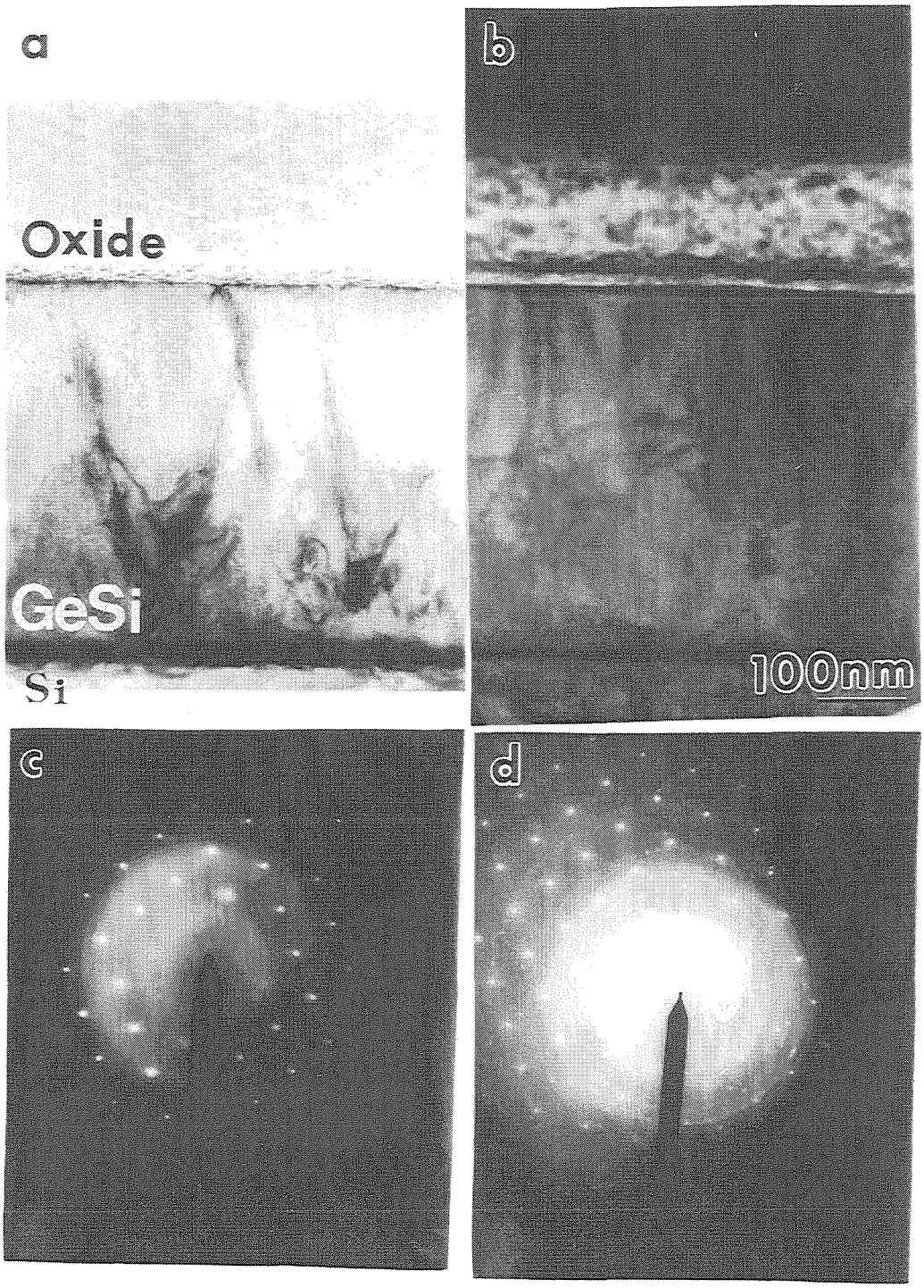

Fi.g 6.1 Cross-sectional bright-field transmission electron micrographs of the partially oxidized sample: (a) before and (b) after the 700°C/1 h hydrogen annealing. The corresponding diffraction pattern obtained from an illumination of both the oxide and the unoxidized GeSi layer are shown in (c) and (d).

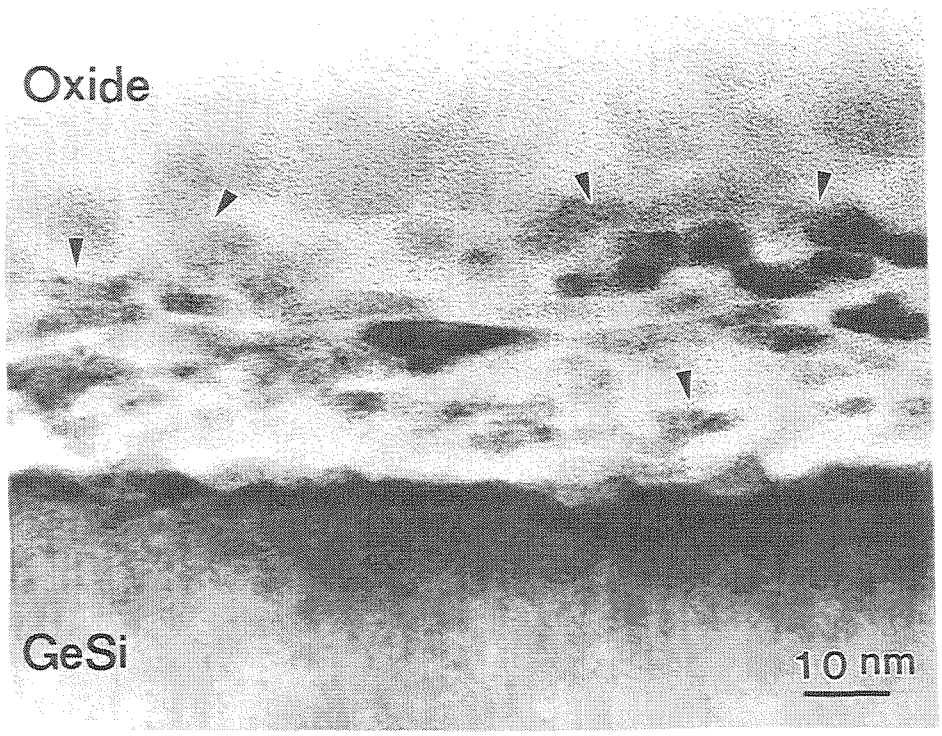

Fig. 6.2 Cross-sectional bright-field transmission electron micrograph of the partially oxidized sample after the hydrogen annealing. Small precipitates are clearly seen. The precipitates show clear lattice fringes of a crystallite, some of which are indicated by the arrows.

crystallites precipitate out of the oxide upon annealing in hydrogen. A similar conclusion is also drawn from the fully oxidized sample after the hydrogen annealing by virtue of the facts that polycrystalline Ge peaks are also found in its x-ray diffraction spectrum and that only absorption peaks belonging to SiO_2, but none belonging to GeO_2 are observed in the infrared spectrum. Both peaks are present before hydrogen annealing. The size of these precipitates in the fully oxidized sample, estimated from the x-ray peaks' width, is about 7 nm, which is similar to that in the partially oxidized sample.

It is thus clear that Ge is reduced from its oxide state, and embedded in the silicon dioxide matrix after the hydrogen annealing in both samples. The thick SiO_2 between the $Ge_{0.38}Si_{0.62}O_2$ layer and the Si substrate in the fully oxidized sample evidently does not inhibit the precipitation of Ge. This proves that the elemental Si has nothing to do with the precipitation of Ge observed here and that Ge does not precipitate via reaction (1) after the hydrogen annealing, unless one accepts the possibility that the diffusivity of the moving species in the SiO_2 (Si and/or the oxidant) required to complete reaction (1) is much enhanced by the presence of hydrogen. If this is the case, that is, that reaction (1) is still the main one, several consequences should be observed. First, the total amount of oxygen in the sample should be reserved. Second, additional Si should be oxidized after the hydrogen annealing. In the partially oxidized sample, this additional oxidation of Si should also result in a decrease of the unoxidized layer thickness and possibly the pileup of Ge near the unoxidized $Ge_{0.38}Si_{0.62}$ layer.

To look for the above consequences, the partially oxidized sample was analyzed by 2 MeV $^4He^+$ backscattering spectrometry. The spectra before and after the hydrogen annealing for 1 h is shown in Fig. 6.3. Within the resolution of backscattering spectrometry, no germanium or silicon is lost after the H_2 annealing, as should obviously be the case according to both reactions (1) and (2). About 40% of the oxygen is lost, however. Because the signals of the oxygen and the Si substrate overlap, we estimate the error of this loss to about ± 20%. It is therefore evident that a significant fraction of the

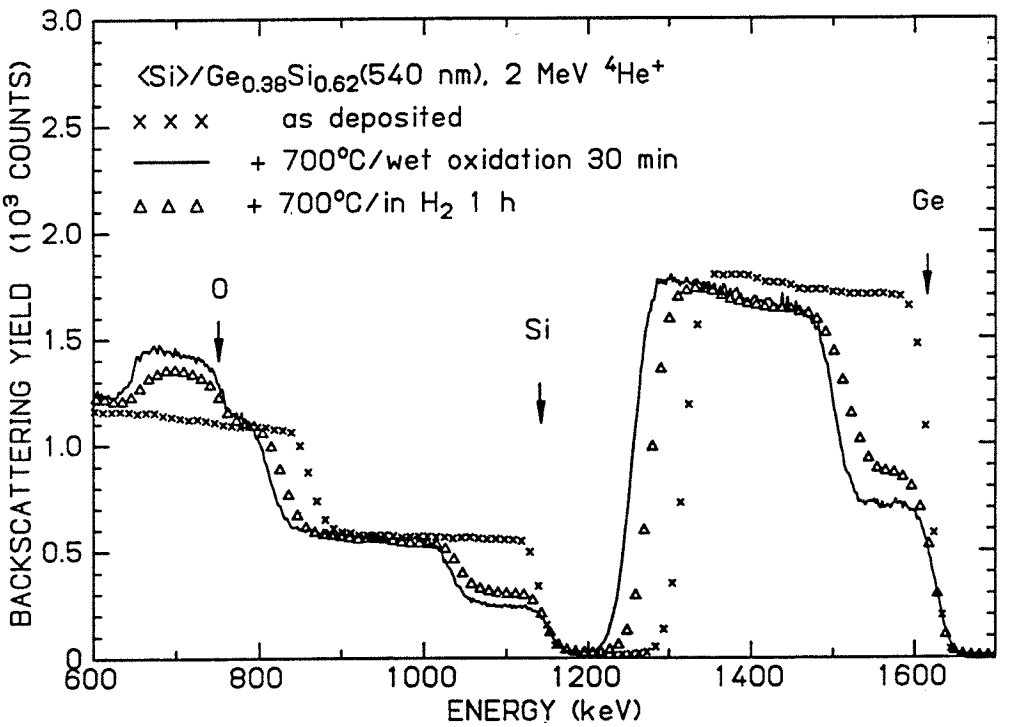

Fig. 6.3 2 MeV $^4He^+$ backscattering spectra of the partially oxidized sample before and after annealing in hydrogen at 700°C for 1 h. (scattering angle of detected particles: 170°, beam incident at 7° from sample normal.)

oxygen is gone after the annealing. The original oxide composition derived from the backscattering spectrometry is uniform and has the composition $Ge_{0.37}Si_{0.63}O_{2.1}$ with an error of ± 5%. This result is consistent with our previous oxidation study in Chapter 3. After the annealing the oxide is still compositionally uniform but has changed to about $Ge_{0.36}Si_{0.64}O_{1.28}$ with an error of ± 5% after the annealing. This composition is equivalent to 0.36 Ge + 0.64 SiO_2 and strongly suggests that the layer is a mixture of elemental Ge and silicon dioxide. Such a composition is consistent with the conclusion drawn from the transmission electron microscopy which indicates that the Ge is reduced from its oxide state after the hydrogen annealing (Fig. 6.1). Furthermore, the unoxidized portion of the GeSi layer remains unchanged in composition and the thickness during the hydrogen annealing within the resolution of backscattering spectra. No pileup of the Ge in the unoxidized GeSi layer is observed. None of the consequence enumerated above are thus observed. Instead, we find further evidence in support of reaction (2). Finally, a partially oxidized reference sample annealed in vacuum instead of hydrogen at 700°C for 1 h has indistinguishable backscattering spectra before and after the heat treatment in vacuum. This outcome is consistent with our previous stability study in Chapter 5 and shows that the reaction of Eq. (1) cannot explain a uniform reaction of $Ge_xSi_{1-x}O_2$ throughout the film thickness at 700°C since such a significant precipitation only occurs in the hydrogen ambient but not in vacuum. The composition change of the oxide observed in Fig. 1 is thus due to the hydrogen ambient.

Since none of the consequence of reaction (1) is observed here, we conclude that the elemental Si is not needed for the precipitation of the Ge observed here. The formation of essentially all of the Ge is thus due to reaction (2).

The standard free energy, G^0, of the reaction (2) is indeed negative, and is about 2.3 kcal/mole after a solid-solution correction of the value of 4.2 kcal/mole for pure GeO_2 at 700°C [6]. This standard free energy is small. The partial pressure ratio of H_2 and H_2O is therefore the key factor controlling the free energy and the way this reaction goes

(reduction or oxidation). It can be simply calculated that under H_2 partial pressure, P_{H_2}, and H_2O partial pressure P_{H_2O}, the free energy of the reaction (2) is given by $G^* = G^0 + 2RT \ln (P_{H_2O}/P_{H_2})$. The partial pressure of H_2 in our system is about 2.5 atm; that of H_2O is unknown, but certainly extremely small as a result of preannealing with Ti getters and multiple purges with H_2 of the high-vacuum tight system. This P_{H_2O}/P_{H_2} ratio thus makes the free energy very negative and greatly drives reaction (2) to the reduction direction. The diffusivity of hydrogen in SiO_2 is high even at 700°C (about 10^{-6} cm^2/s) [7]. A high diffusivity of hydrogen coupled with a large driving force makes the critical radius (the smallest stable precipitate) of the germanium precipitates small and causes the Ge to nucleate homogeneously in the oxide, resulting in nanocrystalline Ge precipitates throughout the oxide.

In conclusion, we have shown that hydrogen reduces GeO_2 to Ge via reaction (2) when a film of the GeSi dioxide is annealed in a hydrogen ambient. Such a hydrogen annealing also provides a new alternative to synthesize the nanocrystalline precipitates of Ge in an amorphous SiO_2 matrix. These precipitates show interesting optical properties and strong photoluminescence.

6.3 A Ge epilayer of improved quality on a Si substrate via $Ge_xSi_{1-x}O_2$ reduction

The growth of a high-quality, totally relaxed Ge epilayer on a single-crystalline silicon substrate is of great technological interest as an intermediate buffer layer for symmetrically strained Si/Ge superlattices or n-channel modulation-doped GeSi structures. Additionally, good quality III-V compounds (such as GaAs or AlGaAs) can be grown on such layers for the purpose of integrating optical and high-frequency III-V devices into silicon-based circuits since the lattice constant and thermal expansion coefficient of Ge are close to those of GaAs. Pure Ge grown on Si results in a very high misfit and threading dislocation density due to the large lattice mismatch (~ 4%) in this system [8]. Recently,

the threading dislocation density could be reduced significantly by introducing the thick buffer layers between the Ge layer and the Si substrate such as the continuously graded Ge_xSi_{1-x} layers [9].

In this section, we report that by annealing the $Ge_{0.82}Si_{0.18}/Ge_{0.82}Si_{0.18}$ bilayer on a Si substrate in forming gas, a fully relaxed Ge epilayer can be formed on top of the $Ge_{0.82}Si_{0.18}$ template. The crystalline quality of this Ge epilayer much exceeds that of the underlying GeSi template.

An elastically unstrained $Ge_{0.82}Si_{0.18}$ film was first grown epitaxially on a (100)Si substrate to a thickness of about 580 nm by molecular beam epitaxy. Pieces of this epiwafer were then oxidized at 700°C in a wet ambient for 30 min. Under such a condition both the germanium and the silicon of this epilayer are oxidized (see Chapter 3). The composition of the oxide has been verified by backscattering spectrometry to concur with that of $Ge_{0.82}Si_{0.18}O_2$. About 280 nm of the GeSi layer is consumed during the oxidation. The unoxidized part of the GeSi layer remains epitaxial and uniform in composition. The oxidized samples were then annealed in forming gas (95% N_2 + 5% H_2) at 700°C for 16 h. The samples were analyzed by backscattering spectrometry, transmission electron microscopy, and x-ray double-crystal diffractometry (The process sequence is also contained in the summary sketch of Fig. 6.7).

Figure 6.4 (a) shows the backscattering spectra of the oxidized samples before and after the annealing in forming gas. After annealing, the GeSi dioxide layer is transformed into an apparent trilayer structure. The top layer consists of Si and O and contains almost no Ge (signals at 0.7 and 1.1 MeV). The atomic composition of that layer is that of SiO_2 within experimental error, and its thickness is approximately 120 nm. The second layer consists of Ge that must be fairly pure, as deduced from the height of the Ge signal in the backscattering spectrum (signal at 1.5 MeV). That second layer is about 140 nm thick. The third layer contains all three elements (signals at 0.6, 0.95 and 1.3 MeV). The thickness of the initially unoxidized GeSi layer decreases from 300 nm to 200 nm; what

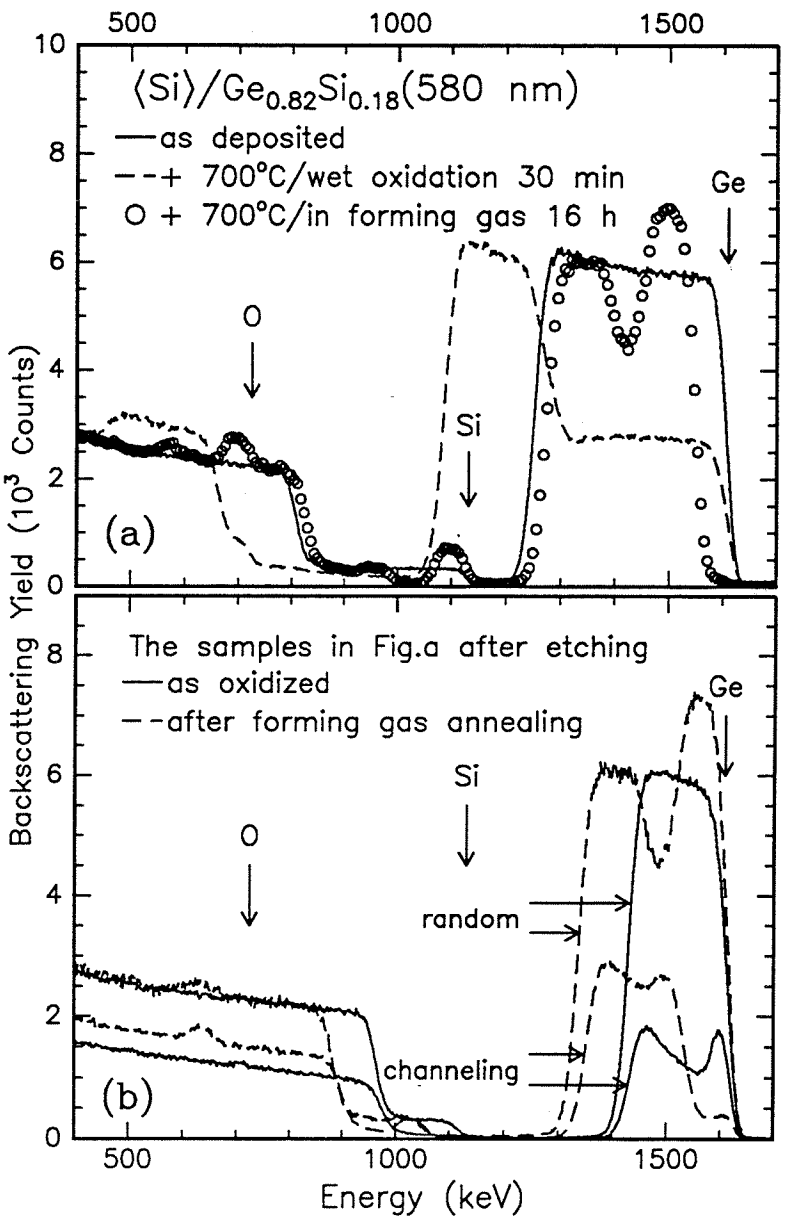

Fig. 6.4 2 MeV $^4He^+$ channeling backscattering spectra of a 580 nm thick epitaxial $Ge_{0.82}Si_{0.18}$ layer grown on a (100)Si substrate, Fig. a: as-deposited (solid line), after oxidation of a part of the epilayer at 700°C for 30 min (dashed line), and after additional heat treatment in forming gas at 700°C for 16 h (circles); Fig. b: the two samples of Fig. a were dipped into a diluted HF solution to remove the top oxide layers. The <100> channeling spectra of both samples are also included in Fig. b. (scattering angle of detected particles: 170°; beam incidence angle: 7° for Fig. 1a and 1b).

remains of it maintains its initial composition. It is also noted that about 18% of Ge is lost during the annealing.

The top oxide layer can be etched off easily by a diluted HF solution. After such an etch the surface of the sample acquires a metallic sheen and is smooth under optical microscopy. For comparison, the $Ge_{0.82}Si_{0.18}O_2$ layer on an oxidized piece of the epiwafer that had not been annealed in forming gas was also etched off. The backscattering spectra for random and <100>-channeled beam incidence of these two etched samples are shown in Fig. 6.4 (b). Comparing the integral of the Ge signals in the two spectra for random beam incidence reveals that the amount of Ge left in the sample annealed in forming gas is about 50% larger than the amount of Ge that remains in the sample that was etched without having undergone an annealing in forming gas. The added Ge must have come from the $Ge_{0.82}Si_{0.18}O_2$ layer, during the second annealing step.

We have demonstrated in Section 6.2 that Ge_xSi_{1-x} dioxide is unstable and that the GeO_2 in it is reduced to elemental Ge in the presence of hydrogen. That instability is obviously observed here also. The decrease of the thickness of the unoxidized GeSi layer noted in Fig. 6.4 (a) can be attributed to an oxidation by moisture that evolves from the reduction reactions of GeO_2. The oxidation rate of GeSi is large even at 700°C in a wet ambient and increases with the Ge content (see Chapter 3). Both Si and Ge may be oxidized because Ge and Si are immobile in GeSi at that temperature; but the instability of GeO_2 ultimately results in a mixture of Ge and SiO_2.

The most striking feature of this reduction process is that it leads to the growth of an epitaxial Ge layer, as the channeling spectrum of Fig. 6.4 (b) shows (signal at 1.6 MeV). The minimum yield of this layer is about 5% which compares quite well with that of a single crystalline (100)Ge wafer (~ 3%). In contrast, the minimum yield of the comparison sample with the exposed GeSi layer is about 15%, which indicates a substantially inferior crystalline quality to that of the Ge layer which grows above it. In

addition, the mixed layer that separates the GeSi layer from the Ge epilayer has Si and O signals that show no channeling at all (at 0.65 and 1.05 MeV).

The cross-sectional transmission electron micrograph of a sample etched after the second annealing in forming gas is shown in Fig. 6.5 and gives a clue as to how that unusual epitaxial growth of Ge is accomplished. Four distinct layers are clearly seen in the figure. The top layer is a 140 nm-thick Ge film and the bottom layer just above the Si substrate is a 190 nm-thick $Ge_{0.82}Si_{0.18}$ film. The selected-area diffraction patterns of both films reveal a single crystal structure with the same (100) orientation. The mixed region identified in the backscattering channeling spectra is seen to actually consist of two sub-regions. A high resolution micrograph of this double region shows a single crystalline matrix that contains large amorphous islands in its upper part and much finer ones in its lower part, thereby causing the two sub-regions seen in the Fig. 6.2. Combined with the channeling result and the instability of GeO_2 mentioned above, the amorphous island should be silicon dioxide and the single crystalline matrix the germanium. The thin and almost continuous oxide layer just above the GeSi layer is caused by the coalescence of the fine oxide islands in the lower part of the mixed region since that layer is not seen in the sample after annealing in forming gas for only 1 h. The dislocation density in the underlying GeSi layer is high (larger than 10^{10} cm^{-2} as estimated from the cross-sectional micrograph) as could be expected since the Ge content in the layer is high. The top Ge layer however has a lessened dislocation density. It is also noted that most of the dislocations in the underlying GeSi layer do not propagate through the mixed region to the top Ge layer.

We measured the strain of the epitaxial layer on a sample of the same configuration as in Fig. 6.5 by double crystal x-ray diffraction using the Fe $K_{\alpha 1}$ line (λ = 1.936 Å) and the (400) diffraction (Fig. 6.6). Two peaks belonging to the fully relaxed Ge and the fully relaxed $Ge_{0.82}Si_{0.18}$ layers are observed. The full-width at half-maximum intensity of the Ge and $Ge_{0.82}Si_{0.18}$ peak is about 660 and 800 arcsec respectively. This width is caused by

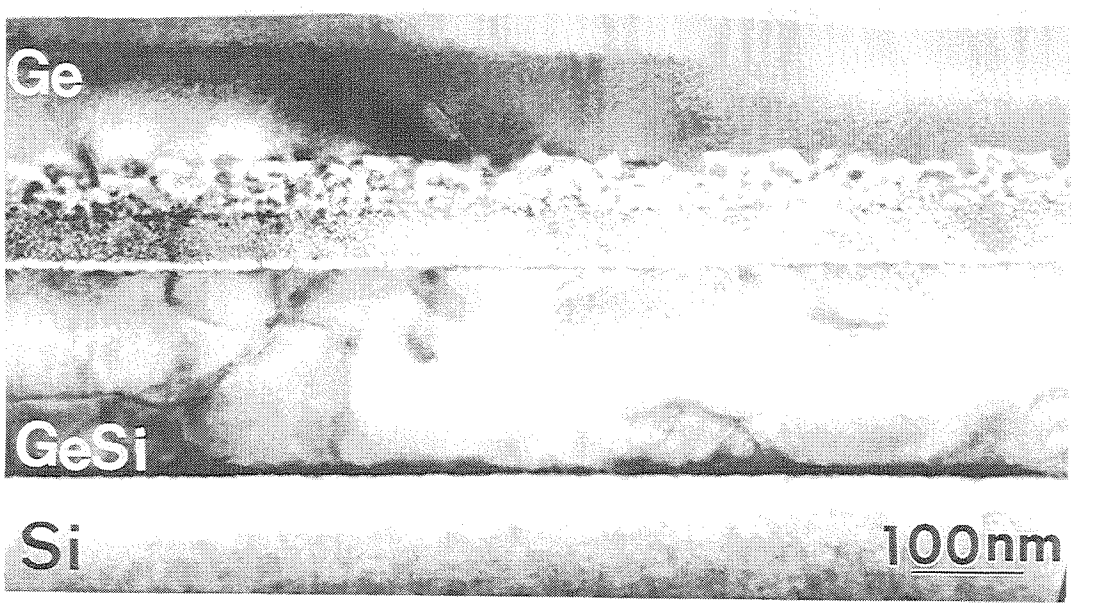

Fig. 6.5 Cross-sectional transmission electron micro graph of the oxidized sample after the 700°C/16 h annealing in forming gas and subsequent removal of the top oxide layer.

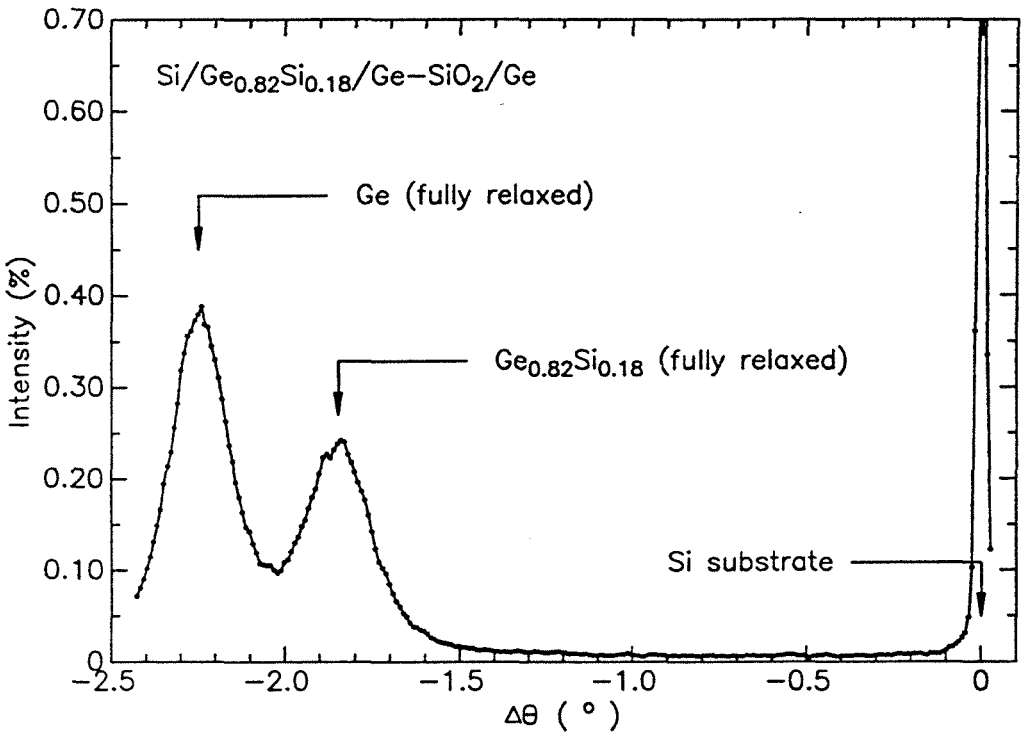

Fig. 6.6 Fe $K_{\alpha 1}$ double crystal x-ray (400) diffraction of a sample in the state equal to that of Fig. 6.5.

the finite thickness of the film and the defects inside the film. The width of the Ge peak doesn't reflect the real quality of the top Ge layer, since some of the broadening of that peak originates from the Ge in the mixed region with single crystalline Ge and SiO_2. In addition, the Ge layer is thinner than the $Ge_{0.82}Si_{0.18}$ and yet has a peak width that is smaller than that of the $Ge_{0.82}Si_{0.18}$ peak. These results are consistent with the channeling result of Fig. 6.4 (a) and the transmission electron micrograph result of Fig. 6.5. They all support the conclusion that the reduction process of GeO_2 leads to the growth of an epitaxial Ge layer that exhibits a higher structural quality than that of the underlying $Ge_{0.82}Si_{0.18}$ template.

The epitaxial nature of this Ge layer obviously originates from the underlying GeSi layer since they are connected through the region with the amorphous oxide islands. The Ge-SiO_2 mixed region between the top Ge and the underlying $Ge_{0.82}Si_{0.18}$ layer evidently plays an important role for the improved crystal quality of the top Ge layer. It is apparent that such a region can block the underlying dislocations from propagating due to the presence of discontinuous second phase of SiO_2 islands in the Ge matrix. This mixed region acts as a filter for dislocations; we thus suggest the name of "percolation layer" for this region. Indeed, most of the underlying dislocations in the GeSi layer terminate in the percolation layer (see Fig. 6.5).

In summary, the sequence of processing steps described here and schematically shown in Fig. 6.7 results in solid-state growth of a layer with better crystalline perfection than that of the seeding substrate. In its essential aspects, this process is similar to patterned epitaxial growth [10], except that the lateral discontinuities beneficial to the epitaxial growth process are self-induced rather than artificially generated.

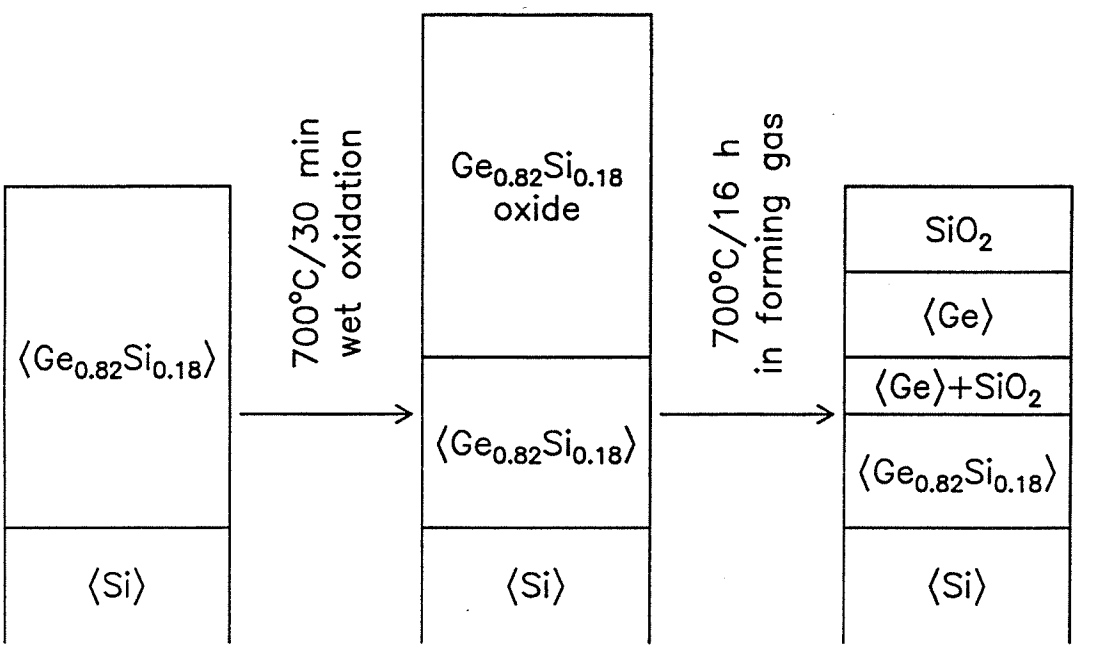

Fig. 6.7 Schematic diagram of the process. The change in the layer thickness are approximately to scale.

6.4 Hydridation and nitridation of GeSi oxide in ammonia

An epitaxial $Ge_{0.38}Si_{0.62}$ film about 540 nm thick was first grown on a (100)Si substrate by molecular beam epitaxy. The film is elastically relaxed as determined from x-ray double-crystal diffractometry. The film was then oxidized at 700°C in a wet ambient for 10, 30 or 90 min. The germanium and silicon are both oxidized during these treatments, resulting in a GeSi dioxide that is about 110 nm thick for 10 min according to its backscattering spectrum and after conversion to a depth scale using an oxide density of 2.1×10^{22} formula units/cm^3 (see Chapter 3). The oxides for 30 and 90 min are about 230 and 380 nm, respectively. Subsequently, these samples were heated at temperatures between 600 to 800°C in flowing NH_3 at one atmosphere in an open tube quartz furnace. The nitridation lasted 4 h. The nitrided samples were examined by the Auger electron spectroscopy, backscattering spectrometry, x-ray photoelectron spectroscopy, and secondary-ion mass spectrometry.

Figure 6.8 shows the Auger electron spectra obtained by sputter-profiling with a 5 keV argon beam of a 110 nm thick $Ge_{0.38}Si_{0.62}O_2$ layer, nitrided in NH_3 at 700°C for 4 h. Peak-to-peak heights of Si(KLL), Ge(LMM), N(KLL) and O(KLL) transitions are depicted as a function of sputtering time. A clear nitrogen signal is observed in the oxide, with a maximum near the surface and a gradual decrease in the oxide. No nitrogen is observed near the interface of the oxide and the underlying GeSi layer. The decrease in the nitrogen signal with increasing duration of sputter-profiling time coincides with an increase in the oxygen signal. This suggests that nitrogen has replaced the oxygen in the oxide during the annealing. The Ge signal first dips within the oxide and then increases fairly rapidly to its value at the oxide interface. The Si signal has a profile that tends to run opposite to that of Ge, exhibiting first a maximum and then a delayed rise to its value at the oxide interface.

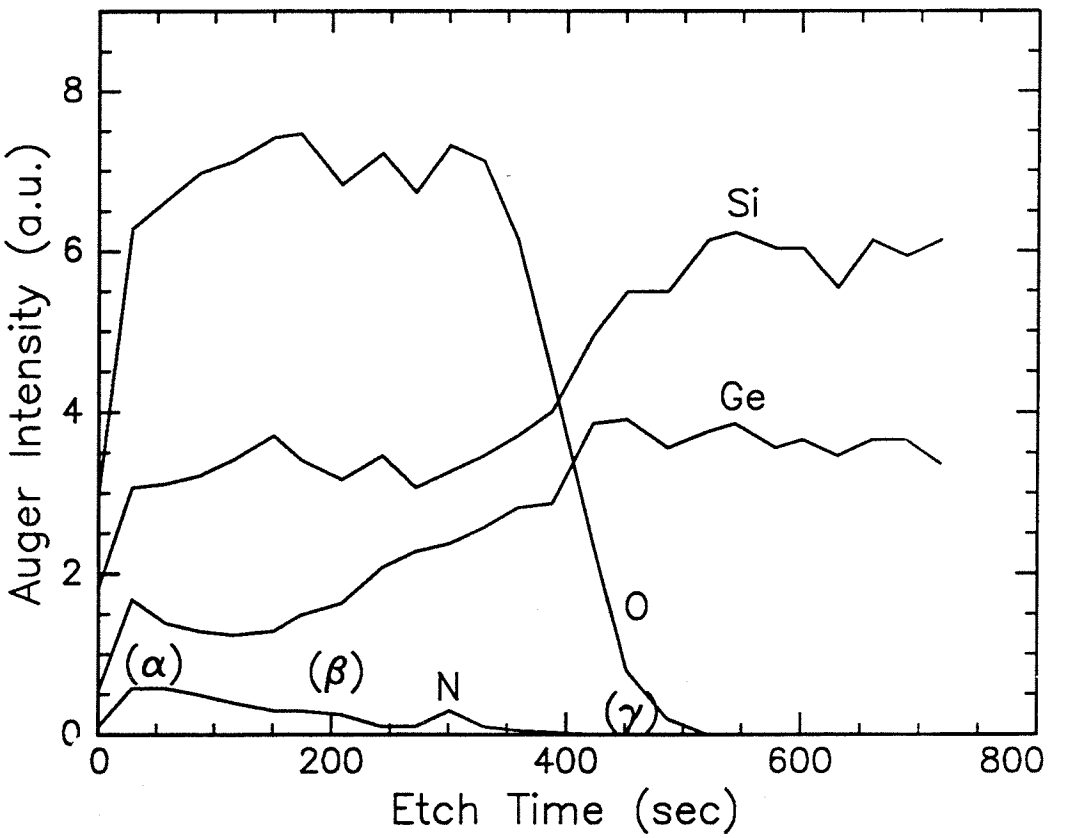

Fig. 6.8 Auger electron depth profile of a 110-nm $Ge_{0.38}Si_{0.62}O_2$ layer on $Ge_{0.38}Si_{0.62}$, annealed in ammonia at 700°C for 4 h.

A minimum in the Ge profile of the oxide is also observed by backscattering spectrometry (Fig. 6.9). Before the ammonia annealing, the Ge profile is uniform through the oxide with a composition close to $Ge_{0.38}Si_{0.62}O_2$. This composition indicates that both Ge and Si are oxidized (see Chapter 3). After the ammonia annealing, a significant decrease of the Ge content is seen just below the surface (near 1550 keV in Fig. 6.9) , while an enhancement is visible at the interface (near 1510 keV). Again Si changes inversely to Ge; its enhancement is clearly visible near 1060 keV at a position which corresponds to the Ge dip (at 1550 keV).

To investigate the chemical states of Si and Ge in these regions, oxidized samples before and after the ammonia annealing were also analyzed using x-ray photoelectron spectroscopy and sequential sputter-etching. Before the annealing in ammonia, both Ge and Si are in their fully oxidized states everywhere. The spectra of the Ge($2p^3$) and Si(2p) peaks obtained after the annealing at the positions α, β and γ indicated in Fig. 6.8 are shown in Fig. 6.10. One can see that the Si in the nitrided oxide (position α and β) is only in the Si^{+4} state and thus bonded as SiO_2. At the GeSi/oxide interface (position γ), the peak of Si in its elemental state also emerges. The peak of Si at 101.8 eV characteristic for Si_3N_4 is absent in all three positions. This result demonstrates that the chemical state of Si is unaffected by the annealing in ammonia. The incorporated nitrogen seen in Fig. 6.8 then must be bonded to Ge. This conclusion is also supported by the mixed chemical sates observed for the Ge in the nitrided oxide. The two peaks detected at position α then correspond to the states of germanium bonded to oxygen and to nitrogen. At position β, besides these two peaks, a third peak that corresponds to the state of the elemental Ge is also observed. That peak could also correspond to a binding between Ge and Si, but this is ruled out since no elemental Si state is found at position b for the Si(2p) transition. Elemental Ge is thus present at position β as well. This is true upto the position corresponding to the etch time of about 320 sec in Fig. 6.8. This region coincides with the

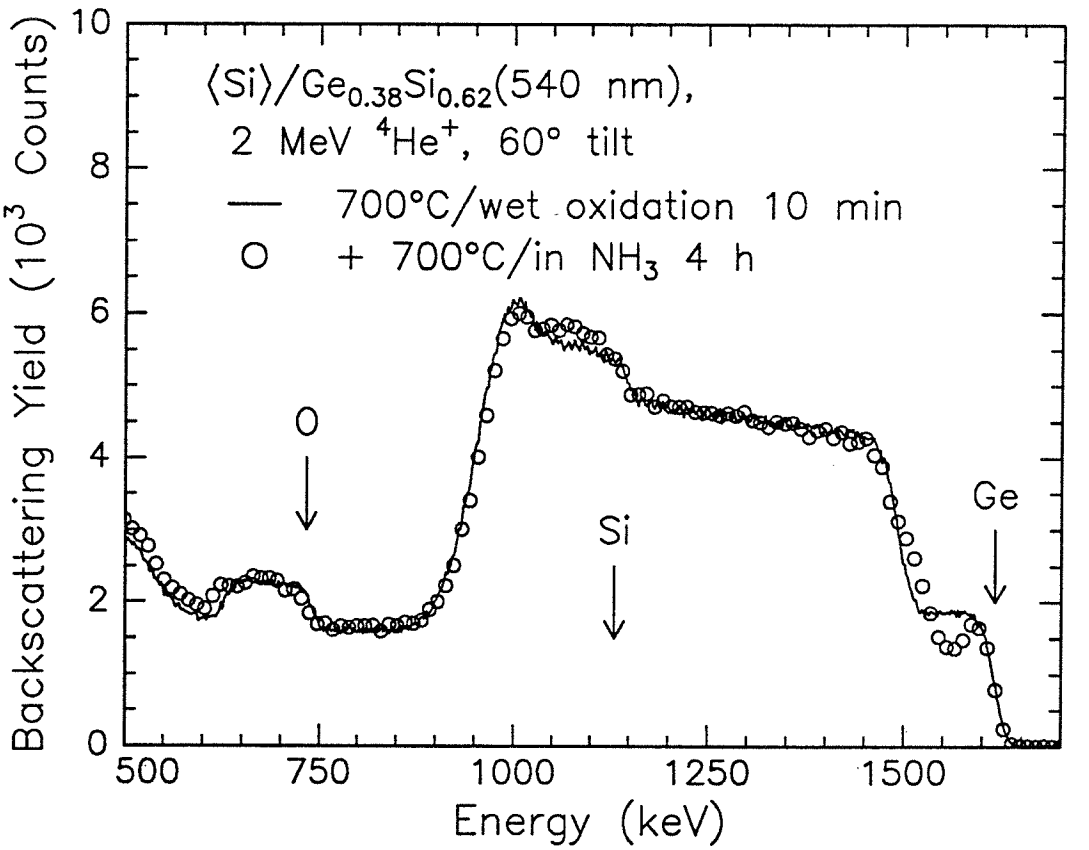

Fig. 6.9 2 MeV $^4He^+$ backscattering spectra of a 110-nm thick $Ge_{0.38}Si_{0.62}O_2$ layer on $Ge_{0.38}Si_{0.62}$ before and after annealing in ammonia at 700°C for 4 h. (The surface normal is tilted by 60° away from the beam line; the scattering angle of detected particles is 170°.)

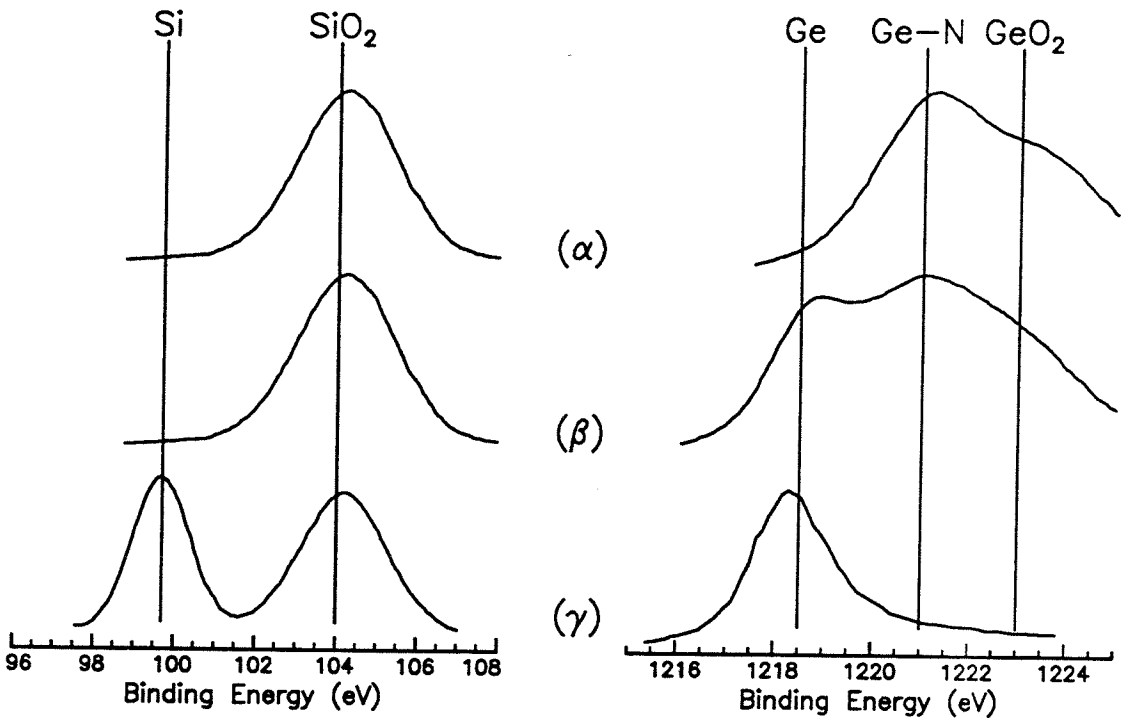

Fig. 6.10 X-ray photoelectron spectra of the Si 2p and Ge2p^3 signals taken at the three different depth of a 110-nm thick $Ge_{0.38}Si_{0.62}O_2$ layer on $Ge_{0.38}Si_{0.62}$ after ammonia annealing at 700°C for 4 h.

increase of the Ge in the oxide. Beyond that 320 sec point, only the elemental Ge signal remains. The significant increase of the Ge content near the GeSi/oxide interface in Fig. 6.9 is thus due to a preferential precipitation of elemental Ge there. A simple possible interpretation of these findings is that the elemental Ge appears first near the GeSi/oxide interface and then extends into the bulk of the oxide. This scenario also explains the fact that only the elemental Ge peak is observed at position γ.

It is then clear that after the ammonia annealing at 700°C, the silicon dioxide remains stable in the GeSi oxide. The germanium in the dioxide, however, partly binds to nitrogen near the surface and partly transforms to elemental Ge near the GeSi/oxide interface. The germanium nitridation we observe is consistent with a previous study that shows ammonia as an effective nitridant of GeO_2 [2].

Figure 6.11 shows the secondary-ion mass spectra of the annealed sample of Fig. 6.8. The detection of nitrogen in the oxide is consistent with the Auger electron spectroscopy results of Fig. 6.8. In addition, the hydrogen is also observed throughout the oxide. No such detectable level of nitrogen or hydrogen is observed in the sample before the ammonia annealing. This supports that the nitrogen is incorporated after the ammonia annealing and that is a result of nitridation of GeO_2 as shown in Fig. 6.8 and 6.10. The hydrogen quite likely comes from the dissociation of the ammonia. Germanium dioxide is unstable in the presence of hydrogen and will be reduced to elemental Ge (see Section 6.2). The elemental Ge identified in Fig. 6.10 thus results from a hydridation of the germanium oxide.

To investigate this hydridation effect further, samples of all three oxide thicknesses (110, 230 and 380 nm) were annealed in ammonia at 700 and 800°C for 4 h. The interfacial Ge peak (the emergence of the elemental Ge at the GeSi/oxide interface) is seen in all three samples. An oxide as thick as 380 nm thus doesn't hinder the hydridation reaction near the GeSi/oxide interface. This fact implies a high mobility of hydrogen in the nitrided GeSi oxide, which is very likely since hydrogen diffuses very fast in SiO_2 (the

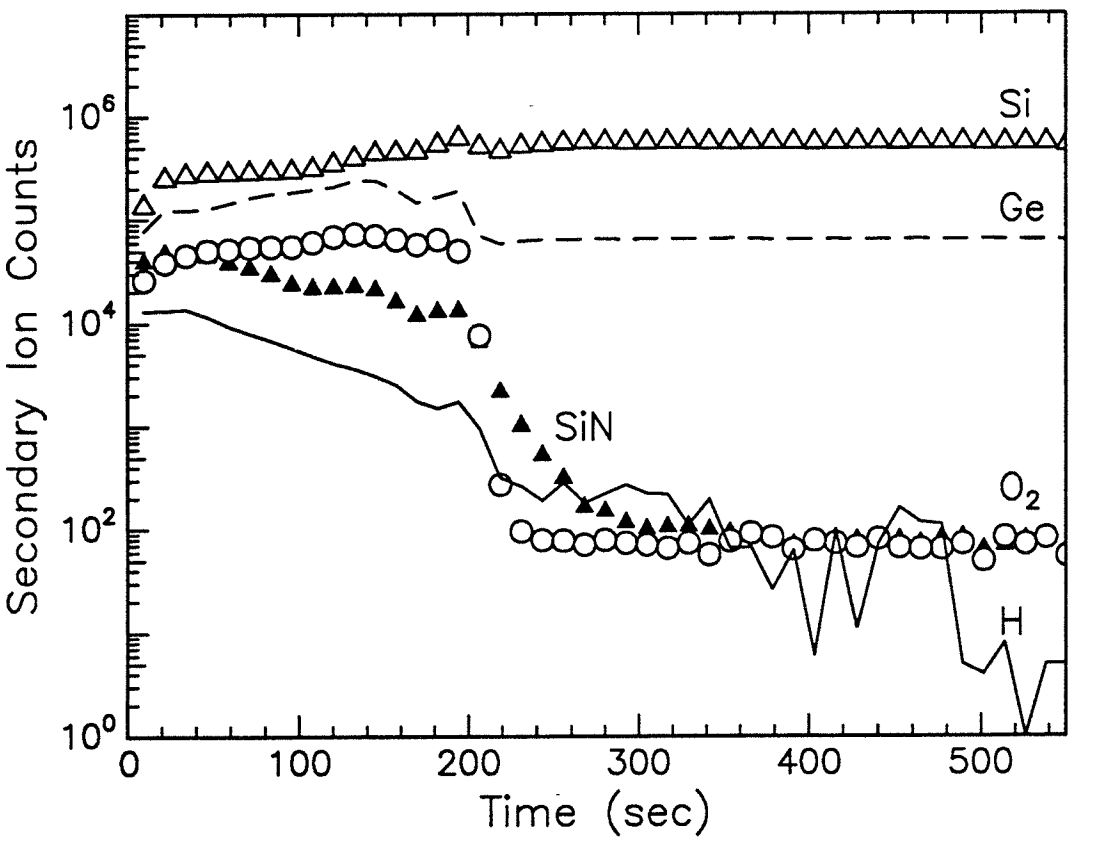

Fig. 6.11 Secondary-ion mass spectra of a 110-nm thick $Ge_{0.38}Si_{0.62}O_2$ layer on $Ge_{0.38}Si_{0.62}$, annealed in ammonia at 700°C for 4 h.

diffusivity is about 2×10^{-6} cm^2/sec at 700°C) [7]. Figure 6.12 shows the backscattering spectra of a 380-nm thick $Ge_{0.38}Si_{0.62}O_2$ sample before and after annealing in ammonia at 800°C for 4 h. A uniform GeSi oxide composition is again seen in the spectrum before the annealing in ammonia. After that annealing, the emergence of a peak in the Ge signal at 1460 keV is quite evident. This Ge is in an elemental state according to results such as those of Fig. 6.10 and accumulates near the GeSi/oxide interface. This Ge accumulation depletes the adjacent germanium in the oxide, creating the dip in the Ge signal at 1520 keV in Fig. 6.12 and a corresponding rise in the Si signal around 1050 keV. The surfacial Ge, however, is not depleted which can be attributed to the formation of a nitride there. Since germanium oxynitride exists and is stable during ammonia annealing of germanium dioxide [2], the nitride formed here should be stable in the hydrogen ambient which results from the dissociation of ammonia. In addition, a minor dip in the Ge signal is also observed at 1430 keV, i.e., just at the bottom of the oxide. A likely cause for this local decrease of Ge is that the underlying GeSi layer is attacked by moisture released in the reduction of GeO_2 by hydrogen and the remaining hydrogen. SiO_2 thus forms between the accumulation of Ge and the unoxidized GeSi layer.

The nitridation of the oxide surface alters the oxide properties significantly. Figure 6.13 shows the backscattering spectra of a 30-min oxidized sample after a 4 h ammonia annealing at 700°C that was followed by reoxidation in a wet ambient for another 30 min at 700°C. As seen in Fig. 6.13, only very little of the remaining underlying GeSi layer is further oxidized after the sample is nitrided. Without the nitridation step, the oxide would have increased in thickness by a factor of $\sqrt{2}$ because the growth law of the oxide is parabolic under this condition (see Section 3.3). The nitrided oxide evidently acts as a barrier for moisture.

Germanium dioxide is not stable in the presence of hydrogen while SiO_2 is (see Section 6.2). Hydrogen dissociated from ammonia thus only reacts with the GeO_2 but not with SiO_2. For the nitridation of a SiO_2 layer on a Si substrate, it has been shown by

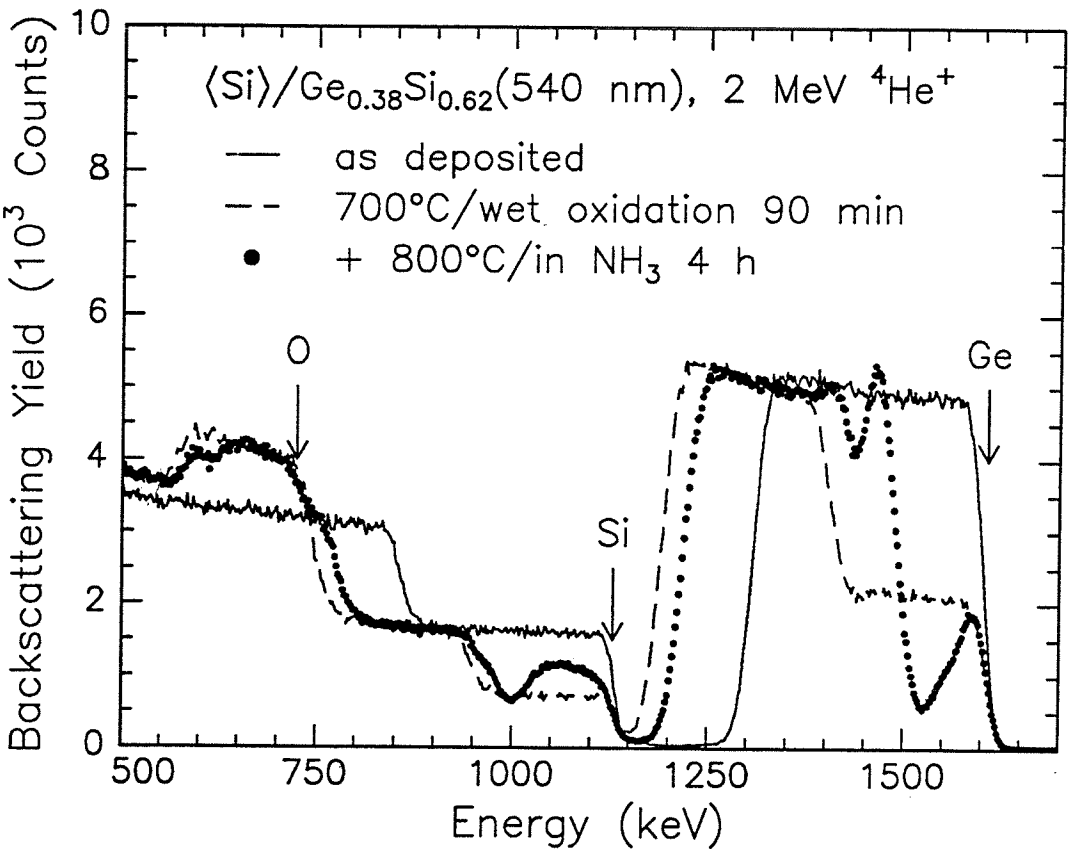

Fig. 6.12 2 MeV $^4He^+$ backscattering of a $Ge_{0.38}Si_{0.62}O_2$ layer 380 nm thick on $Ge_{0.38}Si_{0.62}$ before and after annealing in ammonia at 800°C for 4 h. (Near-normal beam incidence; scattering angle of detected particles: 170°.)

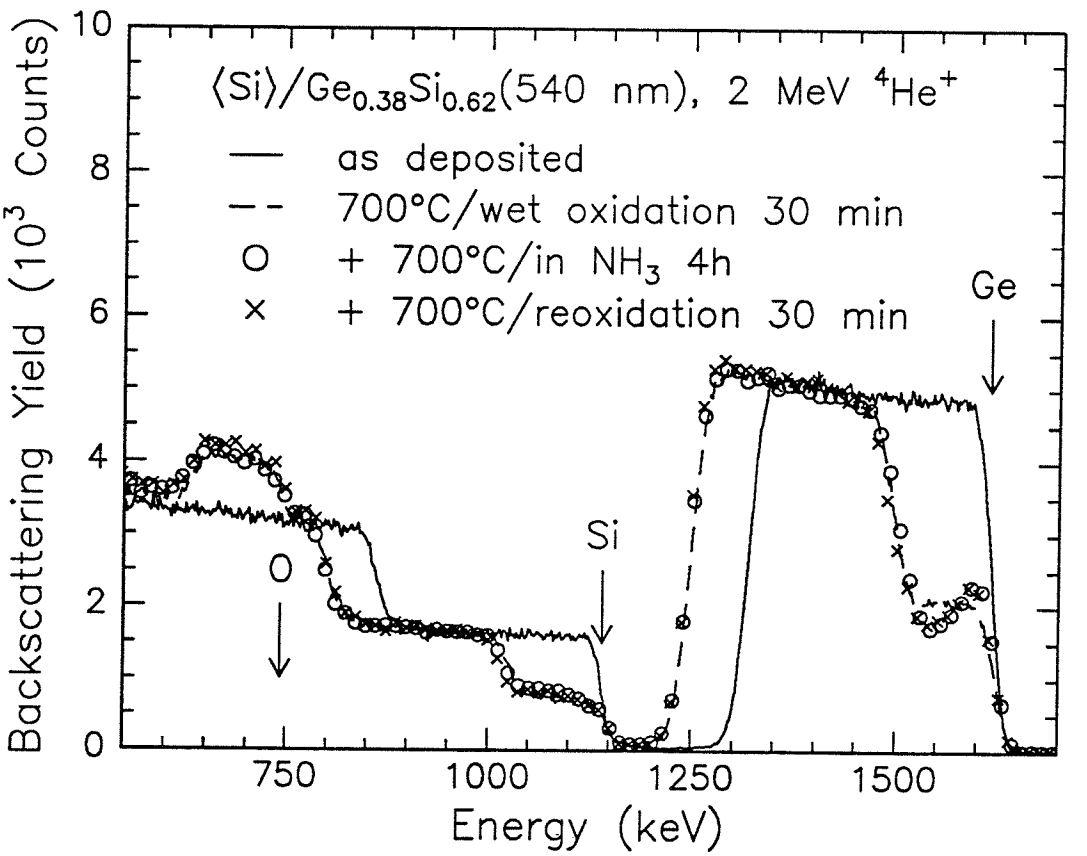

Fig. 6.13 2 MeV $^4He^+$ backscattering spectra of a 230-nm thick $Ge_{0.38}Si_{0.62}O_2$ layer on $Ge_{0.38}Si_{0.62}$ before and after annealing in ammonia at 700°C for 4 h followed by reoxidation in steam for 30 min. Only little additional oxide grows during that reoxidation, suggesting that the nitrided oxide acts as a barrier against further oxidation.

Habraken *et al.* [1] that the nitrogen is included near the oxide surface and the Si/oxide interface after annealing in ammonia. This nitridation of SiO_2 occurs at temperatures between 800°C to 1160°C. On the other hand, the nitridation of GeO_2 in ammonia can occur at a temperature as low as 600°C [2]. Since the temperature in our experiment is only about 700°C, the finding that GeO_2 is converted to nitride and elemental Ge and SiO_2 is not is thus consistent to those studies [1,2]. This outcome also confirms that GeO_2 is much easier to nitridize than SiO_2. We may therefore ignore SiO_2 and discuss the reaction of nitridant and hydridant with GeO_2 only.

As seen in Fig. 6.8, the nitrogen concentration decreases gradually with increasing distance from the surface. No elemental Ge is found in this surface region. On the other hand, the elemental Ge tends to segregate near the GeSi/oxide interface. No nitrogen is observed in this interfacial region. Both nitridation and hydridation therefore occur in parallel, with nitridation winning at the surface and hydridation at the interface. The question arises what determines which reaction dominates where. The process can be viewed as the competition of both reactions with GeO_2 at the surface and at the interface and is discussed as follows:

Habraken *et al.* [1] have suggested that in the nitridation of SiO_2 the ammonia dissociates into NH_x (nitridant) and H_{3-x} (hydridant), and that it is the nitridant NH_x that reacts with SiO_2 to form silicon nitride or oxynitride. This dissociation evidently takes place also in our case. The nitridant and hydridant, while reacting with GeO_2 in the GeSi dioxide, will both produce H_2O. Near the surface, this moisture can easily escape from the oxide while near the GeSi/oxide interface, a further oxidation of the underlying GeSi layer is the most likely process. These two boundaries act as sinks of water that enhance the reactivity there as compared to the bulk of the $GeSiO_2$ film, which explains why reactions occur predominately at the surface and the interface.

In the surface region, both the nitridant and hydridant can react with GeO_2. Hua et al. [11] have shown that germanium nitride films of a thickness less than 15 nm can be grown

by thermal reaction with ammonia from pure Ge substrate at growth temperatures between 600 and 650°C. The reaction between elemental Ge and the nitridant is therefore also feasible and that suggests that even if elemental Ge formed via the hydridation reaction of GeO_2, it can be converted into germanium nitride as well, which makes the absence of the elemental Ge in the surface region possible. On the other hand, the germanium nitride is stable in the hydrogen ambient formed from dissociated ammonia, as explained above in Fig. 6.12. The germanium nitride is therefore the only product observed in this region.

In the interfacial region, the diffusivity of the reactant in the oxide also enters in the reaction process. The finding of hydridation but not of nitridation in the interfacial region can be viewed as an explanation of a much faster diffusion of the hydridant than that of the nitridant in the GeSi oxide. This is certainly conceivable considering the fast diffusion of hydrogen in SiO_2 [7]. The incorporation of nitrogen in the surface will most likely hamper the diffusion of the nitridant more than that of the hydridant which will further enhance the hydridation process over that of the nitridation at the GeSi/oxide interface.

We have examined the structure of amorphous $Ge_{0.38}Si_{0.62}O_2$ after ammonia annealing. Some nitrogen is incorporated in the surface which is bonded to germanium. This nitrided surface acts as a barrier for moisture. On the other hand, some elemental Ge is observed at the GeSi/oxide interface. The emergence of this elemental Ge must be taken into account when considering the use of this nitrided oxide in a device environment.

References

[1] F.H.P.M. Habraken, A.E.T. Kuiper, and Y. Tamminga, J. Appl. Phys. **53**, 6996 (1982).

[2] D.J. Hymes and J. Rosenberg, J. Electrochem. Soc. **135**, 961 (1988).

[3] L.T. Canham, Appl. Phys. Lett. **57**, 1046 (1990).

[4] D.C. Paine, C. Caragianis, and Y. Shigesato, Appl. Phys. Lett. **60**, 2886 (1992).

[5] D.C. Paine, C. Caragianis, T.K. Kim, and Y. Shigesato, Mater. Res. Soc. Symp. Proc. **283** (1993).

[6] CRC *Handbook of Chemistry and Physics*, 70th ed., edited by R.C. Weast, D.R. Lide, M.J. Astle, and W.H. Beyer (CRC, Boca Raton, 1989).

[7] H.F. Wolf, *Silicon Semiconductor Data* (Pergamon Press, New York, 1976), p. 256.

[8] *Proceedings of the 2nd International symposium on Si MBE*, J.C. Bean, Ed. (Electrochemical Society, Pennington, NJ 1988).

[9] E.A. Fitzgerald, Y.-H. Xie, M.L. Green, D. Brasen, A.R. Kortan, J. Michel, Y.-J. Mii, and B.E. Weir, Appl. Phys. Lett. **59**, 811 (1991).

[10] R. Hull, J.C. Bean, G.S. Higashi, M.L. Green, L. Peticolas, D. Bahnck, and D. Brasen, Appl. Phys. Lett., **60**, 1468 (1992).

[11] Q. Hua, J. Rosenberg, J. Ye, and E.S. Yang, J. Appl. Phys. **53**, 8969 (1982).

Chapter 7
Epitaxial Ge Layers on Si via $Ge_xSi_{1-x}O_2$ Reduction

7.1 Introduction

To grow device-grade GaAs epitaxially on a single crystalline Si substrate for integrated electronic and optical devices is of great technological interest. Because the lattice constant and thermal expansion coefficient of Ge are close to those of GaAs but those of Si are not, efforts to form an epitaxial interlayer of Ge on Si started early [1-5]. The fact that device-quality heteroepitaxial GaAs has been grown on Ge substrates vindicates this concept [6].

We have demonstrated in Section 6.3 a novel way to grow an epitaxial Ge film on a Si substrate via the reduction of $Ge_xSi_{1-x}O_2$. The reduction process is driven by the reaction:

$$GeO_2 \text{ (in solution with } SiO_2) + 2\ H_2 = Ge + 2\ H_2O. \qquad (1)$$

This process involves the production of a percolation layer and a reduction of GeO_2 to Ge which grows epitaxially on this percolation layer. In this chapter, we investigate, in detail, the formation of this novel epitaxial growth process and characterize the defects of the grown top Ge layer. A possible mechanism for the epitaxial growth is proposed. We also investigate the effect of the hydrogen partial pressure on this epitaxy growth. It is shown that two quite different Ge structures can be obtained by changing the hydrogen partial pressure, which we depict schematically in Fig. 7.1. The role of the Ge content in the sample is also examined. Finally, conditions under which this epitaxial growth takes place are discussed.

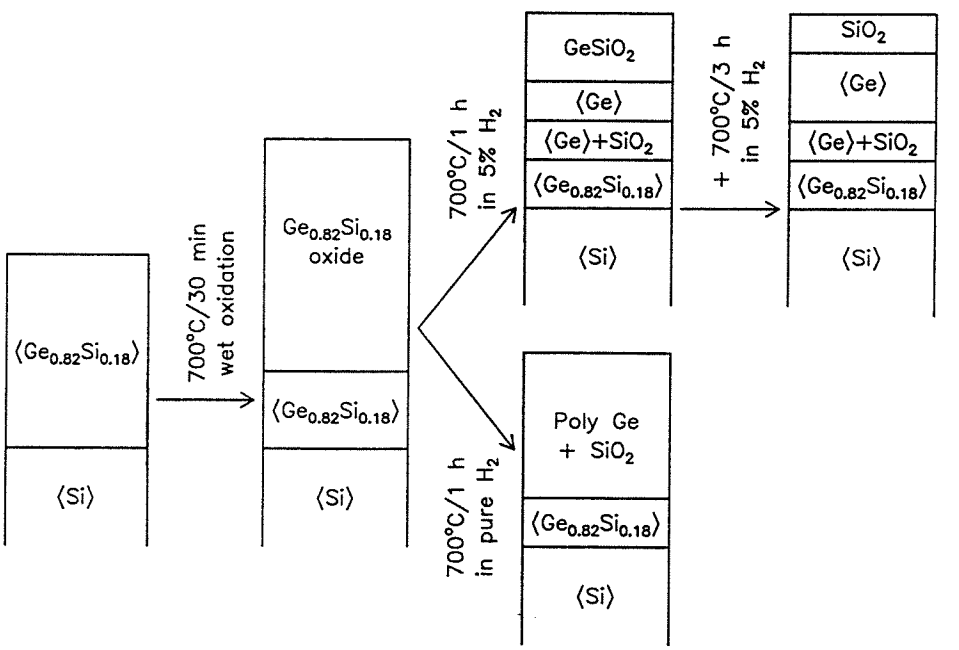

Fig. 7.1 Schematic diagram of the process sequence to obtain an epitaxial growth of Ge or a polycrystalline Ge formation. Both sequences involve the reduction of $Ge_{0.82}Si_{0.18}O_2$ (reaction (1)). The hydrogen partial pressure, however, determines the final structure.

7.2 Experiment

Elastically relaxed Ge_xSi_{1-x} alloys with x = 0.52 and 0.82 were grown epitaxially on (100)Si substrates by molecular beam epitaxy. The thickness for x = 0.52 and x = 0.82 are 540 and 580 nm, respectively. Both samples are then oxidized in a tube furnace at 700°C in a wet ambient. In order to produce a similar oxide thickness, the sample with x = 0.52 was oxidized for 90 min, resulting in an oxide about 680 nm thick, and the sample with x = 0.82 was oxidized for 30 min to produce a 600 nm-thick oxide. The values of the oxide thicknesses were determined from the backscattering spectra and the appropriate oxide density (see Section 3.3). These oxidations did not completely oxidize the GeSi films for both samples. The unoxidized GeSi layer remains epitaxial and uniform in composition. The unoxidized part of the $Ge_{0.82}Si_{0.18}$ layer is about 300 nm thick and that of the $Ge_{0.52}Si_{0.48}$ is about 250 nm thick. These samples shall be referred to as the oxidized samples x = 0.52 and x = 0.82. The purpose of using these two samples is to see what role the Ge and GeO_2 content in the underlying GeSi and in the oxide layers play during the reduction process. Both sample types were then annealed in an open-tube furnace with forming gas (95% N_2 + 5% H_2) at 700°C for 1 to 4 h. Some oxidized samples x = 0.82 and x = 0.52 were also annealed in a closed-tube furnace with pure hydrogen at 700°C for 1 h. The purity of the hydrogen gas used was about 99.95%. The pressure of hydrogen was initially 1 bar above atmospheric pressure and rose to 1.5 bar above atmospheric pressure at 700°C. This rise is less than that of the absolute oven temperature because the furnace heats up only part of the tube. The comparison (5% vs. pure H_2) of the two ambients is to see the effect of the hydrogen partial pressure during the reduction process.

7.3 The Ge growth mechanisms and structure characterization

Figure 7.2 (a) and (b) show the cross-sectional transmission electron micrograph of the oxidized sample x = 0.82 after annealing in N_2 + 5%H_2 for 1 and 4 h. The oxidized sample before annealing is a GeSi/oxide bilayer structure on a Si substrate. After 1 h annealing, a Ge epilayer emerges near the GeSi/oxide interface with a percolation layer underlying the Ge epilayer. This epilayer exhibits the same orientation as the remaining GeSi layer below and has fewer defects than the GeSi layer. The Ge layer is about 80 nm thick and is not defect-free. Some dislocation and microtwin are observed. The percolation layer just next to the top Ge layer consists of two sub-regions with large amorphous islands in its upper part and much finer ones in its lower part. The unoxidized GeSi layer is about 200 nm thick at this stage, which is about 100 nm less than its initial value of 300 nm before annealing.

After 4 h annealing, the Ge epilayer has grown to about 140 nm. Again, some dislocations and microtwins are seen. The defect density is about the same as that after 1 h annealing. The top oxide shrinks to about 120 nm. Some Ge crystalline precipitates are embedded in the oxide. This is concluded from the selected-area diffraction pattern of these precipitates. Compared to that just after 1 h annealing, the unoxidized GeSi layer remains unchanged. Some fine oxide islands in the lower part of the percolation layer coalesce during this further annealing. This is evidenced by the thin and almost continuous oxide layer just above the GeSi layer and by a big oxide island as labeled in the figure in the lower part of the percolation layer, which are not observed in Fig 7.2 (a).

To investigate the percolation layer further, the high resolution cross-sectional transmission electron micrograph of that layer in the sample after 4 h annealing was taken (Fig. 7.3). The upper part of the percolation layer contains an interconnected network of Ge with embedded oxide pockets. The Ge in the network is single-crystalline as evidenced by lattice fringes that are all oriented in the same directions. The network is

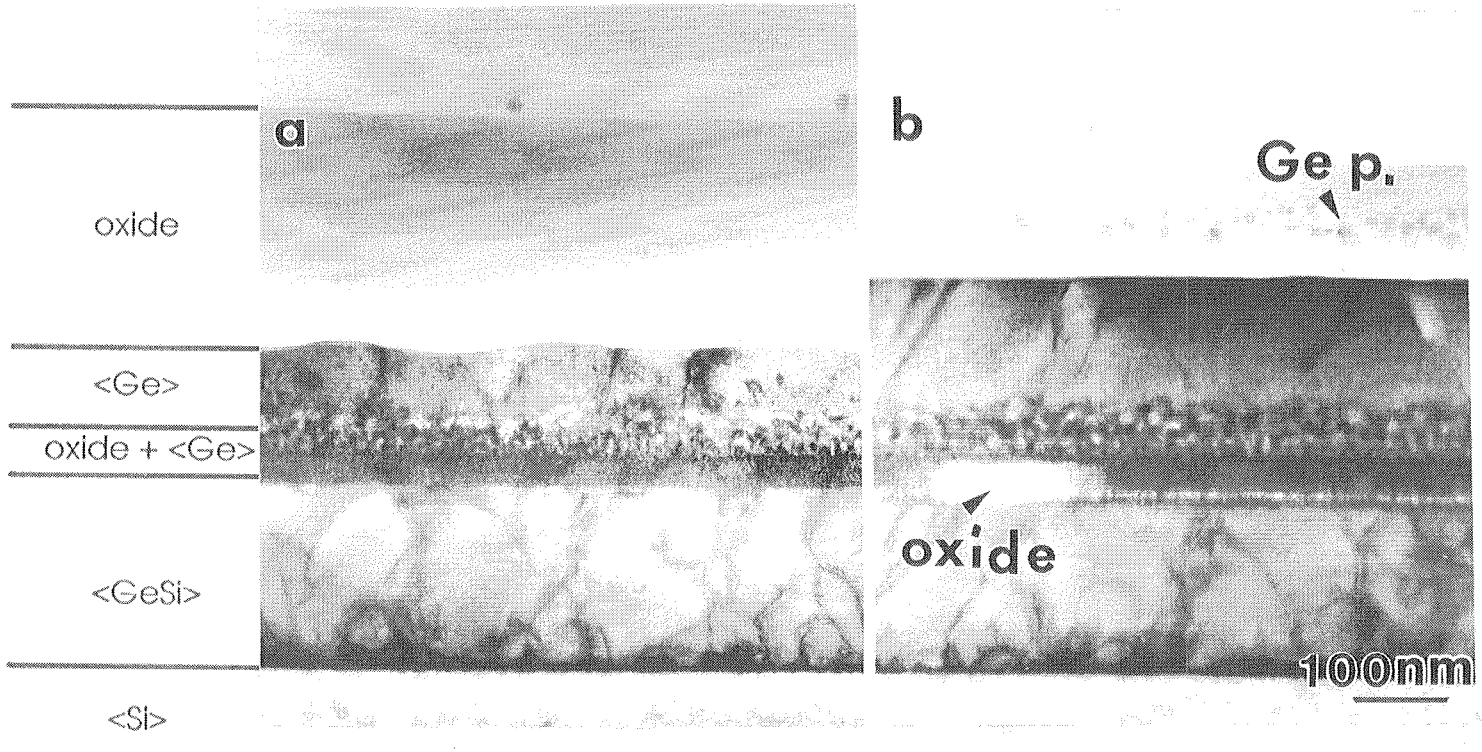

Fig. 7.2 Cross-sectional transmission electron micrograph of the oxidized sample x = 0.82 after the 700°C annealing (a) for 1 h and (b) for 4 h in 5% hydrogen.

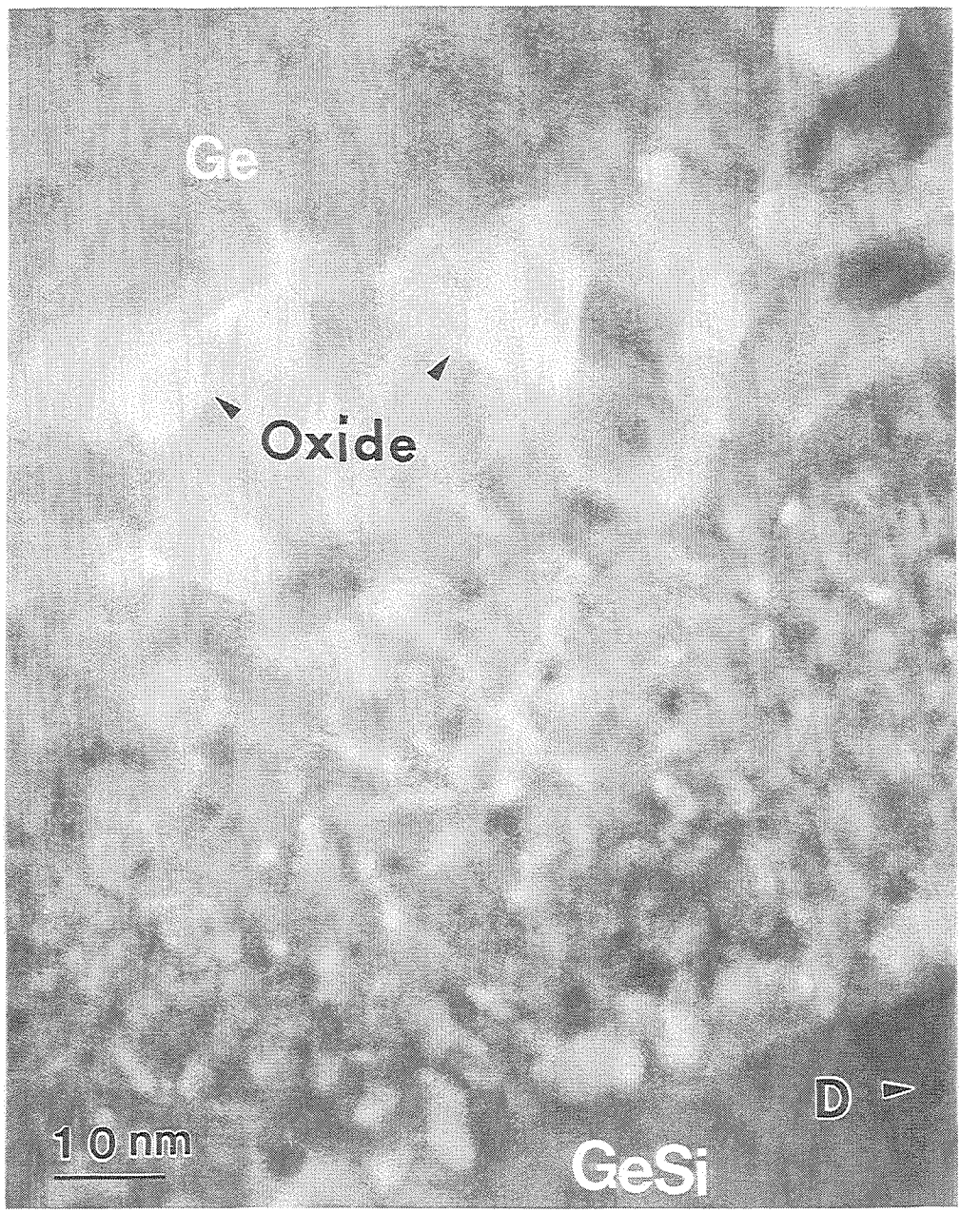

Fig. 7.3 High resolution cross-sectional transmission electron micrograph of the percolation layer in the oxidized sample x = 0.82 after annealing at 700°C in 5% hydrogen for 4 h.

epitaxial with the Ge layer above. The oxide pockets are amorphous. The lower part of the percolation layer contains smaller Ge nodules than that in the upper layer. The nodules seem to be largely connected. Lattice fringes can be seen in these Ge nodules too, which indicates that the Ge nudules are crystalline and have the same orientation. Furthermore, the lattice fringes in the nodules have the same orientation as the underlying GeSi layer. It is then clear that the epitaxial nature of the Ge layer above originates from the underlying GeSi layer since they are connected through the percolation layer.

Figure 7.4 shows the corresponding backscattering spectra of the above annealed samples. The oxidized samples before and after annealing for 2 h are also included. After 1 h annealing, material is lost, as evidenced by the shift of the low-energy edge of the Ge signal. About 18% of Ge is lost, probably in the form of GeO which is volatile and goes to the ambient, as can be seen from the decreasing total number of counts in the Ge signal. About 50% of O is also lost. The Ge layer formed near the GeSi/oxide interface generates a peak signal near 1400 keV but is too thin to be fully resolved in the spectrum. The thickness of the initially unoxidized GeSi layer decreases from 300 nm to 200 nm. The composition of that layer, however maintains its initial value. When annealing further for 2 or 4 h, no more Ge is lost. However oxygen is continuously lost (67% lost for 2h and 75% lost for 4 h). The Ge epilayer also grows thicker. Si remains conserved for all annealings.

We monitored the strain of the grown Ge films by measuring their x-ray rocking curves using Fe $K_{\alpha 1}$ line (λ = 1.936 Å) and the (400) diffraction (Fig. 7.5). It clearly shows that the Ge film is relaxed from the beginning of the growth. The peak is as broad as that of the underlying GeSi layer, presumably because it also contains a contributed signal from the Ge in the percolation layer.

From the above analyses, the epitaxial growth mechanism for the Ge layer can be understood as follows: the germanium dioxide is unstable in the presence of hydrogen and will be reduced to elemental Ge. Since the partial pressure of the hydrogen used here is

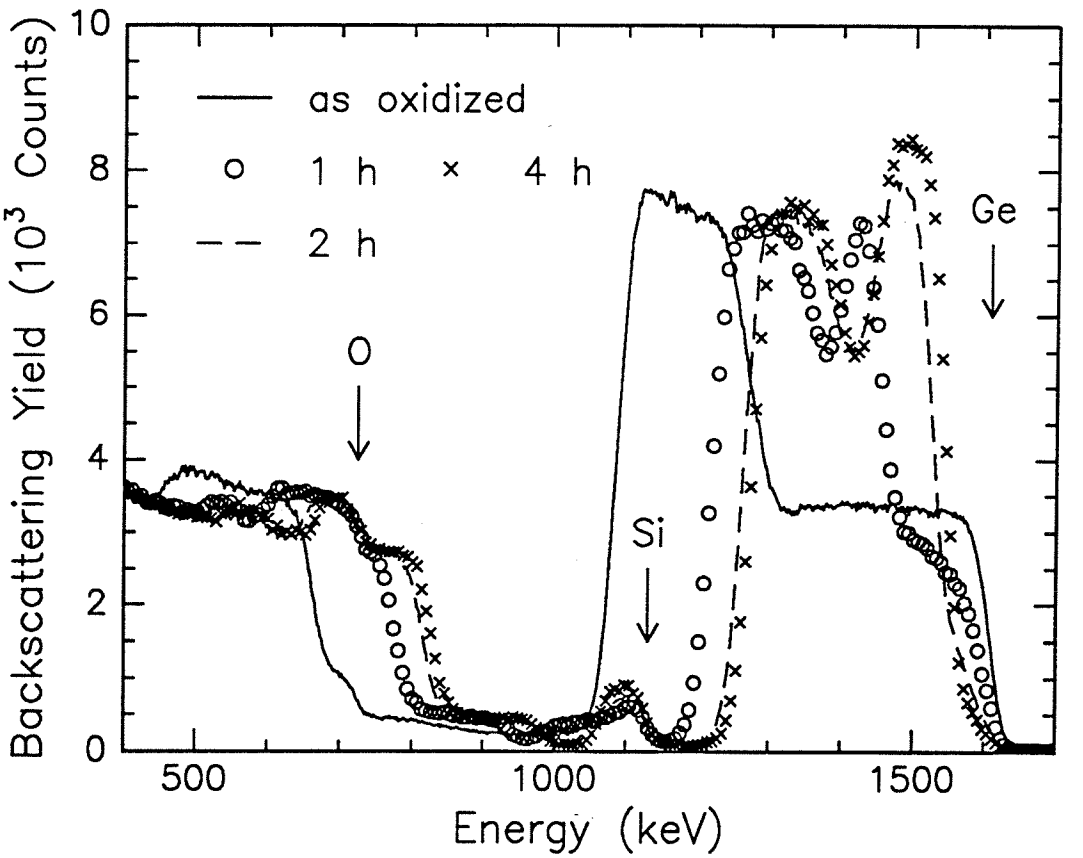

Fig. 7.4 2 MeV $^4He^{++}$ backscattering spectra of an oxidized sample x = 0.82 before and after annealing in 5% hydrogen at 700°C for 1, 2 and 4 h. (scattering angle of detected particles: 170°; beam incidence at 7° from the sample normal).

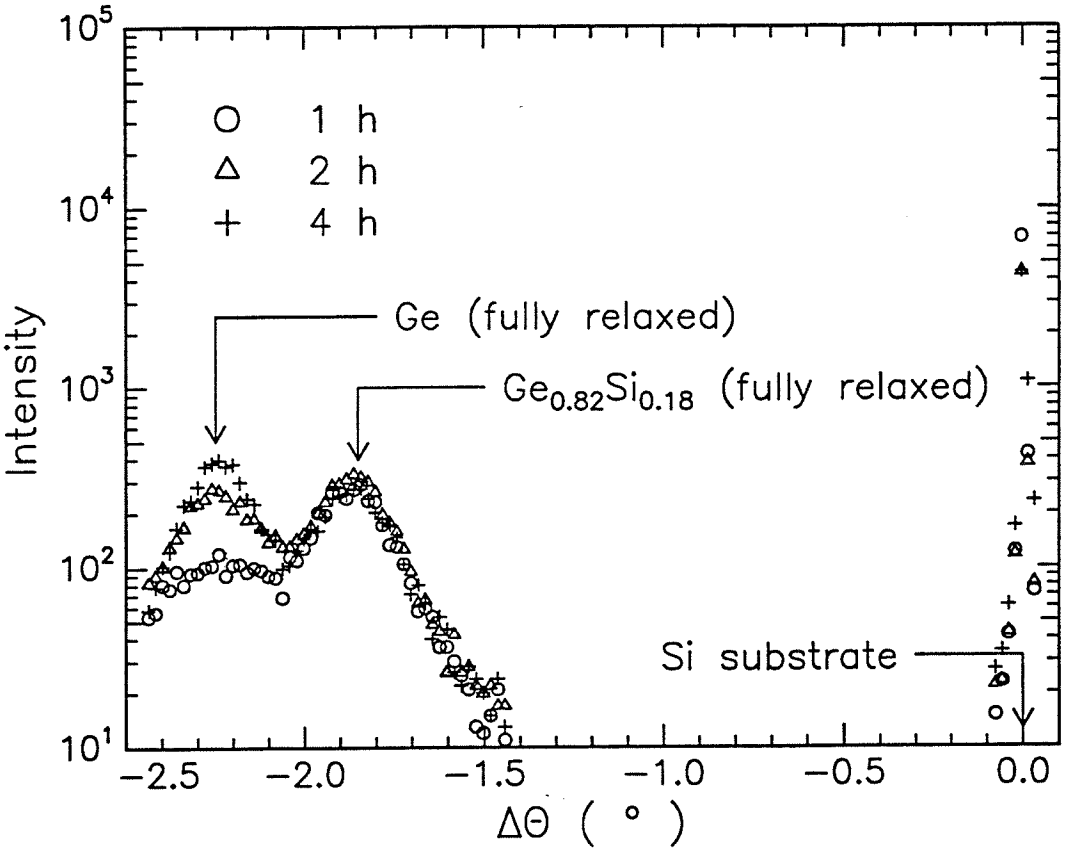

Fig. 7.5 Fe $K_{\alpha 1}$ double crystal x-ray (400) diffraction of the oxidized sample x = 0.82 after annealing at 700°C in 5% hydrogen for 1, 2 and 4 h.

low (5%), heterogeneous nucleation dominates. We will explain this in Section 7.4. The reduction reaction of GeO_2 therefore occurs mainly near the surface and the GeSi/oxide interface. Near the surface, the reduced elemental Ge is converted to GeO which escapes the sample, by reacting with the remaining GeO_2. A SiO_2-rich region is therefore formed near the surface. This surfacial region slows down the further evaporation of Ge as GeO when the reaction progresses into the oxide. No significant loss of Ge is observed after 1 h annealing. Near the GeSi/oxide interface, elemental Ge is able to stay within the oxide. To induce the reaction at this buried interface obviously requires a high mobility of hydrogen in the GeSi oxide, which is quite likely from the fact that the hydrogen diffuses rapidly in the silicon dioxide [7]. While Ge is formed near the GeSi/oxide interface via the reaction (1), the moisture produced from the reaction (1) also oxidizes the underlying GeSi layer. Both Ge and Si can be oxidized since Ge and Si are immobile in GeSi at this temperature. But the GeO_2 is unstable because of the reaction (1) and is thus ultimately reduced, which results in the formation of a mixture of Ge and SiO_2. Another way to view this process is that the moisture released by the reaction of the preexisting GeO_2 leads to an oxidation of only the Si in the adjacent GeSi epitaxial layer, with hydrogen acting as a catalyst. Ultimately, hydrogen will escape out of the sample as H_2 or H_2O.

An approximate description of the resulting region is that of an epitaxial Ge layer with lots of small SiO_2 inclusions. Once established, this layer acts as a seed layer for the heterogeneous nucleation of the Ge reduced from the overlying oxide. After a continuous Ge film is established, the moisture released from the reduction reaction of GeO_2 is unable to oxidize the underlying GeSi layer further. Most of the moisture therefore diffuses out of the oxide. This picture is supported by the unchanged thickness of the unoxidized GeSi layer and the continued loss of oxygen (Fig. 7.2 & 7.4) for a longer annealing (2 & 4 h) compared to those just after 1 h annealing. The continued reduction of GeO_2 to Ge also increases the SiO_2 content in the remaining oxide. Finally, an almost pure SiO_2 layer is left

that contains some Ge precipitates (Fig. 7.2 (b)) which were unable to diffuse to the Ge layer and grow epitaxially in the annealing time applied here.

It is very unlikely that the dislocations in the underlying GeSi would penetrate through the percolation layer into the grown Ge layer since dislocations can not propagate through amorphous material. From Fig. 7.3, the amorphous oxide is distributed quite uniformly, forcing the crystalline Ge into a convoluted network. This convoluted nature of the interconnected network of crystalline Ge hinders the glide or climb of dislocations through that layer into the growing layer. The threading dislocations present in the Ge layer are therefore most likely the result of nucleation and growth of defects occurring during the Ge epitaxial growth.

The amorphous oxides in the percolation layer could themselves act as heterogeneous nucleation sites. It is conceivable that stress in the percolation layer also provides a driving force for the nucleation and growth of defects in the Ge film.

7.4 The role of hydrogen partial pressure

Figure 7.6 shows the backscattering spectrum of the oxidized samples x = 0.82 before and after the annealing in pure hydrogen at 700°C for 1 h. The annealing in 5% hydrogen at 700°C for 1 and 4 h are also included for comparison. As discussed in Section 7.3, the well-defined rectangular Ge signal (Ge signal from 1.45 to 1.53 MeV, circle symbol) in the spectrum of the 4 h anneal in 5% hydrogen corresponds to the Ge epilayer. No such Ge peak is, however, observed after annealing in pure H_2 for 1 h. Rather, Ge is uniformly distributed throughout the oxide. A SiO_2-rich layer is also observed near the surface. Excluding this surface oxide, the composition of the oxide that remains after 1 h in pure H_2 is calculated to be $Ge_{0.8}Si_{0.2}O_{0.4}$, which is equivalent to 0.8 Ge + 0.2 SiO_2 and strongly suggests that this oxide layer is a mixture of elemental Ge and silicon dioxide. This also indicates that almost all the GeO_2 in the GeSi oxide is reduced to the elemental

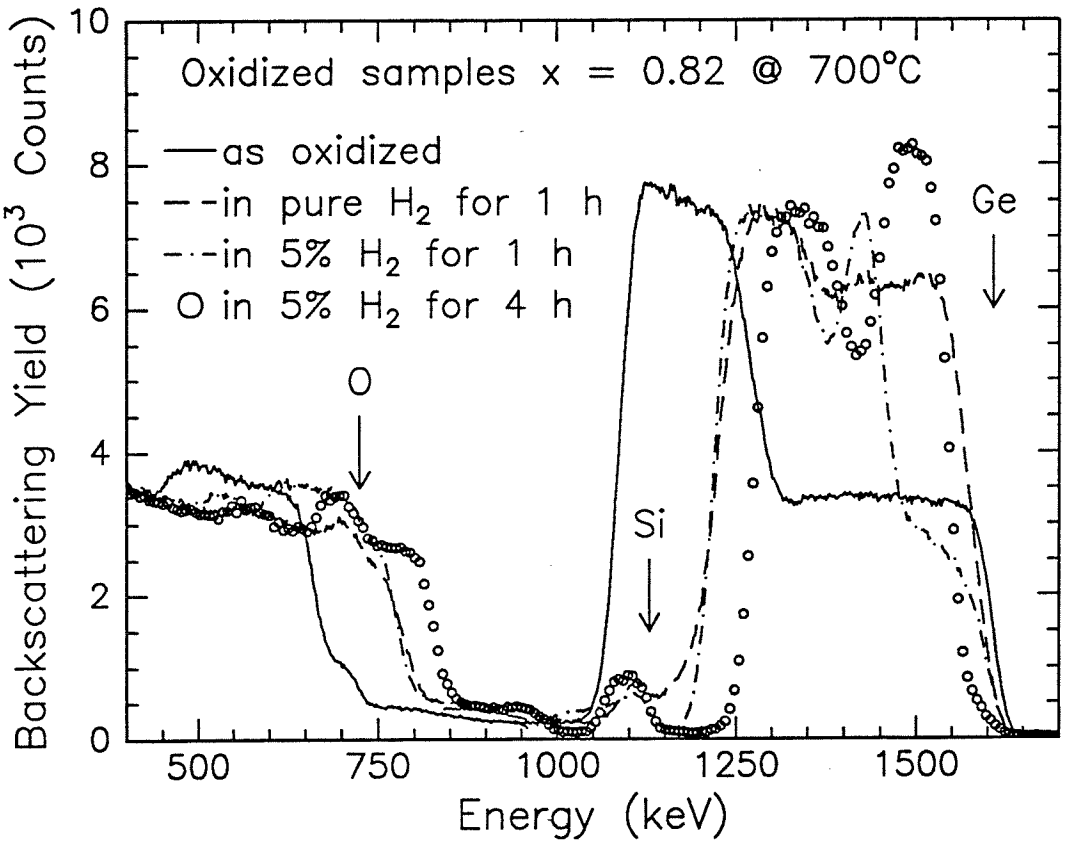

Fig. 7.6 2 MeV $^4He^{++}$ backscattering spectrum of an oxidized sample x = 0.52 before and after annealing in pure hydrogen at 700°C for 1 h. The spectra of the partially oxidized sample after 5% hydrogen annealing at 700°C for 1 and 4 h are also included. (scattering angle of detected particles: 170°; beam incidence at 7° from the sample normal).

state after the pure hydrogen annealing. The area of the Ge signal is indeed observed to decrease only by 5% in that case.

To clarify their crystalline structure, we analyzed the samples by double crystal x-ray diffraction using the Fe $K_{\alpha 1}$ line (λ = 1.936 Å) and the (400) diffraction (Fig. 7.7). As we pointed out previously in Section 6.3 and 7.3 the outcome of this annealing with forming gas annealing (5% hydrogen) is that the formed Ge layer is epitaxial and is of better quality than that of the underlying GeSi seeding layer. The Ge peak is clearly seen in the spectrum of the sample annealed in 5% hydrogen for 4 h. No such peak due to epitaxial Ge is present in the spectrum of the sample annealed in pure hydrogen. Instead, the x-ray diffraction spectrum from an x-ray Read camera shows rings that are characteristic of polycrystalline Ge. The Ge reduced from the GeSi oxide by pure hydrogen thus is polycrystalline, mixed with the silicon dioxide, as already inferred from the backscattering spectrum in Fig. 7.6.

It is thus clear that the reduction reaction (1) occurs upon annealing in both 5% and pure H_2, but the morphology of the crystalline Ge that forms differs much in the two cases, forming an epitaxial layer in one case and polycrystalline precipitates in the other. According to the classical nucleation theory [8], a second-phase particle can nucleate in two basic ways: homogeneously and heterogeneously. In most cases, nucleation is predominantly heterogeneous unless there is a large driving force (free energy difference) for the formation of the second-phase particle. In that case, nucleation may also be homogenous. The different morphology of the crystalline Ge observed here can thus be explained by this theory as being due to a difference in the driving force for these two cases. This difference results in homogenous nucleation in the pure hydrogen annealing system and a heterogeneous nucleation in the 5% hydrogen annealing system. The free energy of the reduction reaction (1) is governed by G = -3.8 kcal/mole + 2 RT ln (P_{H_2O}/P_{H_2}), where P_{H_2O} and P_{H_2} are the partial pressures of the moisture and the

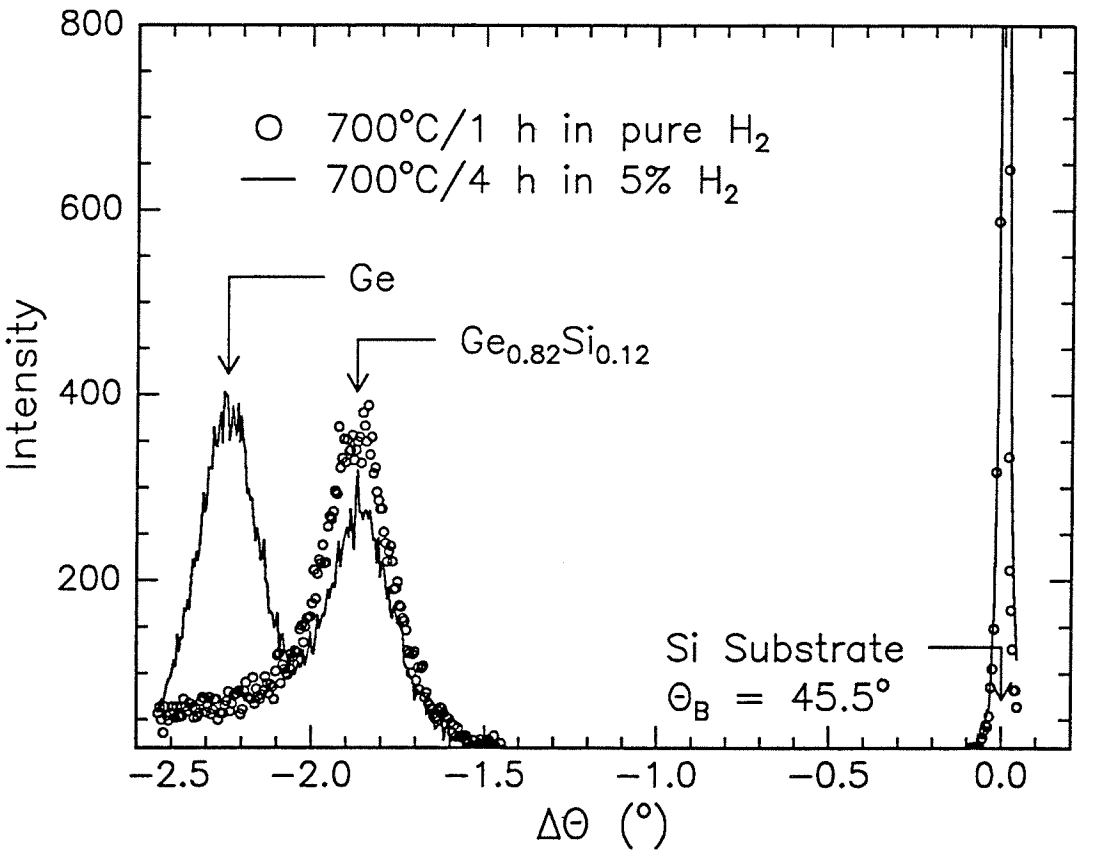

Fig. 7.7 Fe $K_{\alpha 1}$ double crystal x-ray (400) diffraction of the partially oxidized sample x = 0.82 after annealing at 700°C in pure hydrogen for 1 h and in forming gas for 4 h.

hydrogen in the system (see Section 6.2). The different hydrogen partial pressure in the above two systems therefore causes the big difference in the driving force.

The difficulty with this explanation is that it is assumed that P_{H_2O} is the same in both experiments. We did not measure the partial pressure of the moisture in both experiments. It is quite possible that the different gas sources and annealing systems used here result in different P_{H_2O}. Furthermore, it is the concentration in the oxide that actually matters ,which also depends on the generation and consumption of the moisture and hydrogen by the reduction and oxidation reaction. To validate our interpretation will therefore require additional experimental proof.

In the case of pure H_2, homogenous nucleation dominates with the result that Ge randomly nucleates. This homogenous nucleation process hinders the epitaxial growth of Ge. The formation of uniformly distributed polycrystalline Ge throughout the oxide is also observed in the oxidized sample x = 0.52 after the pure hydrogen annealing. In the 5% H_2 case, on the other hand, the reduction of Ge is dominated by heterogeneous nucleation due to a reduced free energy difference. Germanium could epitaxially grow as shown in Section 7.3.

7.5 The role of the Ge content

The formation of this percolation layer of epitaxial Ge with SiO_2 inclusions is therefore the key for the subsequent growth of a pure Ge epitaxial layer. Another key factor for a continued epitaxial growth is the ability to separate the remaining SiO_2 from this epitaxial growing Ge layer. These two factors conceivably are closely related to the Ge content in the original GeSi film.

To demonstrate the importance of this Ge content, an oxidized sample x = 0.52 was annealed in forming gas at 700°C for 4 h. The backscattering spectra of this sample before and after 4 h is shown in Fig. 7.8. A Ge bump (signal at 1.4 MeV) is again

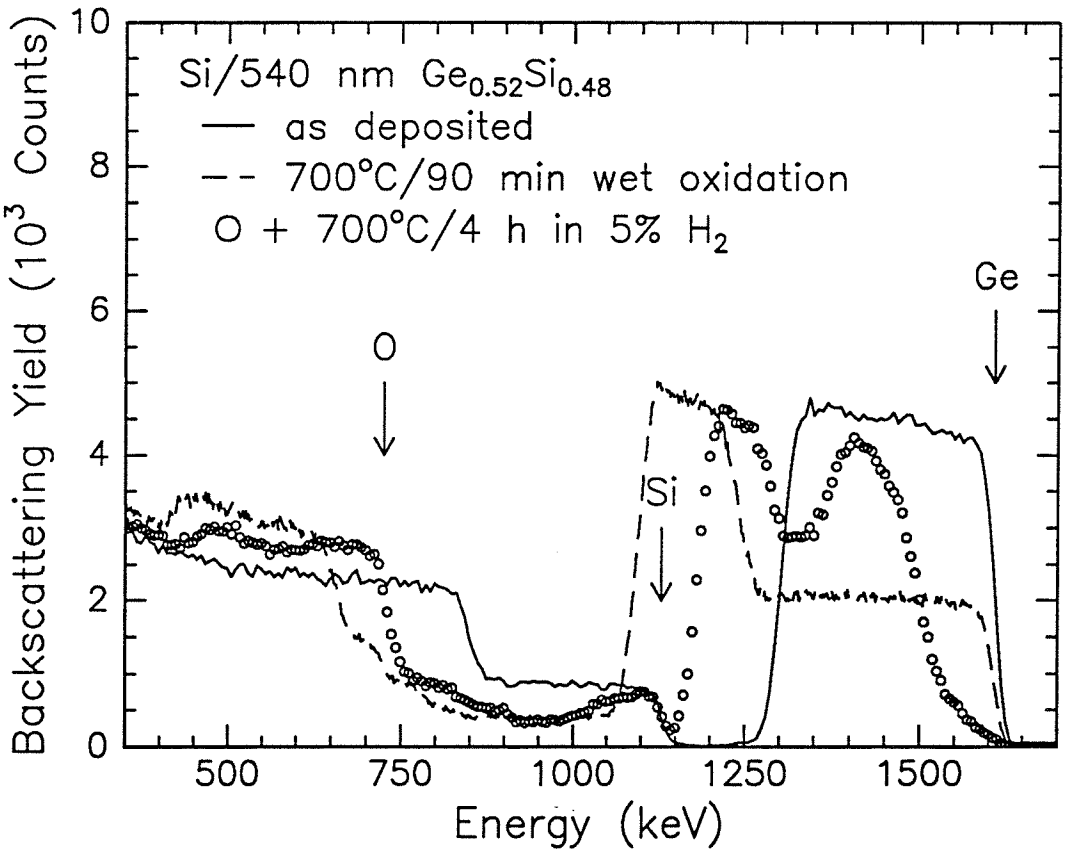

Fig. 7.8 2.9 MeV $^4He^{++}$ backscattering spectra of a oxidized sample x = 0.52 before and after annealing in forming gas ambient at 700°C for 4 h. (scattering angle of detected particles: 170°; beam incidence at 7° from sample normal).

observed near the GeSi/oxide interface. The thickness of the initially unoxidized GeSi film decreases from about 250 nm to about 180 nm but the composition and uniformity of this remaining epitaxial GeSi is unaltered. These facts again prove that the reduction reaction (1) also occurs in this sample and that the reduced Ge accumulates near the GeSi/oxide interface. What is different form the oxidized sample x = 0.82, however, is that the reduced Ge does not develop a layer. From the height and width of this Ge bump, it indicates that the Ge is mixed with the silicon dioxide. The x-ray rocking curve shows no evidence of the existence of a single crystalline Ge. Polycrystalline Ge rings are found form an x-ray Read camera. This demonstrates that although Ge is also reduced initially near the GeSi/oxide interface in this oxidized sample x = 0.52, the Ge layer is polycrystalline, rather than epitaxial.

The Ge content in the GeSi alloy is thus critical for the epitaxial growth of Ge. This content not only decides the Ge concentration in the underlying GeSi layer, but also the germanium dioxide in the oxide layer. In the oxidized sample x = 0.82, the germanium and the germanium dioxide are the majority species in both the GeSi and the oxide layers. This could benefit the epitaxial growth in two ways: first, the selective oxidation of Si to create the percolation layer discussed above does not form a continuous film of SiO_2, but rather SiO_2 islands that precipitate out in a connected network of epitaxial Ge. This Ge becomes a seeding area for the subsequent Ge epitaxial growth. Secondly, the Ge reduced from its oxide state can form a continuous layer out of which the remaining SiO_2 is expelled, forming a top layer above the Ge epilayer (see Fig. 7.6). The inability to grow a Ge epilayer in the oxidized sample x = 0.52 suggests that one of the above two factors, or both, is not present in this sample.

7.6 Conclusions

We have shown that the GeO_2 in $Ge_{0.52}Si_{0.48}O_2$ and $Ge_{0.82}Si_{0.18}O_2$ is unstable upon annealing in the ambients of pure hydrogen as well as forming gas (95% N_2 + 5% H_2). A Ge epilayer is found in the oxidized samples with x = 0.82 annealed in forming gas. A possible mechanism for the epitaxial growth is proposed. The others, however result in the formation of polycrystalline Ge. Conditions under which an epitaxial Ge growth occurs are tentatively proposed to be the following:

(1) The reduction reaction must occur first near the GeSi/oxide interface, i.e., heterogeneous nucleation must dominate during the reduction process. This condition can be influenced by the hydrogen partial pressure.

(2) The Ge content in the GeSi layer near the GeSi/oxide interface must be large enough that the preferential oxidation of Si in this GeSi layer leads to the formation of a percolation layer.

(3) Ge and/or SiO_2 in the remaining part of the oxide must have sufficient relative mobility to segregate into separate layers.

References

[1] B.Y. Tsaur, J.C.C. Fan, and R.P. Gale, Appl. Phys. Lett. **38** 176 (1981).

[2] M. Maenpaa, T.F. Kuech, M.-A. Nicolet, S.S. Lau, and D.K. Sadana, J. Appl. Phys. **53**, 1076 (1982).

[3] P. Sheldon, B.G. Jacobi, K.M. Jones, and D.J. Dunlavy, J. Appl. Phys. **58**, 4186 (1985).

[4] Y. Fukuda and Y. Kohama, Jpn. J. Appl. Phys. **26**, L597 (1987).

[5] Y. Fukuda and Y. Kohama, J. Crys. Growth **81**, 451 (1987).

[6] P.A. Iles, Y.-C. M. Yeh, F.H. Ho, C.-L. Chu, and C. Cheng, IEEE Electron Dev. Lett. **11**, 140 (1990).

[7] H.F. Wolf, *Silicon Semiconductor data* (Pergamon Press Inc., New York, 1976) p.526.

[8] R.E. Reed-Hill, *Physical Metallurgy Principle*, 2nd edition (Monterey, California, 1973) p.368.

Chapter 8
Epitaxial Ge_xSi_{1-x} Layers on Si via Oxidation of Amorphous Ge/Si Bilayers

8.1 Introduction

As we show in Chapter 1, the growth of epitaxial GeSi alloys on Si is of interest for electronic device applications. Although high quality GeSi layers can be grown by molecular beam epitaxy [1] or chemical vapor deposition [2], the cost of these methods and their compatibility with current Si integrated circuit technology are limitations of concern.

Prokes et al. have shown recently that by wet oxidation of an amorphous GeSi film on Si, an epitaxial GeSi heterostructure can be grown regardless of the existence of interfacial contaminations [3-5]. The proposed model involves the diffusion of Si from the substrate through a contamination layer to the forming surface oxide, creating a localized defect supersaturation and resulting in enhanced downward Ge diffusion and epitaxy. In this chapter, we extend the study to a dry ambient. We show that an epitaxial GeSi heterostructure can also be formed by dry oxidation of an initially amorphous Ge/Si bilayer deposited on (100)Si. The quality of this epi-GeSi layer and the mechanism of the formation are investigated and compared to those obtained by wet oxidation.

8.2 Experiment

4-6 ohm-cm type (100) silicon wafers were cleaned in trichloroethylene, acetone, and methanol in a ultrasonic bath, and then dipped in a diluted HF solution. 180 nm thick germanium and 45 nm thick silicon layers were sequentially electron-beam evaporated at

room temperature. The purpose of depositing a thin layer of Si on top is to prevent the loss of Ge in the form of GeO during the subsequent oxidation [6]. The pressure during deposition was less than 4×10^{-7} Torr. Following the evaporation, some samples were oxidized in a dry or wet ambient at 920°C for various durations. For comparison, a sample was also annealed in vacuum at 920°C for 4 h. The samples before and after these annealings were characterized by 2 MeV $^4He^+$ backscattering and channeling spectrometry. Some samples were also investigated by cross-sectional transmission electron microscopy.

8.3 The roles of the oxidation ambients

Figure 8.1 (a) shows the backscattering spectra of samples after dry oxidation for 1, 4, and 15 h respectively. An oxide forms on the surface that is almost pure SiO_2, although a small amount of Ge is found within the oxide (seen only faintly in Fig. 8.1 (a)). Most of the original Ge layer is mixed with Si into a uniform GeSi layer with a fairly sharp interface at the underlying Si substrate, as characterized by the low energy edge of the Ge signals in the spectra. The thickness of this layer is about 250 nm and it contains about 70% Ge. This mixed GeSi layer remains roughly constant in composition and thickness during the oxide growth. Some Si atoms that are transformed to SiO_2 during the oxidation then must come from the Si substrate.

The striking feature of this oxidation process is that the resulting mixed GeSi layer is epitaxial with the underlying Si substrate. The crystalline quality of this epilayer improves with the oxidation duration as is demonstrated in Fig. 8.1(b) where channeling spectra of the samples of Fig. 8.1(a) are shown after the oxide layers were etched off by diluted HF. After 1 h of oxidation, only the region of the GeSi layer located nearest to the interface with the underlying single crystalline Si substrate exhibits channeling; the remainder of the film shows no channeling. After 4 h of oxidation, the upper part of the film also exhibits

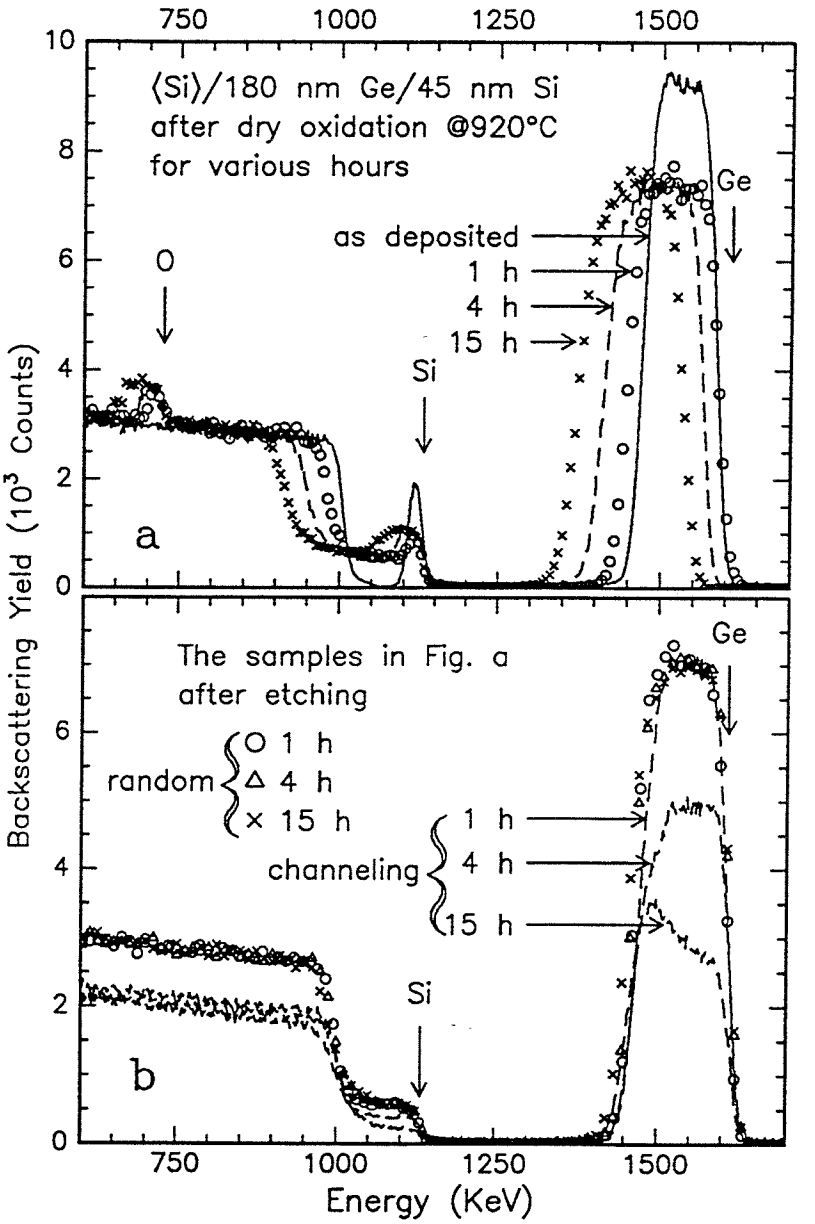

Fig. 8.1 2 MeV He^+ backscattering and channeling spectra (a) of a 180 nm Ge/45 nm Si bilayer on a Si(100) substrate after dry oxidation at 920°C for 1, 4 and 15 h, and (b) of the oxidized samples of Fig. (a) after the oxide was etched off.

channeling. However, the channeling spectrum very clearly displays a two-part structure. After 15 h of oxidation, such a distinct two-part structure disappears. The crystalline quality improves to a channeling yield of about 40% for the Ge signal near the surface.

To view the above structure, a piece of the sample after 4 h of oxidation was investigated by cross-sectional transmission electron microscopy. The bright-field micrograph is shown in Fig. 8.2 (a). A bilayer structure is distinctly seen on top of the Si substrate. The upper layer is about 180 nm thick and the lower one about 70 nm thick. From the electron diffraction, the lower layer is single crystalline. The upper layer is mixed single crystalline and polycrystalline. This configuration is thus consistent with the two-part structure seen in the channeling spectrum (Fig. 8.1(b)). The development of the shape of the channeling spectra described above thus reveals how the structure of the GeSi film evolves during the dry oxidation, which will be discussed further on.

Figure 8.2 (b) is the transmission electron micrograph of the same sample but with higher magnitude than Fig. 8.2 (a). One noticeable observation in this micrograph is that a contamination layer exists between the upper and the lower GeSi layers. This contamination layer appears to be continuous and parallel to the surface. No contamination layer is, however, seen between the lower GeSi layer and the Si substrate.

The growth of an epitaxial GeSi film has also been reported for wet oxidation of an amorphous GeSi layer on a Si substrate.[3] To investigate the effect of the oxidation ambient on the quality of the resulting mixed GeSi layer, we oxidized a piece of our Si(100)/Ge/Si sample in a wet ambient for 40 and 60 min (Fig. 8.3(a)). The oxide layer formed is pure SiO_2 and about 180 nm thick after 40 min of wet oxidation. That thickness is about the same as that obtained after 15 h of dry oxidation. The epitaxial nature of this mixed GeSi film is evidenced by the channeling spectrum of the sample when the top oxide is etched off by HF (Fig. 8.3(b)). The crystalline quality of this film is poor and has a minimum yield of only about 86% for the Ge signal near the surface. Further wet oxidation incorporates most of the Ge into the oxide.

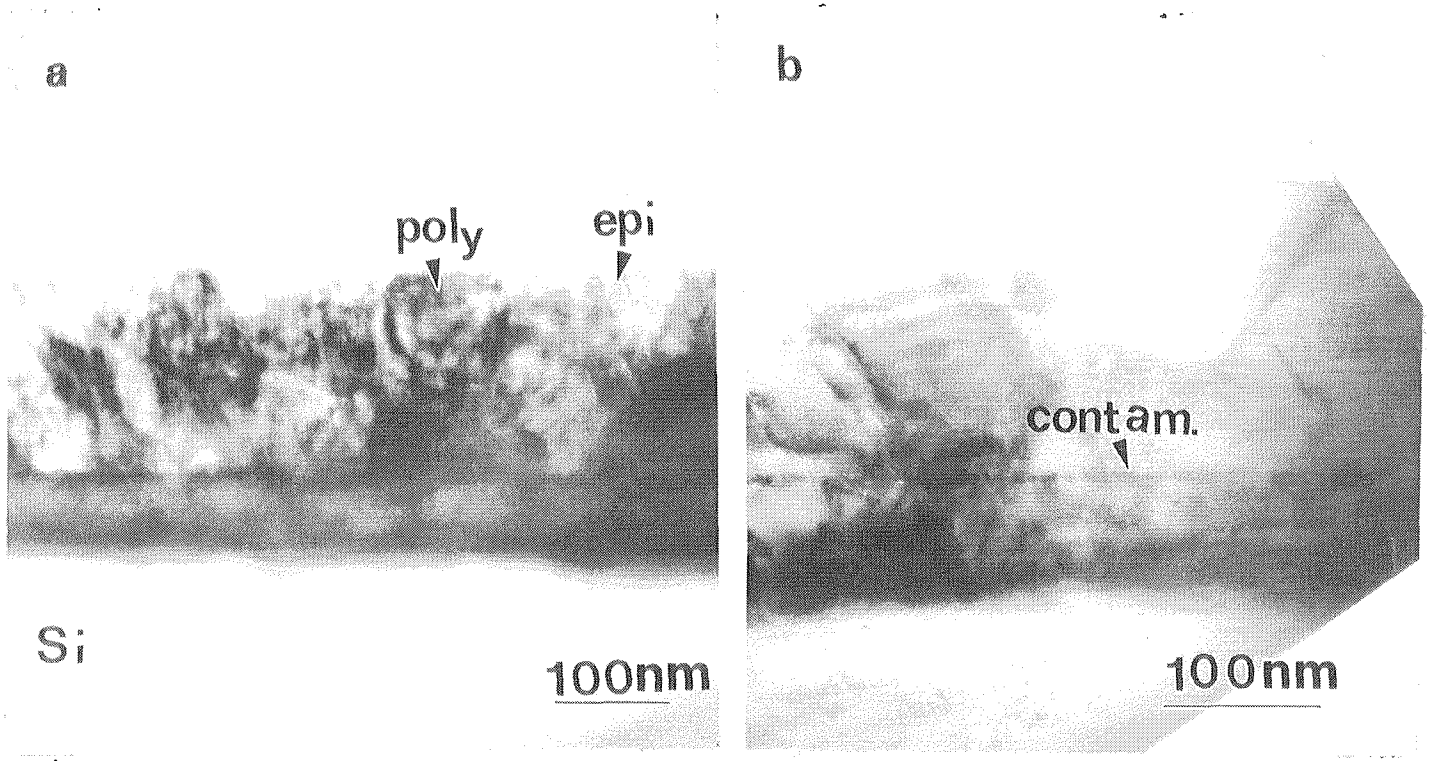

Fig. 8.2 Cross-sectional transmission electron micrographs of a 180 nm Ge/45 nm Si bilayer on a Si(100) substrate after dry oxidation at 920°C for 4 h. The top oxide has been etched off. Fig. (b) shows a similar area with but has a larger magnification than Fig. (a).

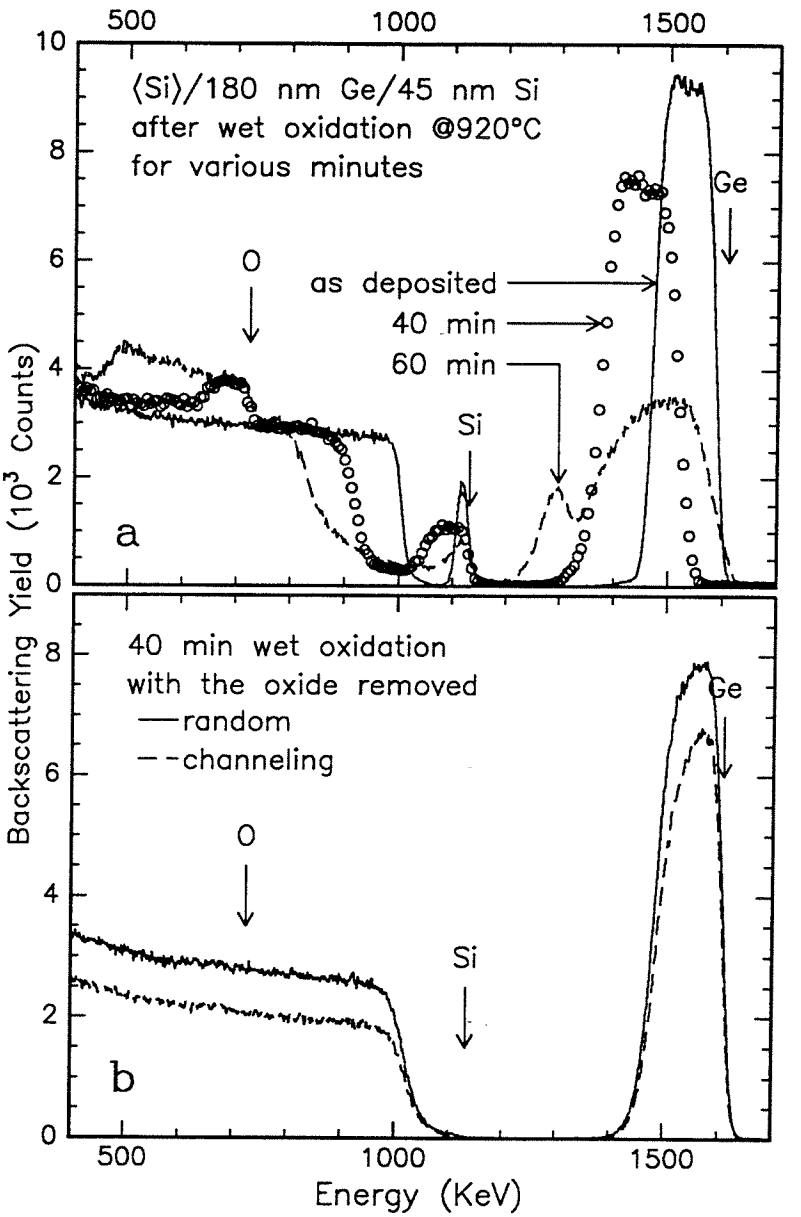

Fig. 8.3 2 MeV He^+ backscattering and channeling spectra (a) of a 180 nm Ge/45 nm Si bilayer on a Si(100) substrate after wet oxidation at 920°C for 40 and 60 min, and (b) of the 40 min-oxidized sample after the oxide was etched off.

The formation of an SiO_2 layer at the sample surface is essential to achieve the epitaxial structure of the GeSi. That this is so follows from the result of an experiment where a sample is annealed in vacuum at 920°C for 4 h (Fig. 8.4). Again Ge mixes with the top Si and substrate Si into a uniform $Ge_{0.6}Si_{0.4}$ film of about 300 nm thick. About 60% of the Si in this film comes from the Si substrate. An epitaxial texture exists near the interface as can be seen in the channeling spectrum, but most of the film shows full dechanneling as an indication of nonepitaxial structure. Upon further annealing for 15 h, some Ge is lost. Again, only the interfacial epitaxial texture is observed, but not the epitaxy of the whole layer.

The crystalline quality of the mixed GeSi film in terms of the channeling yield in the Ge signal and the Si signal near the surface after the above three annealing processes are summarized in table 8-I. The resulting thicknesses and the compositions of the GeSi films are also listed.

Annealing ambient	Oxide thickness (nm)	x/thickness (nm) of Ge_xSi_{1-x}	χ_{min} in Ge (%)	χ_{min} in Si (%)
1 h (dry)	45	0.7/250	100	100
4 h (dry)	90	0.7/250	71	74
15 h (dry)	150	0.7/250	39	40
40 min (wet)	180	0.9/200	86	~
4 h (vac)	~	0.6/300	100	100

Table 8-I The minimum yield of the Ge and Si signals from the near-surface region of the mixed GeSi layers after annealing in the ambients shown. The resulting oxide thicknesses and the Ge contents and the thicknesses of the mixed GeSi films as estimated from the backscattering spectra are also listed.

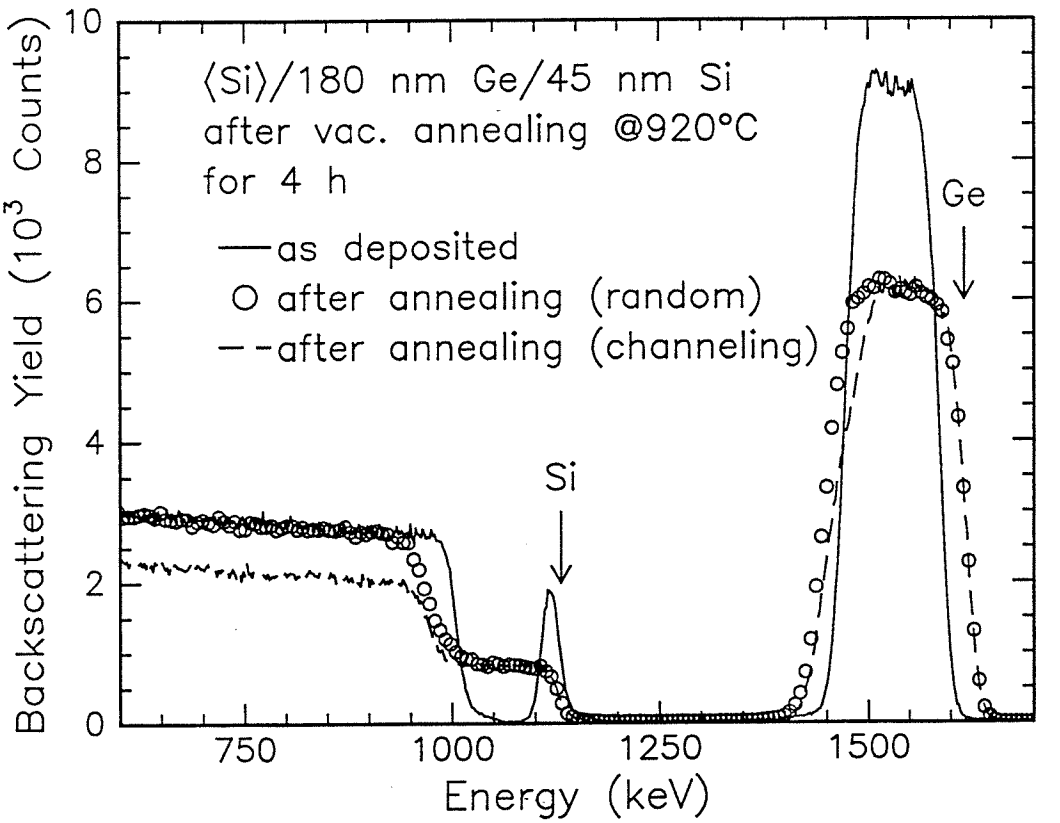

Fig. 8.4 2 MeV He^+ backscattering and channeling spectra of a 180 nm Ge/45 nm Si bilayer on a Si(100) substrate after vacuum annealing at 920°C for 4 h.

8.4 Discussion

Several general conclusions can be drawn from these results. Firstly, although no special precaution is taken to ensure a clean Si surface prior to the Ge deposition, yet epitaxial GeSi films can be formed in both dry and wet ambients. Secondly, the dry oxidation proceeds at a reduced rate which provides a convenient opportunity to follow the evolution of the process. Thirdly, the quality of the resulting GeSi film depends on the annealing parameters chosen. Finally, epitaxy doesn't occur for vacuum annealing. This outcome is expected from similar studies with evaporated Si layers on not cleaned in-situ Si substrates [7-9].

Compared to the wet oxidation, the dry oxidation is a much slower process; fewer defects are generated. This slow process rate thus allows one to capture the evolution of the epitaxial growth of the GeSi film. From Fig. 8.2, no contamination layer is observed in the Si/GeSi interface. Instead, a contamination layer exists within the GeSi film. This layer most likely originates from the initial contamination present on the Si substrate prior to the deposition of Ge and Si, moving up during the dry oxidation. Prokes et al. [5] also observed such a movement during the wet oxidation of an amorphous GeSi layer on Si. This contamination layer probably acts as an inert marker whose upward movement is caused by the downward movement of Ge. As suggested by Prokes et al. [5], this significant movement of the contamination layer is due to the enhanced diffusion of Ge into the Si substrate.

Several mechanisms for this enhancement are possible. Firstly, it is well known that point defects are generated in Si during the oxidation [11]. These point defects may be present and play a role for the diffusion mechanism in GeSi as well. Secondly, the GeSi film remains about constant in thickness and composition during the dry oxidation. Prokes et al. [4,5] have suggested that this diffusion of Si to the forming oxide creates a supersaturation of point defects and results in enhanced downward Ge diffusion.

The intermixing of Ge into the Si substrate produces a noticeable epitaxial GeSi film. At the same time, the Si/Ge exchange through the contamination layer probably creates some weak area which leads to some epitaxy of the top GeSi film just above the contamination layer. This therefore creates a mixture of polycrystalline and single crystal in the top GeSi film as seen in Fig. 8.2. It is also noticed that the corresponding channeling spectrum shown in Fig. 8.1 reflects this bilayer structure. The evolution of the channeling spectra as shown in Fig. 8.1 thus indicates the structural change during the dry oxidation. The spectra suggest that during the initial dry oxidation process, some epitaxial GeSi texture forms below the contamination layer and a polycrystalline GeSi layer remains above (1 h oxidation). With extended oxidation time, the epitaxial texture grows into a layer and some single crystal is also formed in the GeSi film above (4 h oxidation). And finally, with both the growth of the underlying epilayer and grain growth of some properly oriented crystallites in the GeSi film above, a complete GeSi epilayer is formed (15 h oxidation).

References

[1] A.T. Fiory, J.C. Bean, L.C. Feldman, and I.K. Robinson, J. Appl. Phys. **56**, 1227 (1984).

[2] C.M. Gronet, C.A. King, W. Opyd, J.F. Gibbons, S.D. Wilson, and R. Wilson, J. Appl. Phys. **61**, 2407 (1987).

[3] S.M. Prokes, W.F. Tseng, and A. Christou, Appl. Phys. Lett. **53**, 2483 (1988).

[4] S.M. Prokes, and A.K. Rai, J. Appl. Phys. **67**, 807 (1990).

[5] S.M. Prokes and A.K. Rai, Mater. Res. Soc. Symp. Proc. **202**, 639 (1991).

[6] J.T. Law and P.S. Meigs, J. Electrochem. Soc. **104**, 154 (1957).

[7] M. von Allmen, S.S. Lau, D.M. Scott, J.W. Mayer, W.F. Tseng, T.T. Sheng, P. Williams, and J.E. Baker, J. Electrochem. Soc. **80**, 195 (1980).

[8] M.G. Grimaldi, M. Maenpaa, B.M. Paine, M.-A. Nicolet, S.S. Lau, and W.F. Tseng, J. Appl. Phys. **52**, 1351 (1981).

[9] L.S. Hung, S.S. Lau, M. von Allmen, J.E. Mayer, B.M. Ulrich, J.E. Baker, P. Williams, and W.F. Tseng, Appl. Phys. Lett. **37**, 909 (1980).

[10] G.L. Mcvay and A.R. Ducharme, Phys. Rev. **B9**, 627 (1974).

[11] S.M. Hu, J. Appl. Phys. **45**, 1567 (1974).

[12] S.G. Park, W.S. Liu and M.-A. Nicolet, J. Appl. Phys. **75**, 1764 (1994).

Chapter 9
Summary and Future Works

The kinetics and associated mechanisms of thermal oxidation of Ge_xSi_{1-x} on Si, and the properties of the resulting oxides are the two main topics of this thesis. In the first part that deals with the kinetics and associated mechanisms, we establish that the oxidation behavior is determined by the competition between the speed of the diffusive processes in the unoxidized GeSi alloy and the velocity at which the oxidation front progresses. To formulate this model quantitatively, however, requires further investigation, especially regarding the diffusive processes in the unoxidized GeSi alloy. This includes what the main moving species is and how its diffusivity may differ form that in vacuum annealing.

This thesis establishes that wet oxidation of Ge_xSi_{1-x} at temperatures $\leq 700°C$ follows a parabolic growth law; that of pure Si under the same conditions follows a linear growth law [1]. It would be interesting to see how this growth law changes as x approach zero. It is well known that the reaction rate of oxidation of GeSi is significantly enhanced over that of pure Si in a wet ambient, whether Ge is oxidized or not [2-5]. The parabolic law observed in wet oxidation of GeSi at temperatures $\leq 700°C$ also reveals this enhancement. The study of the oxidation kinetics of Ge_xSi_{1-x} for small values of x would shed some light on the origin of this enhancement and on the nature of the oxidation process of pure Si as well

As to the properties of the resulting oxides, this thesis focuses on $Ge_xSi_{1-x}O_2$ on Ge_xSi_{1-x} or Si. It turns out that $Ge_xSi_{1-x}O_2$ is not useful as a passivation layer or as gate oxide, because the $Ge_xSi_{1-x}O_2$ is thermodynamically unstable in contact with Si or GeSi. However, germanium dioxide is also unstable in the presence of hydrogen, while silicon dioxide is stable. That selective instability can be exploited to synthesize nanocrystalline

Ge in SiO_2 or to induce epitaxial growth of Ge on Si. The process is driven by the reaction:

$$GeO_2 \text{ (in } Ge_xSi_{1-x}O_2) + 2\ H_2 = Ge + 2\ H_2O. \qquad (1)$$

By controlling the partial pressures of H_2O and H_2, one can direct the reaction either to reduction or to oxidation.

The loss of Ge is regularly seen in the process of the reduction of GeO_2 (see Chapter 6). This implies that the following reaction is possible:

$$GeO_2 \text{ (in } Ge_xSi_{1-x}O_2) + H_2 = GeO + H_2O. \qquad (2)$$

The annealing of Ge_xSi_{1-x} in mixed ambients of $H_2 + H_2O$ with different partial pressures is therefore of interest. Conceptually, three distinct solid structures will be expected: GeSi dioxide, porous SiO_2 (with GeO to the ambient), and Ge in SiO_2 (with epitaxial, polycrystalline or nanocrystalline Ge). The possibilities contained in this system certainly deserves further investigation.

The basic idea on which these possibilities rest is simple and can be formulated as follows: A homogenous amorphous mixture of two similar binary compounds (oxides, nitrides, etc.) is exposed to a rapidly diffusing species with which one binary compound is thermodynamically stable, and the other not. The result is a two-phase system, the structure of which varies depending on the dominant process of nucleation and growth. The process is similar to a selective chemical reaction in a liquid where the fast diffusion requirement is replaced by agitation.

References

[1] B.E. Deal and A.S. Grove, J. Appl. Phys. **36**, 3370 (1965).

[2] D. Fathy, O.W. Holland, and C.W. White, Appl. Phys. Lett. **51**, 1337 (1987).

[3] F.K. LeGous, R.Rosenberg, and B.S. Meyerson, Appl. Phys. Lett. **54**, 644 (1989).

[4] D.K. Nayak, K. Kamjoo, J.S. Park, J.C.S. Woo, and K.L. Wang, Appl. Phys. Lett. **57**, 369 (1991).

[5] J. Eugene, F.K. LeGous, V.P. Kesan, S.S. Iyer, and F.M. d'Heurle, Appl. Phys. Lett. **59**, 78 (1991).